

Neural Correlates of Sensorimotor Control in  
Human Cortex: State Estimates and Reference  
Frames

Thesis by  
Matias Jafari

In Partial Fulfillment of the Requirements for  
the degree of  
Doctor of Philosophy

The logo for the California Institute of Technology (Caltech), featuring the word "Caltech" in a bold, orange, sans-serif font.

CALIFORNIA INSTITUTE OF TECHNOLOGY  
Pasadena, California

2019  
(Defended May 7, 2019)

© 2019

Matiar Jafari  
ORCID: 0000-0002-2224-4896

## Dedication

For my family past, present, and future.

And

For the love of science.

## Acknowledgements

This work would not have been possible without the backing and support of the people listed here. This work is the product of those who shaped me before and during this time. There is no amount of words I can say to express how grateful I am for each and every person who has been there with me. I could never adequately do justice to you all, but I would like to at least acknowledge a subset of individuals who have directly impacted my work and time at Caltech.

Firstly, I would like to express my sincere gratitude to my advisor Dr. Richard A. Andersen for the continuous support of my Ph.D. work. Your patience, immense knowledge, and resilience especially in the face of adversity have not only helped shape this work, but also my personal life.

I'd like to thank Dr. Tyson N.S. Aflalo, for being an outstanding mentor, friend, and colleague. You have helped shaped my life and career and provided me with a basis set of tools to grow and learn from. While I was not the graduate student that you asked for you took a chance on a young aspiring student who had little to no background in computer programming. I am indebted to you for this work finally coming to fruition, my growth as a scientist, and as a person. You have taught me many lessons both directly and indirectly.

To the rest of my gracious committee Dr. David Chan, Dr. David Prober, and Dr. Ueli Rutishauser: you have exceeded all expectation and obligation, by generously offering your time and constructive input throughout the years.

I'd like to thank my loyal companions, Dr. Aram S. Modrek, Dr. Nicholas D. Olivas, Dr. Ameer Elbuluk, Dr. Srinivas Chivukula, and Dr. Sumner L. Norman. Aram, we grew up dreaming of pursuing scientific questions and here we both stand a decade later ready to face the next set of challenges. The vicissitudes of life that we have shared together over this time, while at times extremely draining, have both helped propel us forward and made us stronger. Nicholas, I thank you for always listening to my crazy ideas and your never-ending encouragement to continue down the road less travelled even when I've lost all hope. I was introduced to neuroscience because of you and I am forever grateful for this and for a friendship of such high caliber. Ameer, like brothers we have always seemingly come to similar conclusions, yet you have always been able to provide a unique and alternative viewpoint. Regardless of what life has thrown at us I have known I could always count on you, this side or the other. Srinivas, you always found a way to uplift me even in moments where I have felt stuck and pessimistic about the future. You always take time to listen and lend a helping hand. Sumner, from bouncing ideas off one another and challenging each another inside and outside the lab you have consistently pressed me to dig deeper and to assimilate any topic. Gentlemen, it has been a privilege having you in my corner and I can confidently say you are not just friends, but brothers for life.

The rest of my family at Caltech: Dr. Spencer S. Kellis, for supporting a taking on a naïve young student and gently guiding and supporting me through my missteps. My Greek family, Vasilieios, Sofia, and Ariadne Christopoulos for always lifting me up, listening, and wisely advising me how to go about any issues I was facing. Dr. Michelle Armenta-Salas, for always being understanding even when I was being difficult. HyeongChan Jo, for the countless memories and laughs we have shared over the years. Kelsie Pejisa, for being my biggest fan and supporter. Dr. Viktor Shcherbatyuk, for always having a joke ready to make me laugh. Also my utmost gratitude to my many other friends and colleagues for productive discussions and making this experience an unforgettable one: Dr. Christian Klaes, Dr. Boris Revechkis, Dr. Luke Bashford, Dr. David Bjanes, Varun Wadia, Sarah Wandelt, Charles Guan, Kelly Kadlec, and Isabelle Rosenthal.

Finally, this work would have not been possible without the steadfast support and love of my family. To my mother, thank you for your unwavering belief in me and for instilling in me that impossible was just a word and it could be overcome. You took the time to teach yourself in hopes of transferring that knowledge to your children. At a young age, you showed me that the world I knew to be filled with magical things was even more majestic when you looked a little deeper. This path began as you guided me while we took apart a pinball machine. It is because of your hard work, sweat, and tears that I was able to embark on this journey. To my father, you have always led by example and been a pillar of strength and resilience. When times have been challenging I have leaned on the lessons you have shown me. My sister, for always knowing how to put a smile on my face and for never letting me feel alone. To my lovely aunt, Marita Tavakoli, for loving me like your own child and supporting me when I have been lost. To Drs. Kamran and Mallika Samakar, as well as Mila and Juliet Samakar, you have all been a source of joy throughout my life and have always found ways to help me focus and embrace the vicissitudes of graduate school. Your support in the past, present, and future is priceless and I am forever grateful. To Media Moussavy, for your unconditional support and passion. Nahid Adibi, my grandmother, for the endless supply of prayers and love. Saba Kashani, for always being so understanding and supportive throughout this journey.

Lastly, to my lovely fiancée, Yasamin Kashani. Yasamin, this journey would be impossible without you. You have been the person who has seen and encouraged me through the bleakest of lows. One could say we have won some and lost some throughout this time, but every moment with you has been a victory. We have gone through graduate school together and I could not have done it without you by my side. While we have lost Akram and Saeed Sarkeshik, I have no doubt they are looking down and are proud of the path we have taken together.

## Abstract

Interacting with our environment involves multiple sensory-motor circuits throughout the human brain. How do these circuits transform sensory inputs into discernable motor actions? Our understanding of this question is critical to behavioral neuroscience and implementation of brain-machine interfaces (BMIs). In this thesis, we present experiments that explore the contributions of human cerebral cortex (parietal, premotor, and primary somatosensory cortices) to sensory-motor transformations. First, we provide evidence in support of primary somatosensory cortex (S1) encoding cognitive motor signals. Next, we describe a series of experiments that explore contributions of posterior parietal cortex (PPC) to the internal state estimate. Neural correlates for the state estimate are found in PPC; furthermore, it is found to be encoded with respect to gaze position. Finally, we investigate reference frame encoding in regions throughout human cortex (AIP, SMG, PMv, and S1) during an imagined reaching task. We find the greatest heterogeneity among brain regions during movement planning, which collapses to a largely single reference frame representation (hand-centered) during execution of the imagined reach. However, this result is dependent upon brain region. These findings yield new perspectives and evidence on the organization of sensory-motor transformations and the location the human brain's internal estimate of the body's state.

# Table of Contents

Abstract.....	vi
1. Introduction.....	1
1.1 Background.....	2
1.1.1. Brain Machine Interfaces .....	2
1.1.1 Reference Frames.....	12
1.1.2 Internal Models .....	16
1.1.3 State estimation in PPC.....	17
2. Neural Correlates of Cognitive Motor Signals in Primary Sensory Cortex.....	22
2.1 Introduction.....	22
2.2 Methods .....	22
2.2.1 Subject Information.....	22
2.2.2 Surgical Planning and Implantation.....	23
2.2.3 Reference Frame Task.....	23
2.2.4 Neural Recordings.....	24
2.2.5 Eye Tracking .....	25
2.2.6 Linear Analysis for Tuning .....	26
2.2.7 Reference Frame Analysis: Gradient Analysis .....	27
2.2.8 Dimensionality Reduction.....	28
2.3 Results.....	29
2.4 Discussion.....	38
3. Neural Correlates of the Internal State Estimate in Human Posterior Parietal Cortex .....	39
3.1 Introduction.....	39
3.2 Methods .....	41
3.2.1 Internal Model Task.....	41
3.2.2 Spatial Match-to-Sample Task.....	43
3.2.3 Behavioral Variable Tuning ANOVA .....	44
3.2.4 Linear Analysis for Tuning .....	45
3.2.5 Gradient Analysis.....	46
3.2.6 AUC Analysis .....	47
3.2.7 Population Decoder Analysis.....	47
3.2.8 Cross-Hand Position Classification Analyses.....	48
3.3 Results.....	49
3.4 Discussion.....	62
4. Diverse Reference Frame Representations Across Human Cortex.....	65
4.1 Introduction.....	65
4.2 Methods .....	69
4.2.1 Subject Information.....	69

4.2.2	Surgical Planning and Implantation.....	70
4.2.3	Reference Frame Task.....	71
4.2.4	Neural Recordings.....	72
4.2.5	Eye Tracking.....	73
4.2.6	Linear Analysis for Tuning.....	73
4.2.7	Reference Frame Analysis: Gradient Analysis.....	74
4.2.8	Dimensionality Reduction.....	76
4.3	Results.....	77
4.3.1	Imagined Reaching Related Activity in Human Cortex.....	79
4.3.2	Reference Frames.....	80
4.3.3	Heterogeneous Representations of Coordinate Frames.....	84
4.3.4	Population Level Encoding of Reference Frames.....	88
4.3.5	Temporal Evolution of Reference Frames.....	96
4.3.6	Decoding Accuracy.....	101
4.4	Discussion.....	104
5.	Conclusion.....	111
6.	References.....	115



## List of Illustrations and/or Tables

<a href="#">Figure 1.1. Different recording modalities</a> .....	10
<a href="#">Figure 1.2. Schematic of Sensorimotor Integration</a> .....	19
<a href="#">Figure 2.1. Behavioral Task, Electrode Location, and Tuning Throughout Task</a> .....	30
<a href="#">Figure 2.2. Example S1 Unit, Gradient Analysis, and Distribution of Gradients of Tuned Units</a> .....	32
<a href="#">Figure 2.3. Idealized Unit Responses Displaying Three Different Reference Frames</a> .....	33
<a href="#">Figure 2.4. Graphical Illustration of Complex PCA Processing</a> .....	35
<a href="#">Figure 2.5. Dimensionality of population level reference frames from S1</a> .....	36
<a href="#">Figure 2.6. Parallel Analysis in S1</a> .....	37
<a href="#">Figure 3.1. Schematic of Sensorimotor Integration, Task Design, and Tuning Across Epochs</a> .....	50
<a href="#">Figure 3.2. Idealized, Sample, and Population Responses during the Mask Epoch</a> .....	51
<a href="#">Figure 3.3. Lack of Coding for Imagined Hand Position in Working Memory Task</a> .....	54
<a href="#">Figure 3.4. Distinct Representations for Hand Position and Potential Reach Targets</a> .....	58
<a href="#">Figure 3.5. Direction Encoding in AIP</a> .....	61
<a href="#">Table 4.1. Criteria for Categorizing Individual Units</a> .....	75
<a href="#">Figure 4.1. Experimental Design, Recording Locations, and Significant Tuning Across Epochs</a> .....	78
<a href="#">Figure 4.2. Eye Position Distribution for Different Task Epochs and Cued Positions</a> .....	79
<a href="#">Figure 4.3. Idealized Unit Responses Displaying Three Different Reference Frames</a> .....	82
<a href="#">Figure 4.4. Example Units from AIP and SMG and their Reference Frames</a> .....	83
<a href="#">Figure 4.5. Heterogeneous Reference Frame Representations Across Brain Regions</a> .....	86
<a href="#">Figure 4.6. Population Level Reference Frames Across Brain Regions</a> .....	89
<a href="#">Figure 4.7. Comparison of Strength of Modulation for Each Vector</a> .....	95
<a href="#">Figure 4.8. Graphical Illustration of Complex PCA Processing</a> .....	97
<a href="#">Figure 4.9. Correlation of Reference Frame Representations over Time and Across Brain Regions</a> .....	98
<a href="#">Figure 4.10. Dimensionality Reduction of Reference Frames</a> .....	99
<a href="#">Figure 4.11. Decoding Target Position from Unique Hand Positon</a> .....	102
<a href="#">Figure 4.12. Decoding Target Position from Unique Eye Positon</a> .....	103

# 1. Introduction

From the eye-hand coordination of a skilled drummer's rhythm to the effortless pouring of freshly brewed coffee into a mug, we have come to observe movements as smooth, accurate, and coordinated actions that interact and adapt to the ever-changing dynamics of our environment. The smooth and unconscious nature of our interaction with surroundings conceals the true complexity of the underlying neural processes. These seemingly effortless actions are driven by a complex electrical symphony built of intricate networks of neurons located in a multitude of sensory and motor brain areas. The electrical potentials emerging across these areas produce precise and fluid representations of the surrounding sensory environment, intended movement, and internal simulation of these dynamics.

An action or behavior that interacts with our surroundings is a dynamic link between our sensory world and our internal motor intentions. The coupling of sensory and motor are partially characterized by the following: 1) sensory information that encodes the spatiotemporal location of a movement goal, and 2) an estimate of the current state of the body, limb, and relevant effector. For example, when you visually identify a desired object in space and subsequently engage the musculature required to reach for it, your brain must integrate sensory information about the location of the target with information about the position of your body and effector (e.g., hand) in order to generate a smooth sequence of movements toward the goal.

These characteristics of sensory-motor control are discussed in Chapters 2, 3, and 4. In this chapter we will provide background on the pertinent literature with respect to the following topics: 1) a brief history and introduction to brain machine interfaces, 2) coordinate frame (i.e. reference frame) transformations, and 3) neural evidence in non-human primates (NHPs) of internal state estimates. These will build a groundwork upon which Chapter two (Neural Correlates of Cognitive Motor Signals in Primary Sensory Cortex.) and four (Diverse Reference Frame Representations Across Human Cortex) will build upon. In Chapter three (Neural Correlates of the Internal State Estimate in Human Posterior Parietal Cortex), we will provide single-unit evidence of an internal state estimate of limb position in the posterior parietal cortex (PPC) of an adult human, which to the best of our knowledge is the first human single unit evidence to show that PPC encodes an internal state estimate.

## 1.1 Background

### 1.1.1. Brain Machine Interfaces

In 1924, a psychiatrist named Dr. Hans Berger arguably made the first giant leap towards how we try to understand the brains function. His discovery of electroencephalography (EEG) was just the beginning and it would take almost half a century (1976) until Dr. Jacques Vidal at UCLA published his seminal paper “Real-time detection of brain events in EEG.” Vidal and colleagues went on to show the first evidence that they could detect and classify individual evoked responses with reliability, and furthermore coined the term brain machine interface (BMI). In essence, what Dr. Vidal had shown was the realization

that by recording from the brain he and his team could utilize brain signals effectively enough to control a cursor through a two-dimensional maze (Vidal, 1973; Wolpaw and Wolpaw, 2012).

The annual incidence of spinal cord injury (SCI) is estimated to be 40 cases per million population in the United States, approximately 12,500 new SCI cases per year. These cases exclude those who die at the scene of the accident (National Spinal Cord Injury Statistical Center, 2015). Unfortunately, many high-level spinal cord injuries result in tetraplegia, that is, the total or partial paralysis of all four limbs and torso as well as loss of sensation below the level of injury. Per consequence, many tetraplegic patients are unable to perform many activities of daily living (ADL), such as eating and bathing. Fortunately, recent advances in neuroprosthetics and brain-machine interfaces (BMIs) have helped propel the translation of nearly a half century's worth of NHP BMI work to human clinical trials in tetraplegic participants. While BMIs have numerous potential applications, the scientific community has identified that enabling direct brain-machine communication for tetraplegic patients would have a significant impact on both the personal and financial aspects of SCI patients' lives: the long term aim of such research is to provide autonomy for patients to perform ADLs.

Prior to the initiation of the first intracortical BMI clinical trials (Hochberg et al., 2006) the field was built upon decades of NHP research. Early evidence began to accumulate in the late 1960s. An initial set of experiments completed by Eberhard E. Fetz showed that

NHPs reliably modulated single neurons when given visual feedback of an analog signal correlated to their spiking activity, in an operant conditioning paradigm (Fetz et al., 1969). This fortuitous finding came while Fetz and colleagues were trying to determine the motor analog to sensory receptive fields, wherein it was established that many of the operantly rewarded responses were associated with active limb movements (Fetz and Baker, 1973). As the rewarded unit was continuously driven by the animal for a reward, the associated movements became more discrete and often dropped out entirely, further adding that the central volitional drive on cells can be modulated independent of peripheral input (Fetz, 2007). These findings along with a series of other impressive demonstrations of neural control set the foundation for the field now referred to as brain-machine interfaces (BMIs) (Wolpaw and Wolpaw, 2012).

Brain-machine interfacing (BMI) refers to a wide array of techniques and applications that all share the characteristic of using signals directly from the brain to control an external device and/or using electrical or magnetic stimulation methods to “write” information to the brain. Interfaces technologies can be invasive or noninvasive; thus, the application of different recording techniques are often decided by technical and surgical constraints. Examples of recording methods that measure neuronal electrical potentials, either directly or indirectly, include electroencephalography (EEG), electrocorticography (ECoG), and intracortical microelectrode arrays (MEAs). EEG measures electrical potentials at the scalp that reflect the activity of billions of neurons whose summed potential has propagated through tissue and bone in a process called volume conduction.

ECoG is an invasive technique that involves implanting an array of electrodes underneath the skull, now capable of measuring the local field potentials of more specific cortical neuron populations. MEAs measure local field and single unit activity by implanting small 4 mm x 4 mm intracortical arrays in carefully localized brain areas of interest. There are also methods of measuring brain activity indirectly through neurovascular coupling for the purpose of a BMI control signal. These techniques include functional magnetic resonance imaging (fMRI), functional near-infrared spectroscopy (fNIRS) and functional ultrasound (fUS). For more detail on these methods, we direct the reader to Wolpaw and Wolpaw, 2012. In clinical practice, the number of BMI applications and recording techniques are still narrow. The most commonly implanted BMI is the cochlear implant, where auditory sensory information is conveyed to the user via electrical impulses from a medical device that replaces the function of a dysfunctional inner ear (House, 1976). More recently, BMI applications aimed to replace (Collinger et al., 2013) or assist (Norman et al., 2018) motor function in people that are severely paralyzed due to neurological injury. For example, BMIs have been shown to be capable of controlling cursors, robotic limbs, and functional electrical stimulation (FES) of the user's own body (Aflalo et al., 2015; Ajiboye et al., 2017; Chaudhary et al., 2015; Collinger et al., 2013; Hochberg et al., 2006). As a result, BMI technology and science has garnered increasing attention within academic, private, and public domains.

As the number of independent neural signals we can record from grows, much BMI research has turned its focus on the interpretation of those signals, leveraging analysis

techniques from various fields including control theory, information theory, and artificial intelligence. BMI-neuroprosthetic applications, e.g. control of robotic limbs and computer cursors, has primarily leveraged the dynamics of neural firing rates in cortical regions where the subjects' motor intentions are hypothesized to be encoded. The link between firing rates of various motor related cortices has been established with half a century of scientific progress demonstrating that these populations can accurately predict overt motor intentions. This was expanded upon by Georgopoulos et al. (1982) with a demonstration that a simple linear sum of the preferred directions of neurons with overlapping tuning curves could predict arm movements. These findings, along with others in other cortical regions, helped propel the field forward toward extracting movement parameters from populations of neurons.

Traditionally, a BMI model is fit during a training period, wherein the brains representations of movements are recorded in parallel with the subject mimicking or attempting an instructed action. During this time the subject has no overt control and is rather attempting or imagining the movement so as to create a training set of data with stereotyped actions. For example, a subject will be asked to concurrently attempt the same movements as a predetermined cursor trajectory is displayed on the screen. The neural data from this training set will then be used by a neural encoder to relate the neural activity that with a given label or movement direction. These models are then used during a testing period to decode neural information in an attempt to predict the user's movement intention in real time. Neural encoders and decoders are composed of a

multitude of varying linear and non-linear methods, a fast-growing and important topic outside the scope of this work. For recent work, we refer the reader to (Glaser et al.; Kao et al., 2015; Pandarinath et al., 2018).

Neural decoding in a BMI context leverages the electrical potentials of many neurons firing as the basis set upon which predictions on the world are made. Hence, it is important to know what kinds of information can be and are encoded in a given brain region within the context of the desired BMI. For example, researchers have shown that activity in motor and parietal cortices could be used to drive movements in a BMI context (Aflalo et al., 2015; Ethier et al., 2012; Hochberg et al., 2006; Kim et al., 2008; Serruya et al., 2002). In contrast, others have shown that location based information could be predicted by leveraging the information encoded in hippocampal cells (Davidson et al., 2009; Zhang et al., 1998). Therefore, decoding information from the brain is not only useful in the context of BMIs but also for determining the amount of information the brain encodes as it pertains to the external world (i.e., behavioral variables, movements, sensations, etc.) and how the available information is differentially parcellated across brain areas (Hernández et al., 2010; van der Meer et al., 2010; Quiroga et al., 2006; Sugata et al., 2016).

One of the more commonly utilized areas for BMI control is primary motor cortex (M1). M1 receives inputs from premotor, primary somatosensory, and parietal areas. M1 itself








encodes low-level motor output and is a final common pathway for the cortical control of movement. Its primary downstream projections are to the spinal cord. As a result, M1 produces reliable, low-dimensional signals that correlate well with motor states such as velocity. These qualities make it desirable for decoding movement states and dynamics (Georgopoulos et al., 1982; Hochberg et al., 2006; Holdefer and Miller, 2002; Morrow and Miller, 2003; Russo et al., 2018), hence its utility in BMIs for spatial cursor or robotic limb control. Furthermore, another advantage to recording from M1 is its topographical representation of motor intent. That is, M1 is divided into separate regions controlling the movement of different muscles and body parts as described in the earliest work by Penfield (Penfield and Boldrey, 1937). Briefly, leg movements are largely elicited on the dorsal medial aspect of M1 and progress to shoulder elbow, wrist, and hand movements more laterally and ventrally, followed by the digits, face, and mouth. This topographical organization enables a spatially intuitive map on which BMIs can be designed. Furthermore, later work went on to show that the densest connections were found to be to the hand area of M1. This is to say, M1 is often-though to be an ideal location for MEA placement for the implementation of BMI for spatial motor control tasks (He et al., 1993; Nuyujukian et al., 2018; Rathelot and Strick, 2006).

Another area that has been used for BMI purposes is the posterior parietal cortex (PPC). The PPC in contrast to M1 encodes higher level intentions and plays a pivotal role in the synergy required for sensory-motor transformations in the brain (Aflalo et al., 2015; Andersen and Cui, 2009; Andersen et al., 2010; Baldauf et al., 2008; Zhang et al., 2017).

The encoding of higher level intentions in PPC along with the ability to decode trajectories make PPC another proven area upon which human BMIs have been successfully implemented (Aflalo et al., 2015; Revehkis et al., 2014). We expand on the posterior parietal cortex and its subdivisions in a later section.

It is clear that the specialization of cortical areas is pivotal to the implementation of a BMI. However, another important aspect of the application of BMIs is the modality of neural code that is analyzed. Most neurons use action potentials (APs) to transmit information. This information is a product of electrical potentials reaching a threshold, at which time a “spike” is seen and the potential travels down the neurons axon towards the synapses of all its downstream post-synaptic neurons. The rate at which a series of APs occur in a single neuron is one example of neural encoding that researchers leverage. This is called a “firing rate” (FR). Electrodes are also capable of sensing the summed activity of large populations of neighboring neurons, the “local field potential (LFP). While FRs and LFPs are in the time domain, researchers have shown that neural codes in the frequency domain can also be used to robustly decode information as it pertains to a task (Adrian and Zotterman, 1926; Butts et al., 2007; Singh and Levy, 2017; Stein et al., 2005; VanRullen et al., 2005). Much of the techniques that try to determine electrical potential changes in the brain parenchyma utilize signals that pertain to the AP. Interestingly, with the advent of functional magnetic resonance imaging (fMRI) researchers found that measuring blood oxygenation levels in regions of the brain is also a practical application for indirectly determining localized neuronal activity. While the

signals associated with hemodynamic methods such as fMRI do not retain the spatiotemporal qualities of invasive electrophysiological methods, they have the advantage of being noninvasive and capable of large-structure or whole-brain imaging.

Recording Modality	fMRI	fUS	EEG	ECoG	MEA
Resolution ( $\mu\text{m}$ )	1000	100	> 50,000	10,000	Single cell
Temporal Resolution (Hz)	0.5	2	> 256	> 1000	spiking
Invasive or noninvasive	Non-invasive	Non-invasive	Non-invasive	Invasive	Invasive
Electrophysiology or Hemodynamics					

**Figure 1.1** Different recording modalities and their associated resolutions, invasiveness, and method for recording brain activity.

Another factor, briefly discussed above, in consideration of BMI recording techniques is invasive versus noninvasive strategies and the required spatial and temporal resolutions desired (Figure 1.1). Invasive strategies for recording neural activity such as microelectrode arrays (MEAs) and electrocorticography (ECoG) are yet unmatched for spatiotemporal resolution. MEAs are implanted directly in superficial cortical areas and allow for direct recording of single neuronal action potentials as well as local field potentials (LFPs) from the summed electrical currents of surrounding neurons. ECoG uses similar recording strategies as EEG; however, due to the invasive nature of ECoG resolution is increased due to the fact that electrodes are placed underneath the cranium,

yielding greater spatial resolution when compared to EEG. Substantial improvements in the spatial resolution of ECoG can be achieved with the use of closely spaced subdural grids and strips of electrodes yielding  $< 5 \text{ mm}^2$  resolution (Buzsáki et al., 2012). Given the above regarding the techniques that utilize electrophysiology more recent implementations of MEAs and ECoG have been shown to reliably be useful for the implementation of different BMIs ranging from decoding motor imagery with MEAs in tetraplegic human subjects and decoding speech in humans with high density ECoG signals (Aflalo et al., 2015; Chartier et al., 2018; Hochberg et al., 2006).

In contrast to the invasive techniques discussed above, EEG, being the oldest of the recording modalities, is the most widely used recording modality; however, it is limited by the distorting and attenuating effects of the tissues and bone that electrical potentials must travel through. Consequentially, single neuronal firing is highly unlikely to be found using this modality, rather the recorded signal from a single electrode more closely relates to a lower resolution (smoothed) version of the LFP in an area about  $10 \text{ cm}^2$  (Buzsáki et al., 2012). Modalities for recording neural activity that utilize hemodynamics as a proxy for neural activity have the advantage of being more non-invasive and sacrificing spatio-temporal resolution (BOLD response and temporal limitations) (Baumann et al., 2010). However, one advantage of fMRI and more recent methods like function ultrasound (fUS) is the greater field of view, allowing for in some cases whole brain imaging that can be of advantage when desiring cortico-cortical interactions (Wander et al., 2016). Given the technical limitations of different recording modalities it is clear that more invasive strategies afford greater resolution. Until technological

advancements improve this tradeoff it is something that researchers must weigh heavily when determining the desired BMI implementation.

### 1.1.1 Reference Frames

As you are reading this, imagine you momentarily look away and reach for your bottled water. After taking a sip, you place the bottle back and continue reading. After some time, you reach again for your bottled water while you continue reading. This time you do not shift your gaze to the bottle. Our ability to complete such a task may not seem a significant one. While both reaches were to the same location in space, the image of the bottle on your retina was different, the latter being in your periphery. While the reach itself can be thought of a vector that starts at the location of your hand and ends at the bottle, the brain must still transform the retinotopic (sensory) coordinates of the bottle to the explicit muscle (motor) based coordinates that will yield the appropriate reach. In this section, we aim to answer the question: How are these robust transformations between multiple coordinates executed at the neural level?

Our brain performs a remarkable number of subconscious coordinate transformations to enable smooth interactions with our environment (Andersen and Cui, 2009; Chivukula et al., 2019). In reaching for the bottle in the above example, the brain determines the appropriate axes to represent in space the configuration of the arm (effector) and the position of the cup (object) to bring one to the other. How does the brain reconstruct the external world and relate it to the body? At a minimum the brain is integrating three

different signals: proprioceptive information, visual information, and motor feedback. Understanding the coordinate transformations that the brain intrinsically computes in the process of motor control is essential in eventually utilizing cortical neural signals for BMI applications. This is vital as algorithms used in BMIs must know what behavioral effectors modulate neural activity in order to yield the best control.

Single neuron data from both humans and NHPs suggest that spatial locations are represented in multiple reference frames and can vary within and across sensory modalities (Avillac et al., 2005; McGuire and Sabes, 2009, 2011). For instance, visual stimuli can be encoded with respect to the eye or the head, and tactile stimuli may likewise be encoded with respect to the eyes or body parts (e.g., hands) (Buneo et al., 2002; Pesaran et al., 2006b, 2010). There appear to be anatomically defined, regional preferences for the coordinate frames utilized. Both visual and auditory stimuli are encoded in a common gaze-centered reference frame by neurons in most regions of the PRR, but in hand-centered coordinates by area 5d (Andersen and Cui, 2009; Crawford et al., 2011; Bremner and Andersen, 2012). However, a recent growing body of evidence is suggestive of gradients of representations including mixed or intermediate reference frames being used throughout the motor system (Batista et al., 2007; Chang and Snyder, 2010; Colby and Duhamel, 1996; McGuire and Sabes, 2011; Pesaran et al., 2006). An explanation as to why a distribution of reference frames may exist is postulated to be due to a reduction in planning variability (McGuire and Sabes, 2009). Moreover, reference frames can dynamically evolve even in the same population of neurons with changing

behavioral demands, ensuring that the most relevant postural and spatial information is encoded at each behavioral stage (Bremner and Andersen, 2014; Chang and Snyder, 2010; Chang et al., 2009).

The process of converting sensory stimuli into motor commands (sensory-motor transformation) has historically been postulated to occur through the remapping of disparate modalities into a common reference frame (Avillac et al., 2005). Neurons in distinct brain areas were predicted to have receptive fields (RFs) with positions invariant of reference frame (Duhamel et al., 1997). However, multiple multisensory areas (such as the superior colliculus) demonstrate partially shifting RFs (Pouget and Snyder, 2000; Trotter and Celebrini, 1999). For instance, when an eye movement is executed, the neural representation of spatial location for eye centered RFs must update. Although these representations change with eye movement, they do so by less than the change in eye position, which suggests, and indeed requires, a shift in the RF itself. These findings also extend to auditory RFs for the same neural units (Pouget et al., 2002). Moreover, the amplitude of the neural response may be modulated by eye position, creating a phenomenon referred to as a “gain field” (Andersen et al., 1985; Pouget and Snyder, 2000).

The multiple modalities and nuances of reference frames across brain areas and even at the individual neuron level suggests that we do not yet fully understand how these

reference frames are maintained, transformed, and integrated. Several hypotheses have been put forward to unify reference frame neural encoding (Chivukula et al., 2019). In one such hypothesis, a mixture of reference frames appears to be heterogeneously distributed around the brain. This may explain partial shifts in RFs, and gain fields (Pouget et al., 2002). Another, more recent concept, mixed selectivity, is increasingly recognized as fundamental to the coding and implementation of brain functions (Rigotti et al., 2013). Mixed selectivity dictates that neurons behave differently in different contexts, belonging to different ensembles that encode explicit but highly context-dependent information (Fusi et al., 2016). The common neural substrate may provide a basis for the transfer of learning: motor skills acquired through one ensemble may be recruited by others (Zhang et al., 2017). This provides an alternative viewpoint for gain fields and multiple reference frames; a single neuronal population may encode many types of information in a context dependent manner. A direct consequence of this is that overlapping activity at the population level may afford the brain significant computational savings through shared resources, such as different views of the object, different starting configurations of the effector, even information from different brain areas (Fusi et al., 2016; Zhang et al., 2017). Within the framework of mixed selectivity, neurons can greatly enhance the diversity and dimensionality of neural representations that can be encoded by a subset of neurons (Rigotti et al., 2013). This has important implications for cortical neuroprosthetics, foremost amongst them that large volumes of data may be extracted from cortical signals derived from strategic neuronal applications. For example, PPC encodes rich, high-level cognitive processing and may thus serve as one such highly-informative cortical brain region for BMI and neuroprosthetics (Aflalo et



al., 2015; Cohen and Andersen, 2004; Zipser and Andersen, 1988). In Chapters 2 and 4 we investigate reference frame representations and the common modes of tuning found across areas during a delayed cognitive reaching task.

### 1.1.2 Internal Models

Our lives are filled with situations upon which we must act faster than our senses allow us. The sensation of catching a falling cup, a major league pitcher throwing a curveball for a strike, or serving a tennis ball with spin, our lives are filled with these scenarios in which we must evaluate and integrate information from our bodies and environment to compensate for physically inescapable sensory delays. A growing body of literature has begun to amount evidence in support of the theory that the brain utilizes internal models during controlled movements, such as those mentioned above.

Internal models utilize outgoing motor signals and sensory feedback to internally simulate the dynamics of behavior during motor control (Shadmehr and Krakauer, 2008; Wolpert and Ghahramani, 2000; Wolpert et al., 1995a, 1995b). Two categories of internal models exist: forward and inverse. Forward models, predict future states of the motor system given the current motor command without the associated sensory input (Jordan and Rumelhart, 1992; Wolpert and Ghahramani, 2000; Wolpert et al., 1995a). Thus, the primary function of a forward model is to predict the relationship between our motor actions and their sensory outcomes. Conversely, an inverse model does the opposite. Inverse models predict the relationship between a current and desired sensory outcome

and the motor actions that will elicit the desired state (for more on inverse models see (Gomi and Kawato, 1996; Katayama and Kawato, 1993)). Given the above, computational models suggest that to do this one must maintain an internal state estimate via efferent motor commands and afferent sensory input. This internal state estimate is stored and integrated further as more motor and sensory information is collected. Integrating this information over time produces a much more stable internal estimate that effectively reduces the noise from motor signals and delayed sensory information.

To do this the brain must maintain an internal state estimate of the body and the PPC has substantially gained evermore evidence that this is where it is stored. The PPC is thought to be the location where this estimate is stored due to the location of this region. PPC associates multiple sensory modalities and subsequently transforms the association into a representation for guiding motor actions (Andersen and Buneo, 2002; Andersen et al., 1997; Colby, 1998). Furthermore, the PPC sits at an intersection of the dorsal visual pathway of the brain where it receives efferent and afferent motor and sensory signals making it a strong candidate for integrating the internal state estimate with information regarding these incoming signals (Desmurget and Grafton, 2000a; Goodale, 1998; Inoue et al., 1998).

### 1.1.3 State estimation in PPC

Strong evidence in support of this theory was published in the seminal work published by Rushworth and colleagues followed by Wolpert and colleagues in NHPs and a case report in subject PJ. Rushworth and colleagues demonstrated a dissociation between the two

areas of the PPC, SPL, and IPL, wherein they found that reaches made in the dark (using proprioception) were dysfunctional when lesions to the SPL were present, but not IPL. In contrast, reaches made in the light (using vision) were dysfunctional when lesions in the IPL were present, and not the SPL (Rushworth et al., 1997). Furthermore, Wolpert and colleagues followed this with their reporting of patient PJ's inability to maintain an internal representation (Wolpert et al., 1998). Patient PJ suffered from an extra-axial cyst encroaching upon the cortex of the left superior parietal lobe. She presented with a progressively worsening symptoms in her right arm. The symptoms initially began with jerking of her right arm and two years later was marked by an increasingly uncertain sense of arm position if her vision of the arm was occluded or out of view. If vision of the arm was not present she reported that over time under a static load the arm disappeared. Lastly, these findings shared share distinct parallels with the studies done by Rushworth

and colleagues in so far that she could maintain constant and stable representations of the hand if she was given visual feedback.

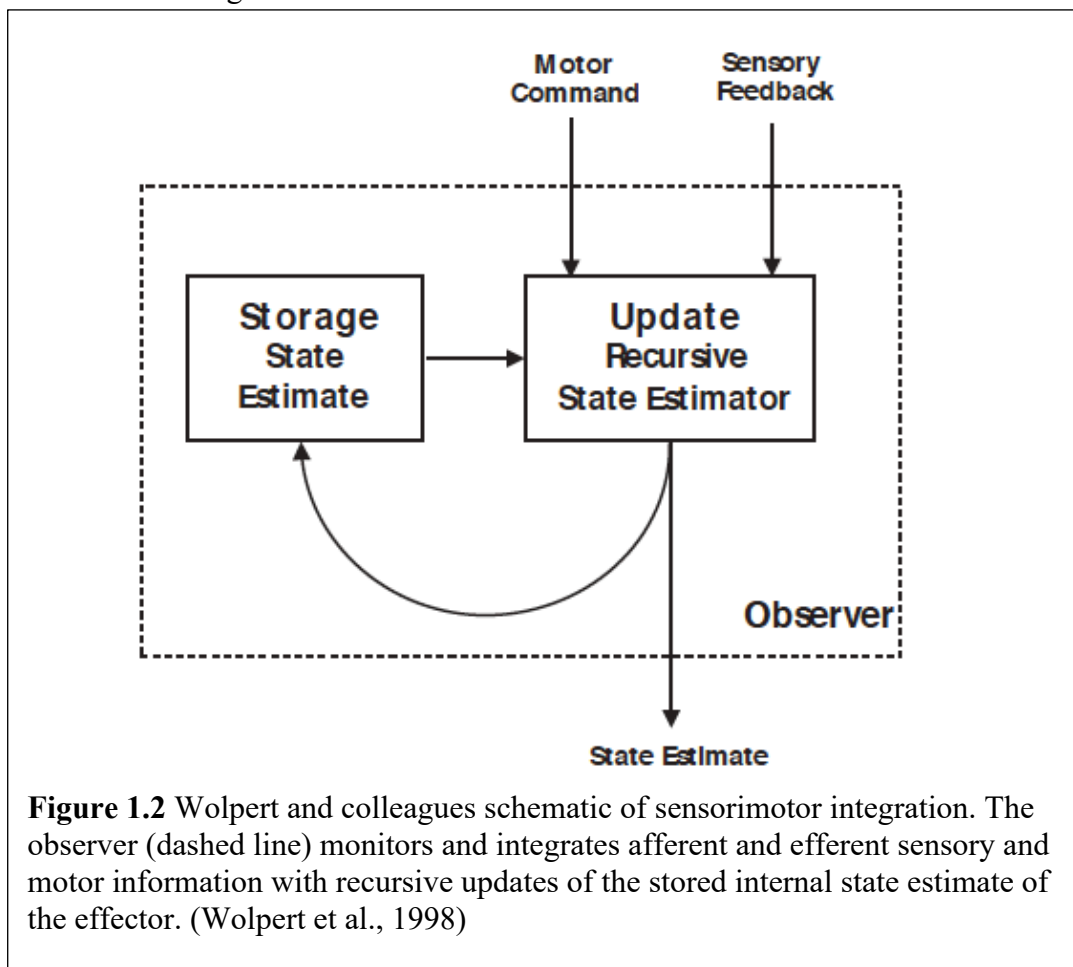


**Figure 1.2** Wolpert and colleagues schematic of sensorimotor integration. The observer (dashed line) monitors and integrates afferent and efferent sensory and motor information with recursive updates of the stored internal state estimate of the effector. (Wolpert et al., 1998)

PPC is known to be involved in not just the specification of a movement plan but also the control of ongoing movements. Perhaps some of the better evidence in support of this can be found in the studies done by Grea et al. (2002) where they observed an inability for a patient with bilateral parietal lesions to reach toward a target if it jumped to a new location during the movement to the initial target location. The patient continued to the initial location as if the target had not been displaced (Gréa et al., 2002). Similarly, TMS studies in subjects with normal parietal function show similar deficits in reaching when given a pulse of stimulation as the reach begins to the initial target (Desmurget et al.,

1999). These studies suggest that either integration of novel sensory information, as it regards to the target jumping during the reach, is affected by a lesion or TMS stimulation. These findings fit in well with Wolpert and colleagues' findings that suggest PPC serves as an observer shaping the internal state estimate of the arm as it is recursively updated. An inability to maintain this estimate would lead to deficits in monitoring the state of the effector and correcting ongoing movements, as was found in the studies mentioned here.

State prediction can also be used in imagined movements. Imagined movements which are found to share the same time course as attempted movements despite the lack of sensory feedback is suggestive of the brain maintaining a state estimate. Interestingly, Sirigu and colleagues found that patients with PPC lesions had significantly different imagined time courses for the same attempted movements (imagined movements were usually faster) (Sirigu et al., 1996). In contrast patients with motor cortex lesions were found not to have differences in these same attempted and imagined movement despite difficulty with the attempted movements. The production of imagined and attempted movements differ in that imagined movements rely solely on the prediction and must change the weight of incoming sensory feedback to zero (Shadmehr and Krakauer, 2008). Deficits in adjusting the weight of sensory feedback would result in deficient estimates of imagined movements. These findings when put together can be explained by the same observer model described by Wolpert and colleagues (Fig 1.2). The most recent physiological evidence in NHPs of state estimates being stored and updated in PPC show that neural data on average occurs at zero lag with respect to behavior indicated a

possible link with the internal model (Mulliken et al., 2008). In Chapter 3 we investigate and provide to the best of our knowledge the first single unit human evidence that internal state estimates are maintained and stored in PPC of a tetraplegic subject during a cognitive reaching task.

## 2. Neural Correlates of Cognitive Motor Signals in Primary Sensory Cortex

### 2.1 Introduction

Somatosensory cortex (S1) is largely studied and understood in its role as the primary sensory region for processing somatic sensory signals from the body. However, recent work highlights a more direct role in motor production: S1 neurons can respond to passive movements alone, active movements alone, or both (London and Miller, 2013; Nelson, 1987) and neurons become activated prior to movement initiation. S1 neurons project to the spinal cord (Rathelot and Strick, 2006; Rathelot et al., 2017), and electrical or optical stimulation of S1 elicits motor movements (Matyas et al., 2010; Penfield and Boldrey, 1937; Welker et al., 1957). Taken together, these results indicate a direct role of S1 in the production motor behavior. However, in many of these studies it is hard to disentangle the degree to which neural signals may reflect motor variables per se or aspects of sensory processing.

### 2.2 Methods

#### 2.2.1 Subject Information

A 32-year-old male tetraplegic subject was recruited who suffered a complete C5/C6 spinal cord injury and consented 1.5 years' post-injury to participate in a clinical trial of a BMI system consisting of intracortical stimulation and recording. Subject FG has residual sensation in the anterior lateral portions of the upper limbs and residual sensation with no

discriminatory ability in the posterior radial section of the upper arm and forearm that is also accompanied with paresthesia. All sensations and motor ability are consistent with the level of the sustained injury. The subject remains intact of all other motor control and sensations above the injury other than those noted above. The study and all procedures were approved by the California Institute of Technology (Caltech), Institutional Review Boards (IRB) of the University of Southern California (USC), and Rancho Los Amigos National Rehabilitation Hospital (RLA). Surgical implantation took place at Keck Hospital of USC. All future study sessions with this subject discussed here were run at RLA.

### 2.2.2 Surgical Planning and Implantation

Surgical planning for subject FG followed the protocols described in (Aflalo et al., 2015; Salas et al., 2018). Based off these experiments analysis of the fMRI data was done in order to determine and identify the areas to implant. Subject FG was implanted in PMv, SMG, and S1. All areas except S1 were implanted with 96-channel Neuroport microelectrode arrays (Blackrock Microsystems, Salt Lake City, UT). S1 was implanted with two 7x7 microelectrode arrays (48 channels per array).

### 2.2.3 Reference Frame Task

Experimental sessions with subject FG were performed at Rancho Los Amigos National Rehabilitation Center (RLA). The subject performed the task in a dim room with his



motorized wheelchair seated so that the task screen covered approximately 45 degrees of visual angle. The subject was asked to minimize any and all head movements throughout the task and was placed in front of the screen with a researcher monitoring his head movements. Subject FG was seated in his motorized wheel chair throughout the duration of the task. At the beginning of each trial the subject was cued to fixate their gaze and imagine their right hand (dominant and contralateral to recording arrays) at one of four locations marked by a circle and hand image, respectively. After 3 seconds a circle was shown above the cued eye and hand positions for 1.25 seconds wherein the subject continued to hold their gaze and imagined hand fixations. A change in the color of the fixation marker was the cue for the subject to begin his imagined reach to the target above. The subject was asked to make an imagined reach and maintain the imagined ending position (target location) until the execution epoch was over (2 seconds). The execution epoch was then followed by an inter-trial interval (ITI) of 2 seconds.

Each run consisted a total of 64 trials for each unique combination of the four eye, hand, and target positions. This task was run 3 times (192 total trials, 3 repetitions) consecutively with a 2-5 minute break between each run. All imagined reaches were asked to be made within the frontal plane of the subject. Each session recording was separated out by at least a week.

#### 2.2.4 Neural Recordings

Initial placement of all arrays was predetermined based on pre-operative fMRI imaging, placement may have differed if the initial location was occluded by vasculature seen during the operation (Aflalo et al., 2015). Neural activity from each array was amplified, digitized, and recorded at 30 KHz using the Neuroport neural signal processor (NSP). The Neuroport system, composed of the arrays and NSP, has received FDA clearance for less than 30 days of acute recordings. However, for the purposes of this study we received FDA IDE clearance for extending the duration of the implant (IDE number: G130100).

Thresholds at -4.5 times the root-mean-square were set after high pass filtering the full bandwidth signal sampled, using the Blackrock Central software suite (Blackrock Microsystems). Waveforms collected consisted of 48 samples, 10 prior to threshold crossing and 38 samples after. These recordings were then sorted (both single and multi-unit) using k-medoids clustering using the gap criteria to estimate the total number of clusters (Tibshirani et al., 2001; Zhang et al., 2017). Offline sorting was then reviewed and adjusted as needed following standard practice (Harris et al., 2016). On average across 4 days of recordings in S1 we analyzed 163 sorted units per session. All sorting was done prior to analysis and blind to channel or unit responses found during the task. Further spike sorting methods can be found in Zhang et al., 2017.

### 2.2.5 Eye Tracking

Subject FG's eye position was monitored using a 120 Hz binocular eye tracking system (Pupil Labs, Berlin, Germany). If the subject's gaze shifted off the cued eye position the task was terminated and ran again ensuring that gaze position remained fixed to the cued eye position. Eye positions were synced to the task and allowed online determination of eye position.

### 2.2.6 Linear Analysis for Tuning

We defined a unit as selectively tuned if the unit displayed a significant tuning based on a linear regression analysis. We created a matrix that consisted of indicator variables for each unique condition separated by either a single behavioral variable or pair, similar to (Zhang et al., 2017). There were 64 unique conditions (4 eye, hand, and target positions) indicator variables. Firing rate was estimated as a linear combination of these indicator variables:  $FR$  is firing rate,  $X_c$  is the vector indicator variable for condition  $c$ ,  $\beta_c$  is the estimated scalar weighting coefficient for condition  $c$ , and  $\beta_0$  is the intercept.

$$FR = \sum_c \beta_c X_c + \beta_0$$

Windows were 750 ms in duration and window start times were stepped every 500 ms. This was done for all units in each sliding window. The significance of each fit was determined using the p-value of the F-test of overall significance for the linear analysis (p

< 0.05, FDR-corrected). Units that were found to be significant in this analysis were then determined to be tuned and further analyzed in the reference frame analysis.

### 2.2.7 Reference Frame Analysis: Gradient Analysis

For every individual unit three trials per condition were analyzed. Trials were subsequently aligned to the cue execution epoch (0 s). The delay epoch is defined as -1 s to -0.25 s. Gradient analysis was used to determine the degree of modulation each behavioral variable had on the firing rate of the unit when comparing across each unique combination of variable pairs (Hand-Gaze (HG), Target-Gaze (TG), and Target-Hand (TH)) (Bremner and Andersen, 2012; Buneo et al., 2002; Peña and Konishi, 2001; Pesaran et al., 2006). For each tuned unit we created a four by four matrix (response matrix) representing each unique behavioral variable position and its associated mean firing rate. We averaged across trials and the third variable. Gradients were determined using the gradient function in Matlab 2019a (Mathworks). For each gradient a resultant angle and length are generated indicating the modulation by each variable and its strength (Fig. 2.3). However, as we can see in Fig 2.3A often times the gradients show a symmetrical pattern that would result in cancellation of symmetrical angles. To avoid this, we double each angle in the matrix and represent each angle from  $0^\circ$  to  $\pm 180^\circ$ . Therefore, the summed resultant angle is represented by  $0^\circ$  for left-right patterns of gradients,  $\pm 180^\circ$  for up-down patterns of gradients, and  $-90^\circ$  for gradients pointed at the diagonal as seen in Fig 2.3A. The summed resultant angle and length, however, cannot be mapped directly onto the response matrix, and thus we have notated the appropriate

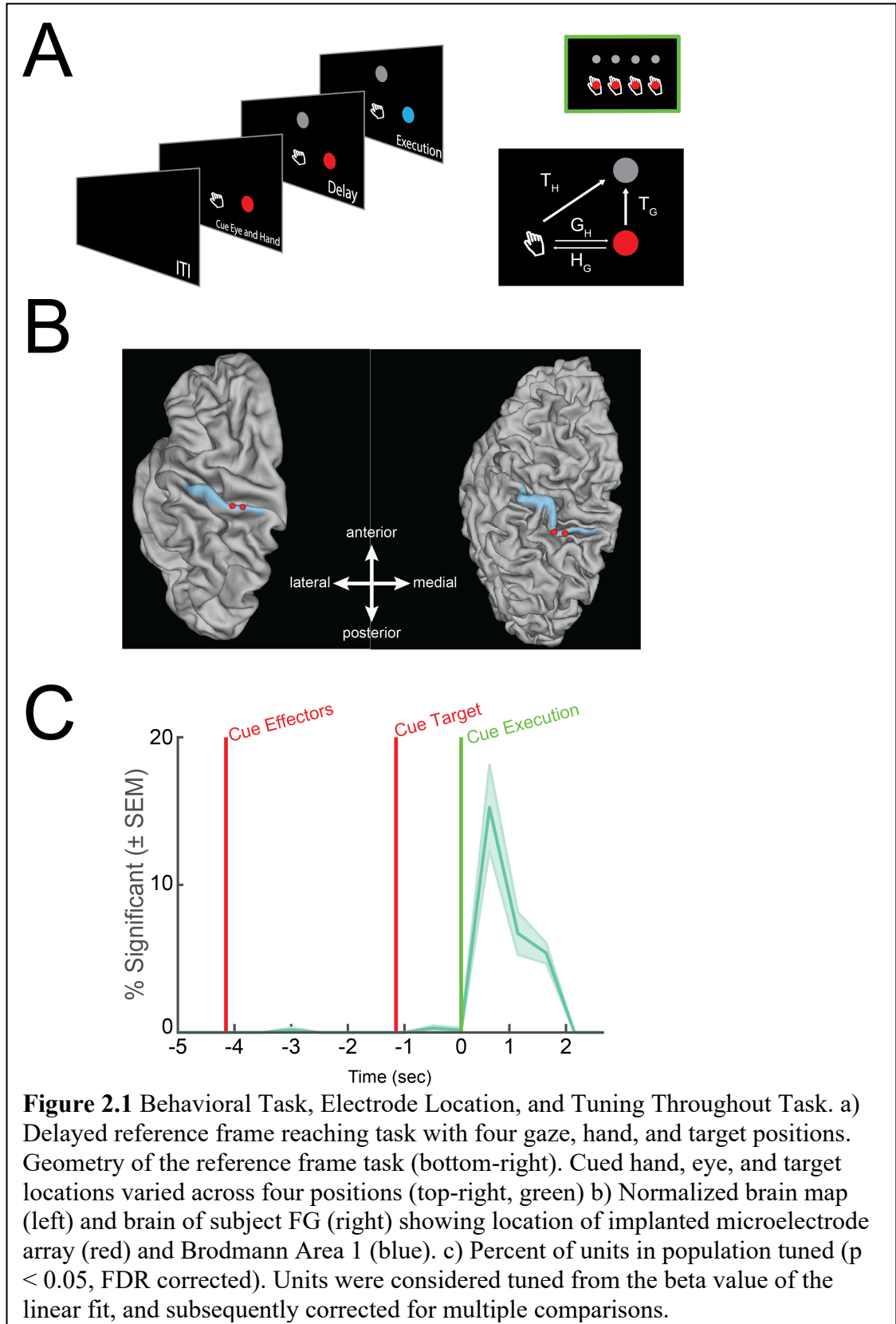
variable and combinations of variables to help with interpretation. For example, in figure 2.3A hand only (H) modulation would be found at  $\pm 180^\circ$ , gaze only (G) modulation is seen at  $0^\circ$ , H+G at  $90^\circ$ , and H-G at  $-90^\circ$ . Therefore, we can use the angle of the resultant angle as a proxy for overall orientation bias for a variable or variable pair.

### 2.2.8 Dimensionality Reduction

We used population level dimensionality reduction analyses to determine the most common modes of reference frame encoding over time in a brain area. The firing rates for all units, trial averages, and time points were arranged in a matrix (unique trials by unit) and reduced down using principal component analysis (Fig. 2.4). For the first 20 components we then ran a gradient analysis for each time window. Time windows were 100 ms in duration and response field angles and lengths were acquired from the start of the cue hand-eye epoch to the end of the cue execution epoch. Analyses done with larger steps showed similar results. Next, we converted all resultant angles and lengths into complex numbers to account for both variables (resultant angle and length) and utilized complex principal component analysis to identify the most common mode of tuning. Previous work on geophysical data sets have successfully used similar methods for identifying dynamics (Horel, 1984). A matrix of each complex value for each time point and each component was then created and reduced to find the components that explained the greatest variance. Furthermore, we used parallel analysis to determine which components from this dimensionality reduction were significant (Fig 2.6) (Franklin et al., 1995).

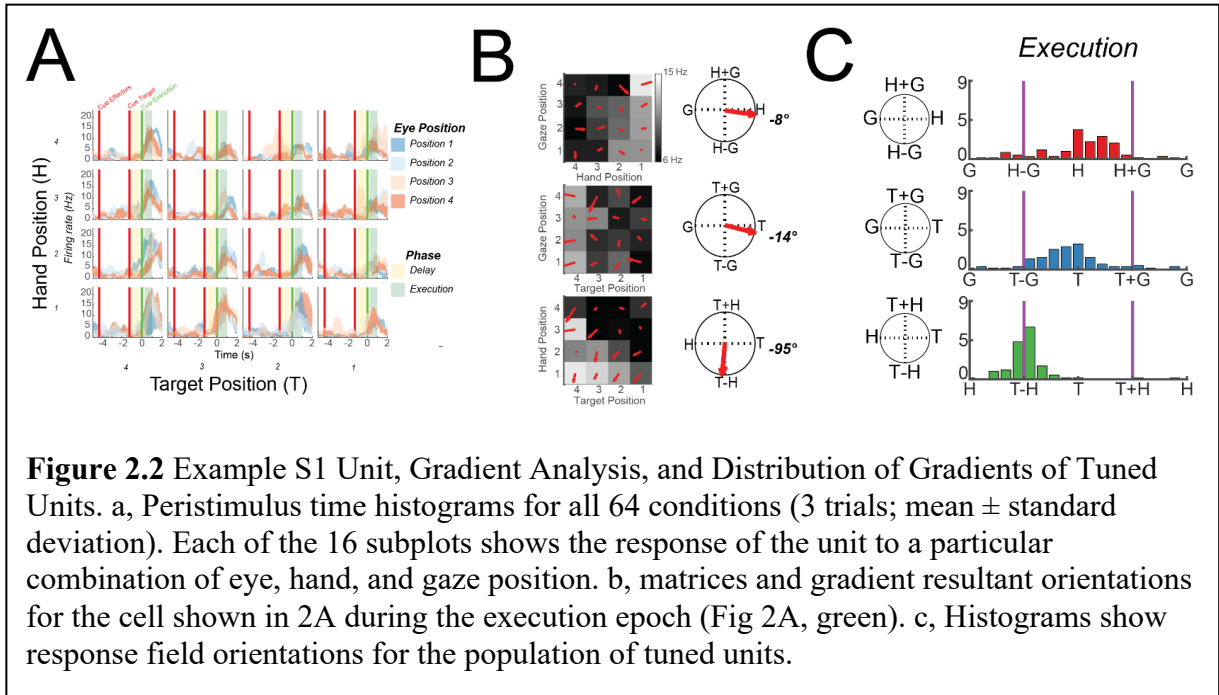
## 2.3 Results

To understand if S1 processes reach intentions in the complete absence of sensation or expected sensations we recorded single unit activity from multi-channel arrays implanted in the sensory cortex (Fig 2.1B) of a 34-year-old tetraplegic male (FG) during a delayed imagine reaching paradigm. The arrays were implanted in S1 as part of an ongoing clinical trial in which we recently showed that microstimulation delivered through these same multi-channel arrays evokes localized and naturalistic cutaneous and proprioceptive sensations (Salas et al., 2018). Our paradigm (Fig 2.1A), adapted from previous non-human primate studies (Bremner and Andersen, 2012; Pesaran et al., 2006), systematically manipulated fixation, imagined initial hand, and reach target locations at distinct points in the trial. Importantly, the subject is capable of moving his eyes and thus direct his gaze to the fixation targets. However, the paralyzed subject did not move his arm, but instead used motor imagery to imagine moving his hand to the initial hand cue location and subsequently move to the final target location. This design allowed us to one, understand how activity in S1 relates to storing information about arm location, movement plans, and movement execution; and two, characterize the reference frame of these signals, e.g., whether movement variables are coded relative to the initial imagined position of the hand, relative to the eyes, or relative to the body or world.

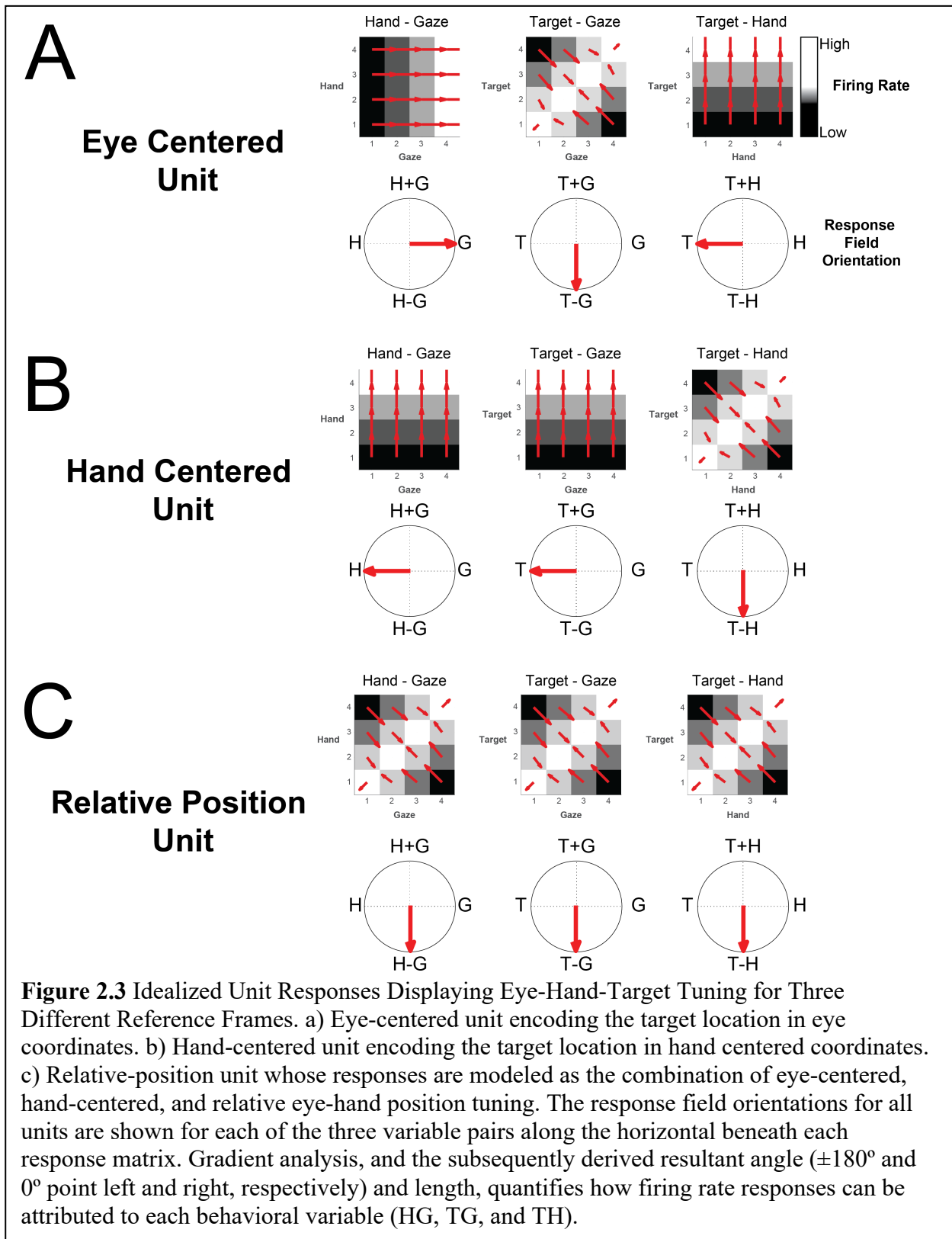


We performed a sliding window analysis to understand whether and when neurons in sensory cortex become active for our cognitive motor task: for each unit, we used a linear model with interactions to explain firing rate as a function of fixation, initial imagined hand, and target locations (Fig 2.2A,  $p < 0.05$  FDR corrected for number of units per time slice, window size: 750 ms, step size: 500 ms). We find negligible selectivity following cueing of the hand and eye positions indicating no neural coding for true eye position or the imagined position of the arm. We also find negligible selectivity following target presentation indicating no encoding of the spatial location of the target or planning activity related to the upcoming motor action. Finally, we found that a significant proportion of the population was selective following the instruction to initiate the imagined reach. Thus, sensory cortex is engaged during a cognitive motor task despite the absence of overt movement and sensory feedback, but only during imagined movement of the limb.



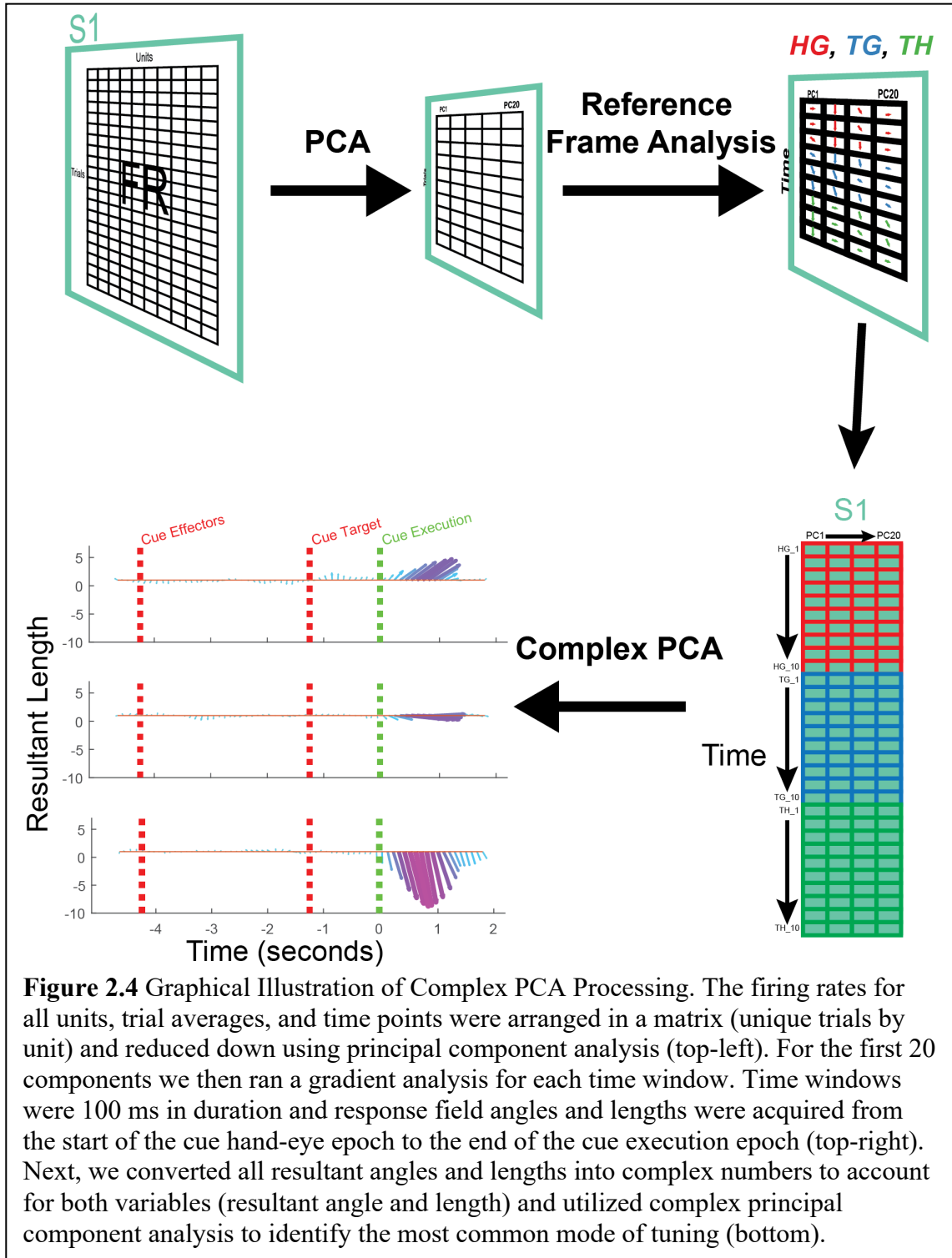


We found that nearly all the neurons selective during the movement execution phase coded movement as the reach vector: the direction of imagined movement of the hand. In other words, selective units coded the location of the target relative to the initial imagined hand position (or, by symmetry, hand position relative to the target). This result was found using a gradient analysis pioneered in NHPs (Buneo et al., 2002): neural responses for each unit were organized into response matrices where the firing rate is coded for each hand, eye, and target position. A gradient field is then computed which describes how the firing rate is sensitive to changes in the behavior variables. Finally, the resultant, or vector sum, of the gradient field summarizes the net effect of behavioral manipulations which can be used to determine whether neural activity encodes target position relative to gaze position (T-G), the target position relative to the hand (T-H), the hand position relative to gaze direction (H-G), or some combination of these vectors (see Fig 2.3). A representative response matrix for a neuron coding the position of the target relative to



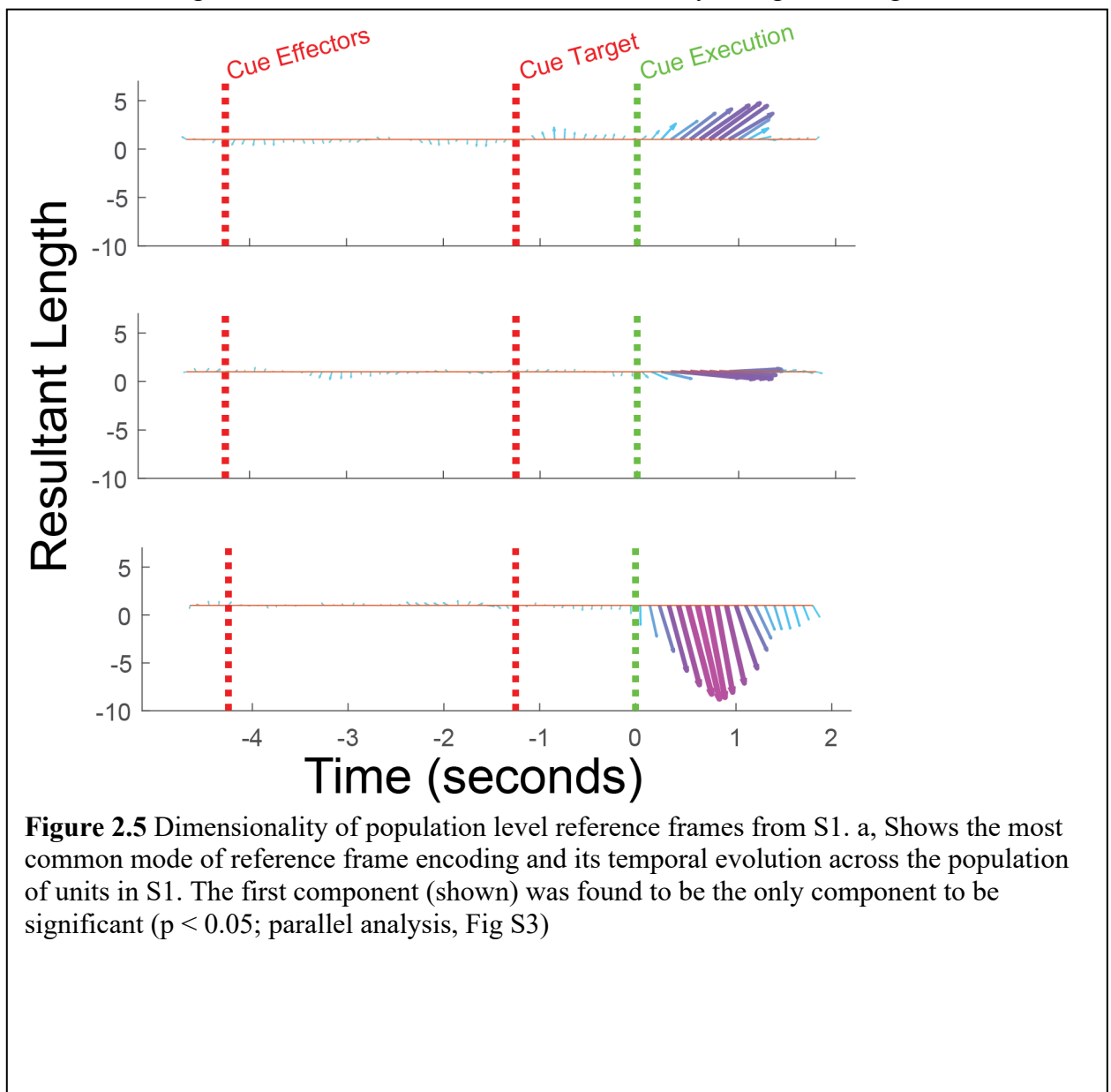
the hand and the population distribution of response gradients is shown in Figure 2.2B

and C. Interestingly, despite no neural coding for imagined hand position prior to movement execution, our result indicates that the neural coding during the imagined

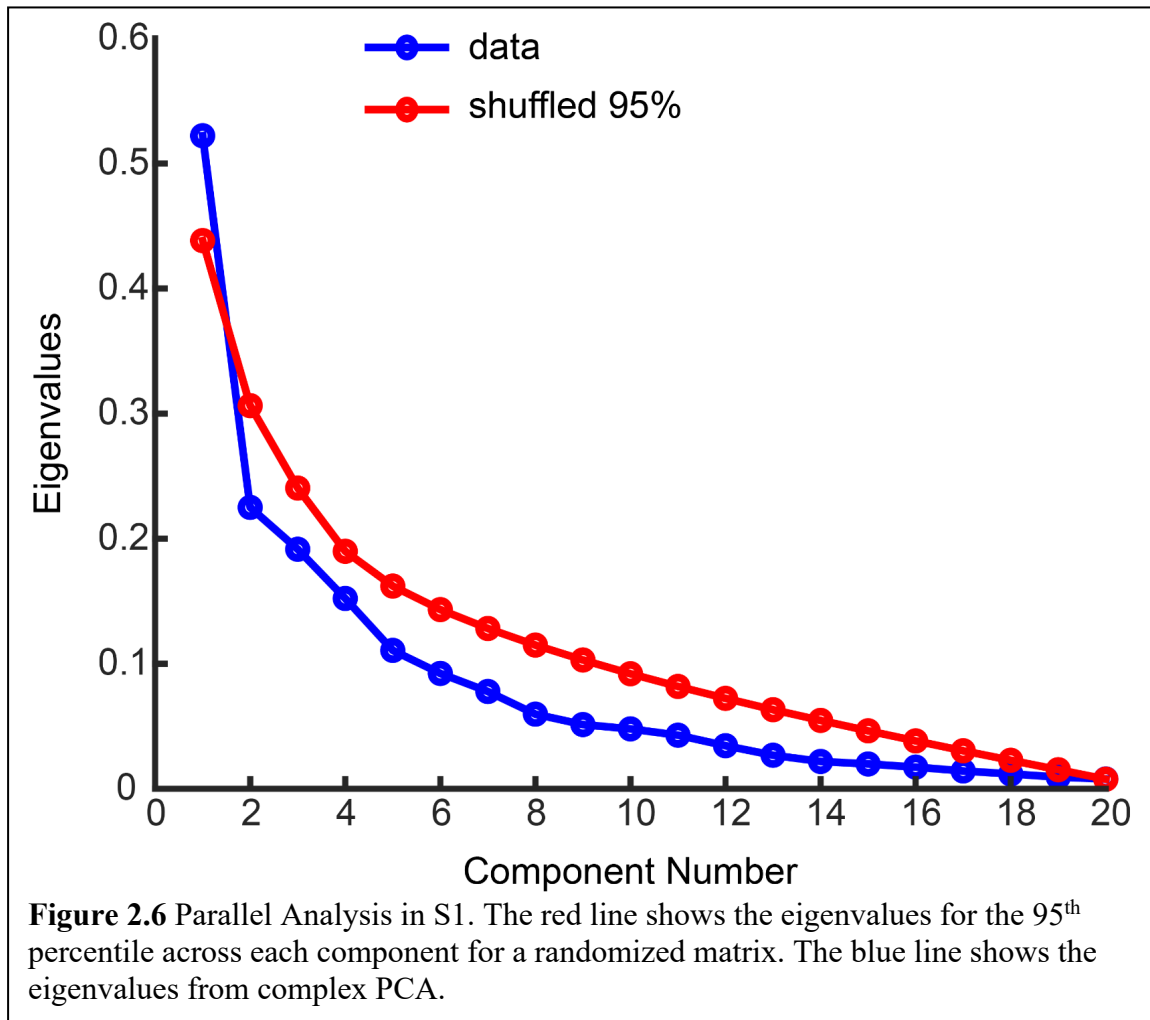


reach incorporates the internal estimate of hand position when computing the reach response.

Single unit analysis shows that the population is dominated by units coding the reach vector. To verify that this interpretation is an adequate summary of S1 encoding, we used complex principal component analysis (cPCA) to characterize the full temporal dynamics of the reference frame of the population as a whole (Fig 2.4). The gradient analysis described above summarizes the sensitivity of a neuron to behavioral variables using the resultant of the gradient, a 2D vector that can be described by a length and angle. cPCA



was used as it is capable of handling our situation where data samples for each observation are described by both a length and angle (Horel, 1984). We find that coding of the reach vector strengthens and peaks around 750 ms after the cue to execute the



imagined reach (Figure 2.5). Further, only the first cPCA component was significant (parallel analysis (Franklin et al., 1995),  $\alpha < 0.05$ , Figure 2.6). This suggests that reach coding in S1 is dominated by a single homogeneous representation of the reach vector exclusively during execution of the imagined reach.

## 2.4 Discussion

We have shown the first single unit evidence that cognitive imagery of movements is represented in the primary somatosensory area of human cortex demonstrating S1 neurons track motor intentions in the complete absence of sensation. Activity is restricted to the time of imagined execution with negligible activity while the subject must actively maintain the position of the limb in memory, maintain fixation at distinct spatial locations, and maintain movement plans. These results suggest that the role of S1 in motor production is restricted to the time of movement execution. Lastly, we show S1 activity codes the reach vector, coding motor intention relative to the imagined position of the hand. These findings are important, as we show deafferented regions of S1 encode functional information that can be leveraged for future neuroprosthetic applications. Furthermore, a possible concern is that these results are unique to individuals who have lost their main peripheral input. However, recent findings from our lab and others have shown these representations are largely stable and reorganization does not result in the production of novel functional sensory representations (Flesher et al., 2016; Makin and Bensmaia, 2017; Salas et al., 2018). These results implicate a role of primary somatosensory cortex in cognitive imagery, and of S1 in motor production in the absence of sensation, and suggest that S1 may provide a source of control signals for future implementations of neural prosthetic systems.

## 3. Neural Correlates of the Internal State Estimate in Human Posterior Parietal Cortex

### 3.1 Introduction

The sensory information that informs movement, comes from a mixture of modalities, and is noisy, frequently incomplete, and delayed (Desmurget and Grafton 2000, Faisal, Selen et al. 2008, More and Donelan 2018). Increasing evidence suggests that the brain overcomes these limitations by utilizing an internal model or mental representation of the body and state of the world (McNamee and Wolpert 2018; Desmurget and Grafton, 2000; Miall and Wolpert, 1996). For example, the brain can use motor command signals to predict how the arm will move and therefore predict upcoming sensory states (Jordan and Rumelhart, 1992; Wolpert et al., 1995a). During movement, these predictions can compensate for sensory processing delays (Scott 2016) which can have a destabilizing effect when sensory feedback is used to guide movement, and can ensure that motor output commands compensate for changing forces that occur during movement (Johansson, Riso et al. 1992, Flanagan and Wing 1993). Such models may also be used before movement to prospectively simulate potential actions and thus understand their possible outcomes prior to committing to a specific action (Cisek and Kalaska 2004). This internal model of the state of the body is frequently called the state estimate and is related to concepts like the body schema.



The posterior parietal cortex (PPC) has been hypothesized to encode such a state estimate. The posterior parietal cortex is well-situated for this role as a functional interface between multi-modal sensory and motor representations (Jones and Powell 1970, Mountcastle, Lynch et al. 1975). Regions of PPC have long been known to play a critical role in representing the state of the body (Graziano, Cooke et al. 2000, Graziano and Botvinick 2002, Ehrsson, Spence et al. 2004). Neural activity recorded in non-human primates during reaching is consistent with coding the state-estimate (Mulliken, Musallam et al. 2008) and the region has long been associated with visuomotor planning (Andersen and Buneo 2002). Lesions to PPC can disrupt an individual's ability to maintain an internal estimate of the state of their bodies (Wolpert, Goodbody et al. 1998), while electrical stimulation can generate the perception of movement, although no such movement has occurred (Desmurget, Reilly et al. 2009). Transient inactivation of PPC using transcranial electrical stimulation during movement can impact error-correction in ways consistent with disruption of the state estimate (Desmurget, Epstein et al. 1999). However, there is little direct electrophysiological recording evidence for internal models in PPC as experiments are complicated; the variables of the state estimate are highly correlated with sensory input and motor output signals that are used to construct the internal estimate. In the most direct evidence to date Mulliken and Andersen found that neural data on average occurs at zero lag with respect to behavior indicated a possible link with the internal model (Mulliken et al., 2008). However, individual neurons covered the entire spectrum from delayed to anticipatory signals, leaving ambiguity as to whether units were encoding a state estimate as such, or simply mixtures of sensory and motor signals.

In an ideal world, we would want an experiment in which sensory and motor variables can be completely dissociated from the output of the internal model. The ability to measure changes in the internal estimate of limb state in the absence of sensory feedback would provide strong evidence for PPC encoding a state estimate. Here we adopt this approach in a tetraplegic human. Motor imagery has been proposed to be the manipulation of an internal state in the absence of overt movement. Here we ask whether an internal estimate of the position the limb is updated and maintained in a motor imagery task that controls for a variety of factors. The data comes from a single subject, participant NS.

## 3.2 Methods

### 3.2.1 Internal Model Task

The subject was positioned so that the screen occupied approximately 25 degrees of visual angle. The task performed by the subject was a center-out imagined reaching task with systematic manipulation of the initial imagined arm configuration and eye fixation point. Figure 3.1B illustrates the behavioral paradigm. At the start of each trial, the subject was asked to fixate her eyes on a small red circle and imagine her hand at the location of a small icon of a hand. All possible combinations of four fixation and hand icon cues were tested for a total of  $4 \times 4 = 16$  possible configurations. The subject was

given 1.75 seconds to fixate and use motor imagery to position her hand at the instructed cue locations. This 1.75 seconds time was determined based on the participant's feedback as it gave her ample time to reach the target prior to the next task epoch. A dynamic white noise mask was then displayed for 2 seconds to extinguish the hand cue from the participant's vision. Critically, during this masking epoch, there was no sensory information available to the subject about the location of the imagined hand position. The mask was then removed revealing the original cued hand position as well as the position of a spatial reach target. The reach target was displayed at one of four positions (up, down, left, or right) equidistant from the hand cue. The subject did not make any imagined movements during this target cue epoch. After a variable interval (1.25-1.75 seconds, randomly sampled from a uniform distribution) the fixation point changed color instructing the subject to initiate an imagined reach to the cued target location. This epoch lasted for 2 seconds and the subject was asked to maintain the final endpoint location until the end of the epoch. For each possible unique combination of the fixation and starting hand location, we presented all four target positions. Thus, in total, there were 64 possible cue configurations (4 eye x 4 hand x 4 target positions). We performed two runs, each lasting approximately 11 minutes, in which each cue configuration was once with the order randomly determined. Our primary interest was in the pattern of neural activity during the masked interval prior to target presentation. Thus, we had 8 repetitions for each of the 16 hand and fixation locations.

We chose the center-out configuration of reach targets for several reasons. As shown in the other chapters, we found that the same cortical population encoded the relative

position of the hand and target which is functionally equivalent to the direction of movement from the starting hand position to the target. Given previous studies showing that potential reach targets can be encoded in higher-order motor regions (Cisek and Kalaska 2010), we chose the center surround arrangement to ensure that initial hand position conveyed no information about potential reach direction and therefore implicit planning signals would not be correlated with initial hand position. In contrast, in the previous target arrangement, starting hand position was at least partially predictive of target direction due to the constraints of the monitor (e.g. for the far left starting hand position all movements were either upwards or to the right while for the far left hand position all movements were upward or towards the right.) Further, the inline arrangement is not optimal for a hand-target relative reference frame: the angular range of directions is relatively small, only targets above the starting hand positions were tested, the set of angles that are tested are hand position dependent (e.g. when the starting position is to the right, all movements are either upward or directed to the left), and direction is partially confounded with movement distance (e.g. when the hand is placed to the far right, the target to the far left is over three times the distance as the target directly above the hand.) Finally, the center-out arrangement also allowed us to compare coding for the relative position of the hand and eye with the relative coding for the hand and reach target (see below).

### 3.2.2 Spatial Match-to-Sample Task

The spatial match-to-sample task was designed to be similar to the internal model task with several key modifications. As in the internal model task, the trial began with the presentation of a fixation cue and hand icon cue, each at one of four spatial locations. The spatial locations of the fixation and hand icon cues were identical to the internal model task. As in the internal model task, the subject was instructed to fixate the fixation cue; however, in the spatial match-to-sample task, the subject was instructed to simply remember the spatial location of the icon without any accompanying motor imagery. As above, all possible combinations of four fixation and hand icon cues were tested for a total of 16 possible configurations (4 eye x 4 hand), and as before the task epoch lasted 1.75 seconds. The dynamic mask was then presented for 2 seconds. Following the dynamic mask the hand icon was presented for one second. For half the trials, the position of the icon was presented at the same spatial location as originally cued while for the other half of the trials, the position of the icon was moved from its original location to one of the other three possible locations (randomly selected from a uniform distribution). Finally, a response screen was presented and the subject verbally reported whether the position of the hand icon was the same before and after the dynamic masking stimulus. We collected eight repetitions of each unique hand and eye combination in a pseudorandom fashion (with each hand eye position tested once prior to repetition.)

### 3.2.3 Behavioral Variable Tuning ANOVA

We performed a sliding-window 4x4x4 ANOVA to quantify the percent of the neural population selective for hand, eye, and target position (4 unique positions per behavioral

variable) throughout the course of the trial. The sliding window of 500 ms was stepped every 250 ms seconds. We tested for main effects resulting in 3 p-values for each unit one for each behavioral variable (eye, hand, and target). The resulting p-value for each factor and time window was then used to visualize temporal tuning and dynamics. Testing for main effects provides limited insight into the nature of how the variables are encoded and thus we performed a reference frame analysis as described below.

### 3.2.4 Linear Analysis for Tuning

We defined a unit as selectively tuned if the unit displayed a significant tuning based on a linear regression analysis. We created a matrix that consisted of indicator variables for each unique condition separated by either a single behavioral variable or pair, similar to (Zhang et al., 2017). There were 64 unique conditions (4 eye, hand, and target positions) indicator variables. Firing rate was estimated as a linear combination of these indicator variables:  $FR$  is firing rate,  $X_c$  is the vector indicator variable for condition  $c$ ,  $\beta_c$  is the estimated scalar weighting coefficient for condition  $c$ , and  $\beta_0$  is the intercept.

$$FR = \sum_c \beta_c X_c + \beta_0$$

Windows were 750 ms in duration and window start times were stepped every 500 ms.

This was done for all units in each sliding window. Significance of each fit was determined using the p-value of the F-test of overall significance for the linear analysis (p

< 0.05, FDR-corrected). Units that were found to be significant in this analysis were then determined to be tuned and further analyzed in the reference frame analysis.

### 3.2.5 Gradient Analysis

Gradient analysis was used to determine the degree of modulation each behavioral variable had on the firing rate of a tuned unit from the linear analysis when comparing across each unique combination of variable pairs (Hand-Gaze (HG), Target-Gaze (TG), and Target-Hand (TH)) (Bremner and Andersen, 2012; Buneo et al., 2002; Peña and Konishi, 2001; Pesaran et al., 2006). For each tuned unit we created a four by four matrix (response matrix) representing each unique behavioral variable position and its associated mean firing rate. We averaged across trials for the third variable. Gradients were determined using the gradient function in Matlab 2018a (Mathworks). For each gradient, a resultant angle and length are generated indicating the modulation by each variable and its strength (Fig. 3.2A). However, as we can see in Fig 3.2A (right) often times the gradients show a symmetrical pattern that would result in cancellation of symmetrical angles. To avoid this, we double each angle in the matrix and represent each angle from  $0^\circ$  to  $\pm 180^\circ$ . Therefore, the summed resultant angle is represented by  $0^\circ$  for gradients oriented along the horizontal directions (Fig. 3.2A left panel),  $\pm 180^\circ$  for gradients oriented along the vertical direction (Fig. 3.2A middle panel), and  $-90^\circ$  for gradients oriented along the diagonal (Fig. 3.2A right panel). The summed resultant angle and length, however, cannot be mapped directly onto the response matrix; thus we have notated the appropriate variable and combinations of variables to help with interpretation.

Therefore, we can use the angle of the resultant angle as a proxy for overall orientation bias for a variable or variable pair.

### 3.2.6 AUC Analysis

We performed a receiver operating characteristic (ROC) analysis to quantify how well individual neurons encoded right from left eye positions and right from left target positions. We used average neural firing rate in the 750 ms window at the end of the masking phase for measuring neural responses to right and left eye positions relative to the hand and we used average neural firing rate in the 750 ms window at the end of the delay phase for measuring neural responses to right and left target positions relative to the hand. We used all trials where the eye or target was presented to the left and right of the hand position resulting in 16 trials per condition. For each unit we summarized the ROC by its area under the curve (AUC). Within our AUC analyses, values above 0.5 indicate that the cue presented to the right generated a larger response while a value below 0.5 indicated that the cue to the left generated a larger response. For each unit, the AUC value for the eye comparison and target comparison were compared with a Pearson correlation to determine if there was any systematic correlation between these values.

### 3.2.7 Population Decoder Analysis

Using the same time windows and binning procedures as the above AUC analysis, we implemented a leave-one out cross-validation procedure to distinguish right from left



cues across the population of units recorded across all sessions: we trained a partialized least squares regression model to predict left versus right eye or target location from the population of neural activity recorded across all sessions using N-1 trials, where N is the total number of trials collected per condition type. The decoder was then applied to the held-out trial of the same condition type (e.g. if the decoder was trained on right and left eye position data, it was tested on the held-out eye position data) as well as the other condition type (e.g. the target data.) In this way we were able to measure how well the neural population was able to distinguish both within condition trials as well as how well the decoder generalized across conditions. In the decoder training, we used the labels of +1 and -1 for left versus right trials respectively. Thus, for each held out trial, the population response would lead to a scalar prediction. These values were saved and their histograms are shown in figure 3.4C. The distance between the distributions of the right and left predictions were quantified using the d-prime measure ( $d' = \frac{\mu_{right} - \mu_{left}}{\sqrt{.5(\mu_{right}^2 - \mu_{left}^2)}}$ ). A permutation shuffle test was used to test whether the d-prime measure was significant.

### 3.2.8 Cross-Hand Position Classification Analyses

To understand the population similarity in coding of target position across hand positions we performed a cross-hand position decode analyses. Classification analyses was performed using linear discriminate analysis. For cross-hand position results, classifiers were trained within a given hand position and applied to the three alternate hand positions. All predictions across folds of the cross-validation procedure were used to compute decode accuracy. This enables us to understand how well the neural

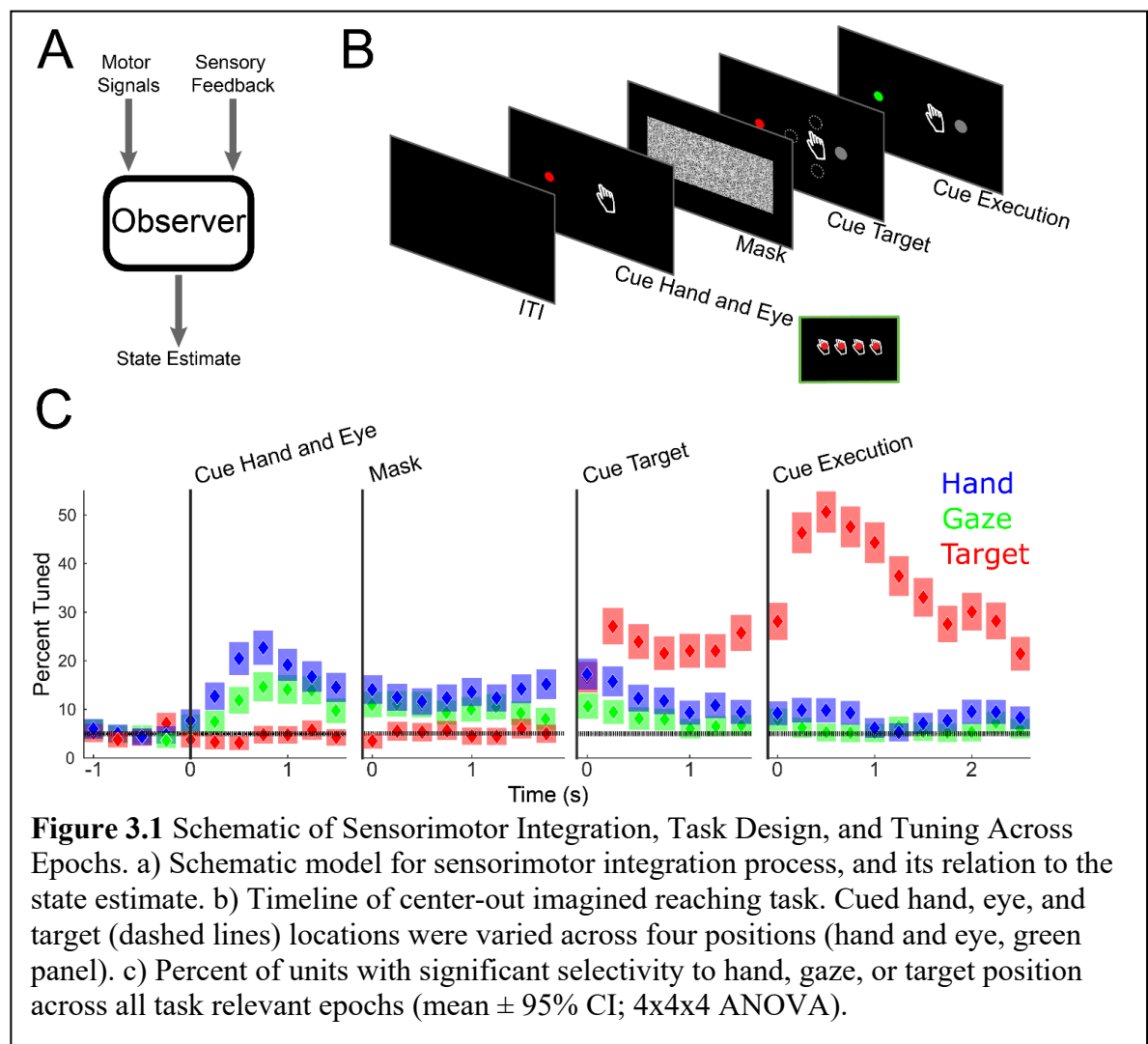
representation of the different target locations generalize to a novel hand position when the definitions of the target positions are preserved across the two positions. The accuracy results were also organized based on the distance between hand positions. A linear regression model was trained to test for a systematic change in classification accuracy as a function of distance between the starting hand positions.

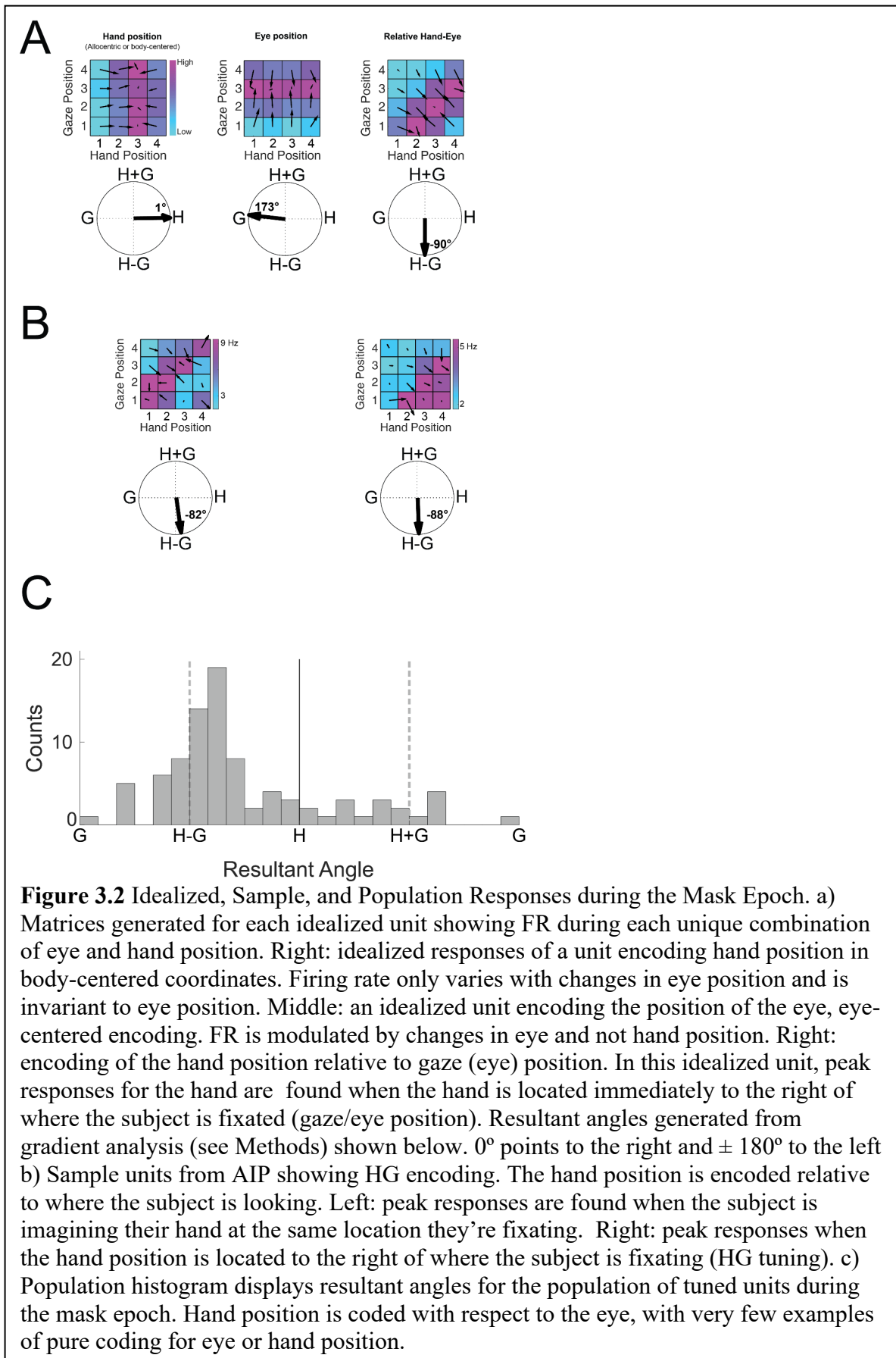
### 3.3 Results

We asked NS to perform a center-out imagined reaching task while systematically manipulating the initial imagined arm configuration and point of fixation (Figure 3.1B). Following an inter-trial interval, a fixation and hand position cue appeared at one of 4 spatial locations and appeared in all pairwise combinations for a total of 16 possible hand and eye configurations. The patient's control of gaze remained intact, and she was capable of fixating the fixation cue. However, due to NS's level of injury, she is unable to move her arm and instead imagines her hand at the cued location without any accompanying body movements. We then presented a dynamic masking stimulus to extinguish the hand position cue. Critically, during this masking phase, there is no sensory (visual or proprioceptive) information related to the imagined position of the hand. The mask was then removed and a reach target was presented at one of four locations in a center-surround arrangement. Finally, the subject was instructed to imagine a movement starting from the imagined hand position out to the target. Note that during the masking phase, the subject must maintain her arm configuration in her mind, but there is no sensory signal that provides any information about the state of the limb nor are there

planning or movement related signals as the subsequent position of the target is unknown.

Thus, we are able to test whether the neural population in PPC maintains an internal





execution, or planning signals (Figure 3.1A).

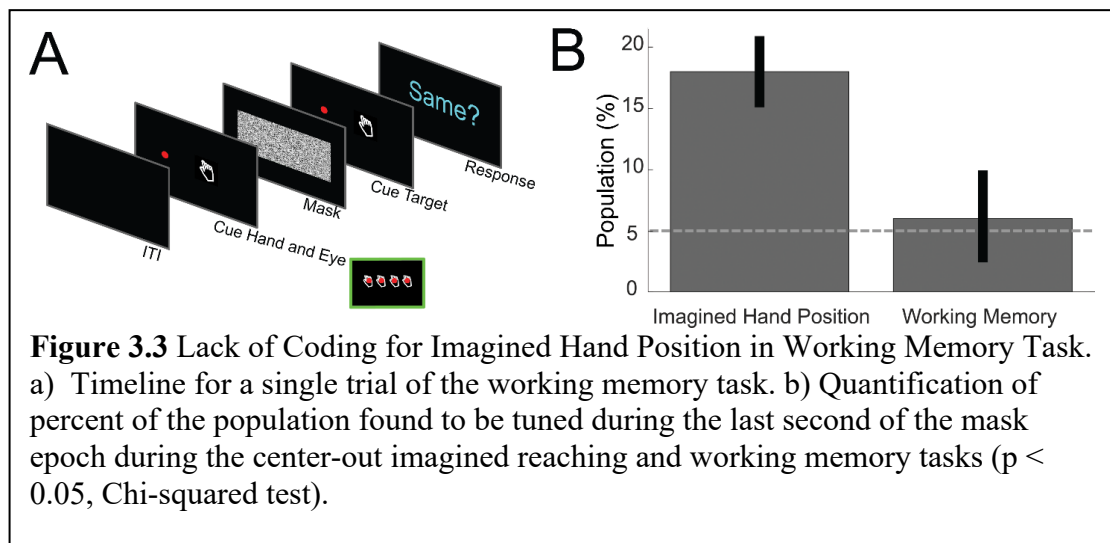
We used sliding window analysis (4x4x4 ANOVA, 500 ms windows stepped at 250ms) to summarize selectivity for hand, eye, and target position throughout the course of a trial (Fig. 3.1C). Analyses was performed on 541 cells acquired over 5 sessions. We found coding for hand and eye position begins with the instructional cue and is preserved throughout the mask phase. Coding for target begins immediately upon target presentation and increases during the imagined reach. Of special importance and a majority of the focus for the current study is the coding of hand and eye position during the dynamic masking phase.

To understand how hand position is coded during the mask phase, we used a gradient analysis (Buneo, Jarvis et al. 2002, Pesaran, Nelson et al. 2006): neural responses for all combinations of the 4 hand and 4 eye positions were organized into a neural response matrix that describes the firing rate at each of the hand/eye combinations. How firing changes across this response matrix determines how the unit codes hand and eye position. Examples of possible coding are shown in figure 3.2A. The left panel shows a hypothetical unit where neural firing changes systematically for changes in imagined hand position but is invariant to changes in eye position. This is characteristic of a neuron that codes hand position independent of the eye. This could reflect body-centered coding of hand position and would require further investigation. The middle panel shows a hypothetical unit that changes systematically for changes in eye position but is invariant

to changes in hand position. This is characteristic of a neuron that codes eye position. Finally, the right panel shows a hypothetical unit where firing rate shifts in a systematic way with changes in hand and eye position consistent with encoding of the relative position of the hand and eye (e.g. in this case the neuron responds maximally when the hand is to the immediate right of the eye). To quantify how firing rate changes for changes of eye and hand position we take the gradient of the response matrix (see arrows within response matrix diagram). The full gradient can then be summarized by a resultant vector that describes the net direction of flow. The resultant vector gives a single value that summarizes the influence of one or both variables on firing rate. The resultants for these hypothetical example units are shown in the bottom row of figure 3.2A. Resultants are mapped so that net changes along the horizontal or hand direction maps to 0 degrees, changes along the vertical or eye position map to 180 degrees, and resultants aligned along this diagonal, for units that code the relative hand-eye position, are mapped to -90 degrees. Together, this analysis allows us to characterize unit responses as tuned to eye position independent of hand position, tuned to hand position independent of eye position, or tuned to the position of the hand relative to the eye (HG).

The results of this analysis for two representative example neurons are shown in figure 3.2B. Each of these cells has a diagonal response vector resulting in a resultant around -90 degrees, hence encoding hand position relative to eye position. The resultants of all the significant units in the population are plotted as a population histogram (Fig 3.2C). There is a clear peak around -90; or in other words, hand is coded relative to the eye with very few examples of pure coding for eye or hand position. The type of hand-eye

relationship we see here can either be coding in a reference frame like manner, coding the relative hand-eye position.



During the masking phase, we found neurons are selective for the subject's imagined hand position. Hand position is coded as the relative position of the hand and eye. At this point there is no sensory information related to hand position and no motor actions or intent. Thus, a preliminary interpretation is that the relative hand and eye neural coding is best understood as an internal state estimate that can be manipulated through motor imagery. However, an alternative explanation of the data is also possible. Neural coding may reflect more general spatial signals such as spatial attention or working memory. To address this issue, we had the participant perform a spatial match-to-sample task (5 sessions, 519 recorded units). The task is shown in figure 3.3A. Following an inter-trial interval, a fixation cue and the hand icon cue were again presented at one of 4 spatial locations and appeared in all pairwise combinations for a total of 16 possible hand icon and eye configurations. However, the subject was asked to not imagine her hand at the

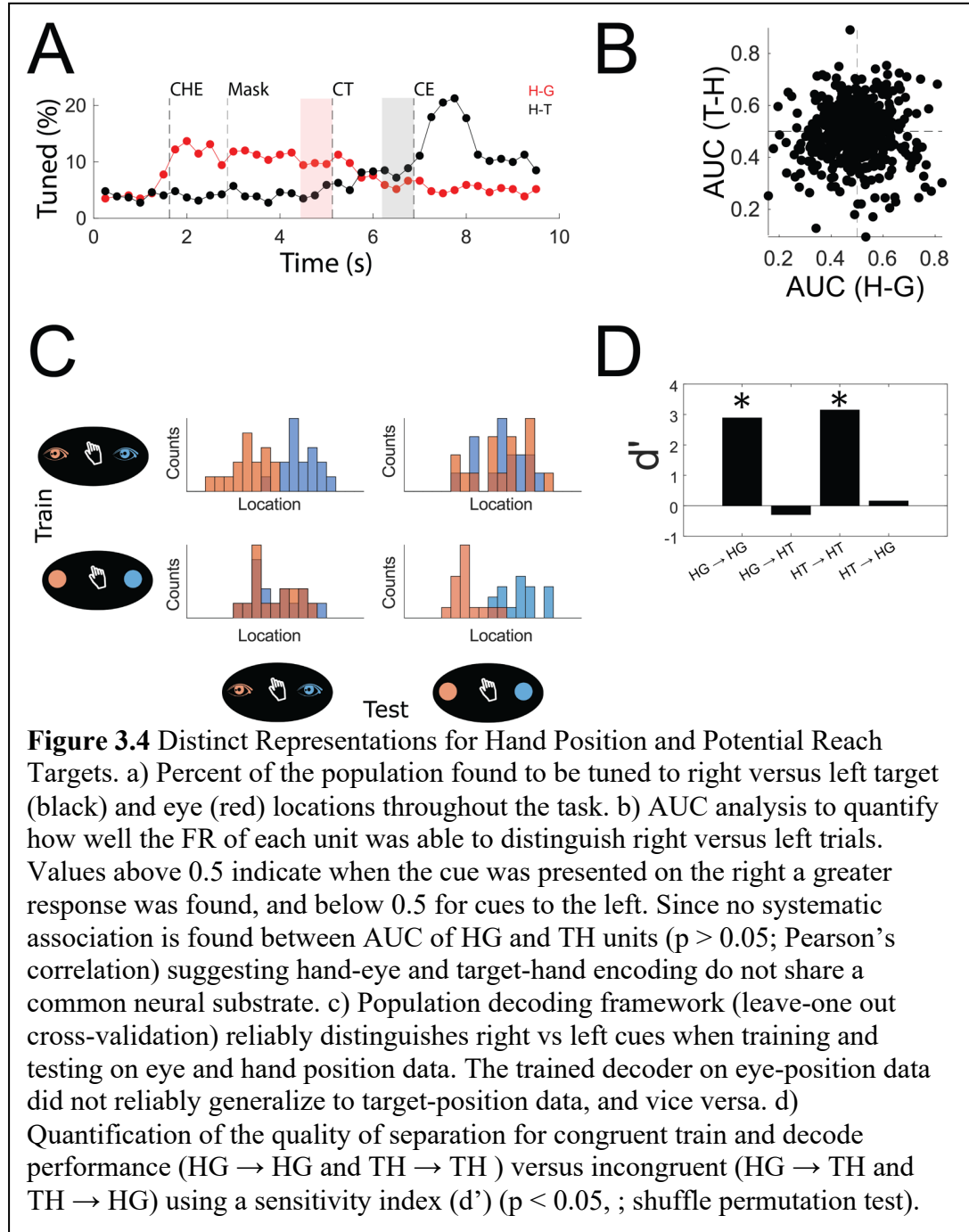
icon but instead to simply remember the position of the icon. The dynamic mask was then presented. Following the dynamic mask, the icon was again shown. However, on 50% of trials, the position of the icon was moved from its initial presentation location to one of the other 3 possible positions (randomly selected from a uniform distribution.) Finally, a response screen was presented and the subject reported whether the position of the mask icon before and after the dynamic masking stimulus were at the same location. Thus the visual elements of the task up through the masking phase as well as the duration of the task phases were identical in the two tasks, and in both tasks the position of the cue was behaviorally relevant and necessary for successful task completion. The primary difference was whether the subject was asked to maintain their imagined arm position at the cue or simply remember the spatial location of the cue. We analyzed the last second of the mask phase using a categorical regression model and found significant selectivity in the imagined movement task but not the match-to-sample task (Fig. 3.3B). Further, the proportion of selective cells was significantly different between the two tasks (Chi-squared test,  $p < 0.05$ ). The neural responses are better described as relating to the internal state estimate of the position of the hand as opposed to a more general spatial signal.

As shown in the next chapter, AIP neurons encode, at least to a first approximation, the relative position of the hand and target. Here we report that AIP neurons also code the relative position of the hand and eye. Are these two distinct neural processes, or does neural coding of the relative position of the hand and eye share a common neural



substrate with coding for the hand and the target? Such might be the case, for instance, if the neural population treated the eye cue as a potential target and formed a motor plan to move the hand to the eye cue location. The set-up of the current task paradigm allowed us to address this possibility. For hand positions 2 and 3, eye cue locations are found that flank the hand position to the right and left. Further, during target presentation, target cue positions flank the hand position to the right and left at an equal distance. If coding of relative hand-eye and hand-target share a common neural substrate, then left versus right coding of the eye and target relative to the hand should be similar. We used a rank-sum statistic to quantify the percentage of the population selective for right versus left eye and target locations as a function of time throughout the task (Fig. 3.4A, sliding window analyses, 0.5 second windows with 0.25 second step size.) Selectivity for left and right targets was found as expected. We used the mean neural response in the 750 ms window at the end of the masking phases to quantify coding for the relative hand-eye position and mean response 750 ms window at the end of the cue target phase to quantify coding for the relative hand-target position. For each unit, we quantified how well the firing rate was able to distinguish rightward from leftward trials using an AUC analyses. Within an AUC analyses, values above 0.5 indicate that the cue presented to the right generated a larger response while a value below 0.5 indicated that the cue to the left generated a larger response. If hand-eye and hand-target share a common neural substrate there should be a tendency for the AUC values to be correlated as the AUC values that express the relative location of the eye and hand should be similar to the AUC values that express the relative location of the target and hand. The AUC values for the hand-eye and hand-target were found to have no systematic association (Fig 3.4B,  $p > 0.05$ , Pearson correlation.) This

single unit analysis was complemented by a population analyses. We used a partial least squares regression model to predict rightward from leftward trials using the entire population of 513 neurons recorded over the 5 sessions. Using a leave-one out cross-validation procedure we found that we could distinguish right and left cues for both the eye and target with relatively high fidelity (Fig 3.4C, diagonal). However, the decoder trained on the eye position data failed to generalize to the target position data and vice versa (Fig 3.4B, off-diagonal). In other words, if you train a model on coding for the intended target relative to the hand, it fails to generalize to eye location relative to the hand. And conversely, if you train a model on eye position relative to hand, it fails to generalize to target position relative to hand. The quality of separation is summarized in figure 3.4D using a sensitivity index ( $d'$ ) to quantify the separation between the right and left cues. The congruent (HG→HG and HT→HT) generalizability is significantly greater than incongruent (HG→HT and HT→HG) ( $p < 0.05$ ; shuffle permutation test). This result is consistent with the single unit analyses of figure 3.4B and demonstrates that coding of the relative position of the hand and eye (HG) and coding of the relative position of the hand and target (HT) do not share a common neural substrate.



We next turn to coding of target location. The center out variant of the task employed here does not have a fixed set of target locations that are the same across all hand positions. Instead, the locations of the target relative to the hand are conserved. This requires a slight reinterpretation of a reference frame analyses relative to the in-line

versions if the reference frame task reported previously (Pesaran, Nelson et al. 2006, Bremner and Andersen 2012) and in the other chapters of this dissertation. Here we focus on the hand and target component of the response as eye position had a negligible impact on neural coding. In the inline version, relative hand-target coding effects appear as a response oriented towards -90 degrees. However, now direction appears explicitly and instead a direction tuning response would be oriented towards the target at 0 degrees. As before, tuning at -180 degrees would appear as pure coding of hand position. Coding at -90 degrees now means that tuning to direction systematically shifts with the starting hand position. A representative example cell along with the population summary is shown in Figure 3.5 A and B. In agreement with the inline results, the population is centered around 0 degrees, showing that the overall trend of the population is to code direction of imagined reaches invariant to starting hand position. However, the distribution is somewhat broad and summarizing the neural response with the resultant of the gradient may fail to capture non-linear dependencies between direction and hand position.

We analyzed the neural population within a decoder framework to understand how large an effect different hand positions have on decoding target location. A linear discriminant classifier was trained to decode target direction for each hand position and applied across all hand positions to construct a cross hand-position confusion matrix to quantify how well a classifier trained on one location will generalize to other hand locations. This analysis was performed separately for each session and averaged to create the result of

figure 3.5C. This data was also used to show how accuracy changed as a function of distance between the starting hand positions (Fig. 3.5D). Classification of target position generalizes between different starting hand positions but accuracy decreases, especially at the largest hand distances. Thus relative coding of hand and target provides a reasonable first order description of the neural responses, however, this coding is not “pure”, as the

starting hand position has some impact on how the relative hand-target relationship is coded.

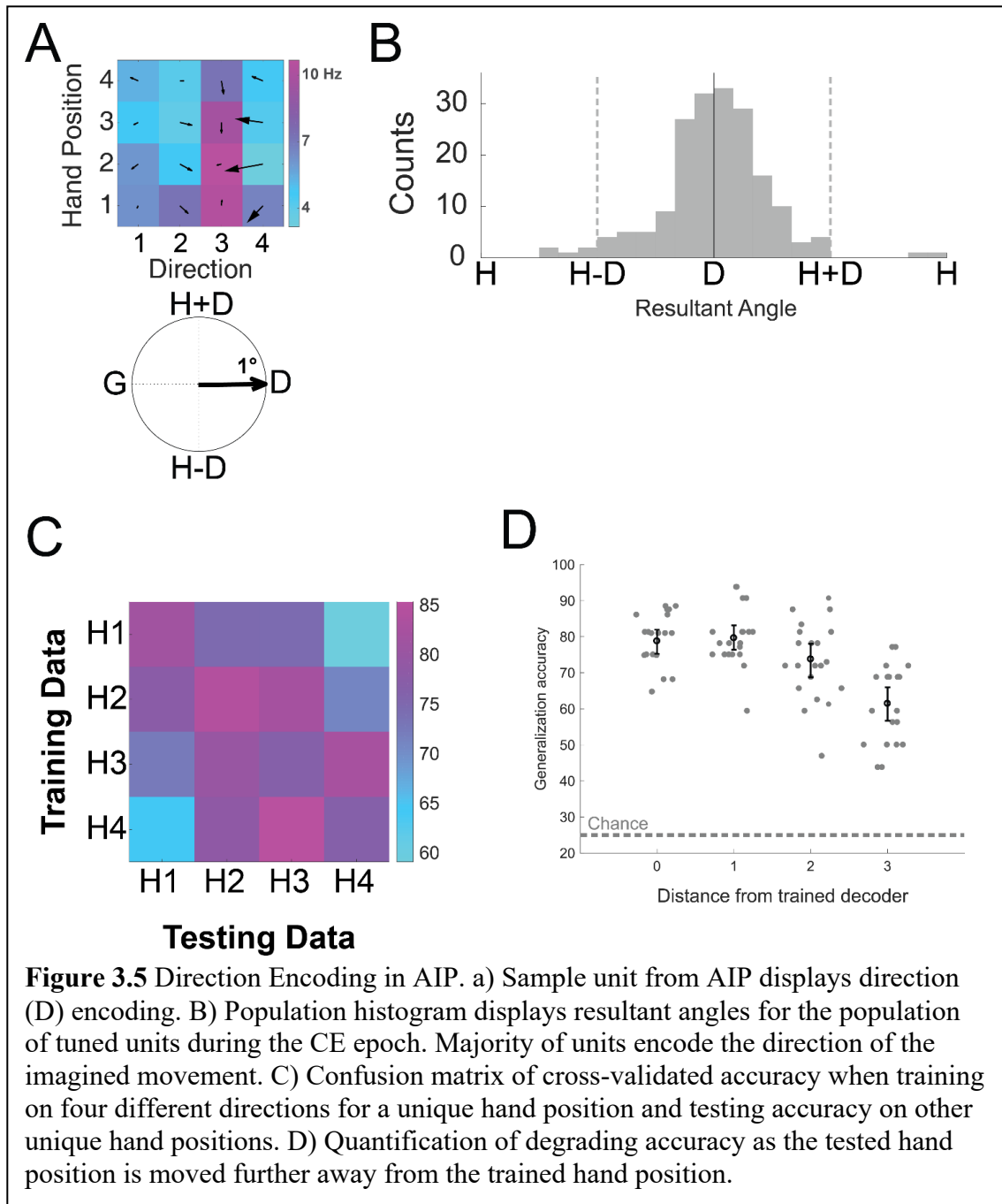


**Figure 3.5** Direction Encoding in AIP. a) Sample unit from AIP displays direction (D) encoding. b) Population histogram displays resultant angles for the population of tuned units during the CE epoch. Majority of units encode the direction of the imagined movement. c) Confusion matrix of cross-validated accuracy when training on four different directions for a unique hand position and testing accuracy on other unique hand positions. d) Quantification of degrading accuracy as the tested hand position is moved further away from the trained hand position.

### 3.4 Discussion

In summary, we show that PPC encodes an internal state estimate of the position of the body that can be manipulated with motor imagery. The internal state estimate of hand position is encoded as the relative position between the (imagined) hand and eye locations. These responses cannot be easily explained as potential planning signals or working memory. Finally, information about target position is coded relative to the state estimate of the hand. There are minor but significant shifts in direction coding relative to the initial starting position of the hand.

We modified the paradigm in two primary ways relative to that used in the other chapters of this dissertation. The first modification was to include a masking phase following presentation of the initial hand position and fixation cue. In the other paradigm, relative coding of the hand and eye could simply have been the consequence of the visual stimulus of the hand position cue relative to the point of fixation. The masking phase was used to ensure that no low-level visual stimuli could confound interpretation of coding for hand position. It remained possible however that edge effects of the masking stimulus or the computer monitor relative to the point of gaze could still drive neural signals. However, such coding with respect to the point of gaze would have shown up as neural coding in an “eye” reference frame (e.g. middle panel Figure 3.2A). Given the negligible portion of the population that coded an eye reference frame (Figure 3.2C) such low-level visual effects did not seem to be an appreciable component of the neural response.

Another modification was the use of a center out movement paradigm. This was primarily used to control against potential planning signals given that rightward starting hand positions would result in leftward reaches for the inline version of the task and vice-versa. It also allowed us to look at the possibility that hand-eye and hand-target relative coding shared a common neural substrate. Finally, this paradigm allowed us to verify that the neural population encoded intentions as the relative hand-target position. This paradigm therefore was a powerful complement to the inline version of the reference frame task.

Our results are interesting from the perspective of neural prosthetics. First, previous studies that decode position for use in neural prostheses have implicitly assumed that position is coded in a body centered reference frame. While such assumptions may hold for other cortical regions, our results contradict this assumption and may partially account for why velocity/direction based decoding methods have outperformed methods that utilize position. Future work is needed to determine if a better understanding of how hand position is encoded can improve online neural decode performance. Second, population level coding for direction of motion changes as a function of starting hand position, even over the relatively limited workspace of the computer monitor. Using decoding algorithm approaches that account for such dependence may improve future implementations of neural prosthesis.

Previous studies in paralyzed individuals have shown neural coding of hand position. However, these studies were not sufficient to support the claim that the hand position was evidence for an internal state estimate. This is because one, these studies did not control



for gaze position or visual differences which is problematic given that eye and head movements naturally follow the controlled effector effectively confounding these sets of variables. Second, the experiments were generally performed using a simple center-out paradigm where coding for hand position is based on intervals of time when the cursor is at the peripheral target locations. In this way, hand position is confounded both with target location as well possible planning signals from the peripheral targets back to the center “home” location. Thus, these studies left it unclear whether neural coding for hand position was an internal state estimate or potential confounding variables.

The finding of internal state estimates in PPC has implications for basic science questions as well. It has been proposed that sensory signals in PPC are too slow to enable rapid updating of reference frames for the purposes of recomputing updated movements plans (Duhamel et al., 1992). However, our results are consistent with the fact that PPC does not need to wait for delayed sensory feedback, but can instead use motor efference signals with delayed sensory feedback to maintain and store an up-to-date estimate of the sensory-state of the body.

## 4. Diverse Reference Frame Representations Across Human Cortex

### 4.1 Introduction

Brain machine interfaces (BMIs) have gained recognition over the previous two decades with seminal work in both non-human primates (NHPs) and humans demonstrating the capability to control cursors and robotic arms with variable degrees of freedom (Serruya et al., 2002, Musallam et al., 2004, Aflalo et al., 2015). In these examples BMIs are used to decode the intended motor goals directly from the neural activity of the recorded population. Understanding the reference frames in which these motor intent signals are encoded and correspond across brain areas is pivotal for the advancement and utility of decoding algorithms (Andersen et al., 2010; Miall and Wolpert, 1996; Musallam et al., 2004; Velliste et al., 2008). For example, if motor intent is encoded in eye coordinates then the location of the eyes would have to be known or fixed in order to maintain accurate decoding from the underlying population. Conversely, if intent is encoded in hand centered coordinates then eye location would not need to be known as the target would be encoded relative to hand position. Thus, knowledge of how motor intent is encoded in a brain area is vital to employing proper decoding algorithms and furthermore may yield insight into how interconnected brain areas variably encode motor intent.

To put this into perspective, let's use an example, imagine you are performing your daily coffee routine and you reach for your favorite coffee mug. As we go throughout our daily

lives performing tasks similar to the one mentioned above our brains are tasked with performing an accurate reach. In doing so our brains must transform incoming information regarding the location of the cup from an initial eye-centered reference frame, like those found in primary visual cortex, to a hand or body-centered reference frame and finally to a set of muscle commands that must be sent to the appropriate muscles. In other words, connected parietal and frontal areas involved in sensorimotor transformations define a set of sensory axes in which to represent the desired motor action (movement) from the initial position of the arm, position of the head, and the visual location of the cup (visual sensory input). Single neuron data from NHPs suggest that spatial locations are represented in multiple reference frames that can vary within and across sensory modalities (Avillac et al., 2005). For instance, visual stimuli can be encoded with respect to the eye or the head or hand, and tactile stimuli may likewise be encoded with respect to the eyes or body parts (e.g. hands) (Buneo et al., 2002; Pesaran et al. 2006; Pesaran et al., 2010). However, from the NHP literature there is conjecture as it regards to anatomically defined and regional preferences for the reference frames utilized. Understanding how these transformations are uniquely encoded in human cortex can yield further insight into the degree of functional specificity of different brain areas.

Population level analyses of reference frame representations in NHPs has yielded insight into how parietal and frontal areas encode reaches. Work in parietal reach region (PRR) has shown that the intended target is largely represented in gaze-centered coordinates (Pesaran et al., 2006, Andersen et al., 1998, Batista et al., 1999). Conversely, studies in

area 5d have shown reaches to a target are largely encoded in hand centered coordinates (Bremner and Andersen, 2012). Interestingly, while largely eye or hand centered representations of intended reach targets are found in some regions of PPC, physiological evidence from areas like dorsal premotor cortex (PMd) and ventral intraparietal area (VIP) have found that responses are not entirely encoded purely in eye or hand centered coordinates but rather encode intended actions in an intermediate space. For example, VIP has been shown to employ a reference frame wherein unit responses are modulated by an intermediate of eye and head centered coordinates (Duhamel et al., 2005). Furthermore, findings in PMd were shown to encode the locations of the eye, hand, and target relative to each other, employing what was termed a full relative position code (Pesaran et al., 2006). However, there still remains debate with regards to the employment of a largely unitary reference frame in areas especially close to the sensory input. (Batista et al., 2007).

To assess diversity of reference frame representations in human cortex during an imagined reach we used a range of target, hand, and gaze positions while analyzing firing rates in four brain areas: a region near ventral premotor cortex (PMv), supramarginal gyrus (SMG), primary somatosensory cortex (S1) in subject FG and anterior intraparietal area (AIP) in subject NS. PMv is an area of interest as work in NHPs has shown this region to be involved not only for sensorimotor transformations of arm movements but also hand shaping during both movement preparation and execution (Genitlucci et al, 1983; Kakei et al., 2001; Fluet et al., 2010). PMv was found to encode these movements

in body-centered coordinates (Kakei et al., 2001). SMG a subregion of the inferior parietal lobule (IPL) is a rich region that is responsive to different sensory stimuli and has many reciprocal connections to frontal and parietal areas such as the superior parietal lobule (SPL). The reference frames in which intentions in PPC are encoded has been found to vary from predominantly hand-centered (parietal area 5d) to eye-centered (PRR). The AIP area is a region known to be important in planning and organizing of grasping movements and was shown by our lab in a tetraplegic human to encode high-level cognitive aspects of a movement (Aflalo et al., 2015). While much research has focused on more caudal and superior areas of PPC very few have investigated the rostral areas of IPL (Rozzi et al., 2008). Mountcastle and Powell, in 1959, identified neurons in the NHP somatosensory cortex that encode proprioception and kinesthesia helping to establish a primary role of S1 in coding body sensations. Subsequent studies suggest a role of S1 in motor movements and the finding that pre-movement activity is encoded in S1 upon presentation of a target for reach (Nelson et al., 1989). More recently, S1 has been histologically demonstrated to contribute to corticospinal projections (Rathelot and Strick, 2006), and that executed arm reaches can be decoded from S1 (Fujiwara et al., 2017).

While studies have been conducted in NHPs on reference frames in parietal and premotor areas finding eye-centered, hand-centered, intermediate and heterogeneous representations. Few have successfully identified common and distinct modes of reference frame encoding across human cortex (Bremner and Andersen, 2012). Here we

explore the reference frame encoding of imagined arm reaches in two human subjects with chronically implanted cortical electrode arrays in four brain areas: ventral premotor cortex (PMv), supramarginal gyrus (SMG), and primary somatosensory cortex (S1) in subject FG and anterior intraparietal cortex (AIP) in subject NS. Of interest is understanding to what degree potentially interconnected brain regions vary or are similar in reference frame representations during the different behaviorally demanding epochs of an imagined reaching task. We find a greater proportion of heterogeneous reference frame representations during the planning epoch; however, all areas encode the reach in predominantly hand-centered coordinates during the cued execution epoch of a delayed-imagined reaching task.

## 4.2 Methods

### 4.2.1 Subject Information

#### 4.2.1.1 *Subject NS*

A 59-year old female tetraplegic subject who suffered a complete C3/C4 spinal cord injury was recruited and consented for a clinical trial for a BMI system. Subject NS has no control or sensation below her upper arms but maintains normal control and sensations for all areas innervated above the level of her spinal cord injury. The study and all procedures were approved by the California Institute of Technology (Caltech), Casa Colina Hospital and Centers for Rehabilitation, and the University of California, Los Angeles (UCLA) Institutional Review Boards (IRB). Informed consent was obtained after explanation of the objectives and possible risks involved. Surgical implantation took

place at Ronald Reagan UCLA Medical Center. All study sessions with subject NS took place at Casa Colina Hospital and Centers for Rehabilitation.

#### 4.2.1.2 *Subject FG*

A 32-year-old male tetraplegic subject was recruited who suffered a complete C5/C6 spinal cord injury and consented 1.5 years post-injury to participate in a clinical trial of a BMI system consisting of intracortical stimulation and recording. Subject FG has residual sensation in the anterior lateral portions of the upper limbs and residual sensation with no discriminatory ability in the posterior radial section of the upper arm and forearm that is also accompanied with paresthesia. All sensations and motor ability are consistent with the level of the sustained injury. The subject remains intact of all other motor control and sensations above the injury other than those noted above. The study and all procedures were approved by the California Institute of Technology (Caltech), Institutional Review Boards (IRB) of the University of Southern California (USC), and Rancho Los Amigos National Rehabilitation Hospital (RLA). Surgical implantation took place at Keck Hospital of USC. All future study sessions with this subject discussed here were run at RLA.

#### 4.2.2 Surgical Planning and Implantation

Surgical planning for both subjects followed the protocols described in (Aflalo et al., 2015; Salas et al., 2018). Based off these experiments analysis of the fMRI data was done in order to determine and identify the areas to implant. Initial placement of all arrays was predetermined based on pre-operative fMRI imaging, but placement may have differed if

the initial location was occluded by vasculature seen during the operation. Subject NS was implanted in the left superior parietal lobule more specifically the AIP area and subject FG in an area near PMv, SMG, and S1. All areas except S1 were implanted with 96-channel Neuroport microelectrode arrays (Blackrock Microsystems, Salt Lake City, UT). S1 was implanted with two 7x7 microelectrode arrays (48 channels per array).

#### 4.2.3 Reference Frame Task

Experimental sessions with both subjects were performed at their respective facilities. Both subjects performed the task in a dim room with their motorized wheel chairs seated similar distances from their task screen. The subjects were asked to minimize any and all head movements throughout the task and were placed in front of their screen with a researcher monitoring their head movements. Subjects were seated in their motorized wheel chair throughout the duration of the task. The task screen approximately occupied 45 degrees of visual angle. At the beginning of each trial the subject was cued to fixate their gaze and imagine their right hand (dominant and contralateral to recording arrays) at one of four locations marked by a circle and hand image, respectively. After 3 seconds a cue was shown above the cued eye and hand positions for 1.25 seconds wherein the subject continued to hold their ocular and imagined hand fixations. A change in the color of the fixation marker was the cue for the subject to begin their imagined reach to the target. The subject was asked to make an imagined reach and maintain the imagined ending position (target location) until the execution epoch was over (2 seconds). The execution epoch was then followed by an inter-trial interval (ITI) of 2 seconds.



Each run consisted a total of 64 trials for each unique combination of the four eye, hand, and target positions. This task was run 3 times (192 total trials, 3 repetitions) consecutively with a 2-5 minute break between each run. All imagined reaches were made within the frontal plane of the subject. Each session recording was separated out by at least seven days.

#### 4.2.4 Neural Recordings

Neural activity from each array was amplified, digitized, and recorded at 30 KHz using the Neuroport neural signal processor (NSP). The Neuroport system, composed of the arrays and NSP, has received FDA clearance for less than 30 days of acute recordings. However, for purposes of this study we received FDA IDE clearance for extending the duration of the implant (IDE numbers: G130100 and G120287).

Thresholds at -4.5 times the root-mean-square were set after high pass filtering the full bandwidth signal sampled, using the Blackrock Central software suite (Blackrock Microsystems). Waveforms collected consisted of 48 samples, 10 prior to threshold crossing and 38 samples after. These recordings were then sorted (both single and multi-unit) using k-medoids clustering using the gap criteria to estimate the total number of clusters (Tibshirani et al., 2001; Zhang et al., 2017). Offline sorting was then reviewed and adjusted as needed following standard practice (Harris et al., 2016). Units from all arrays in AIP, PMv, SMG, and S1 were analyzed. On average across 5 days of recordings in AIP we analyzed 84 sorted units per session in subject NS. In subject FG, on average per session we analyzed 90, 178, and 163 sorted units across 6, 6, and 5 days of

recordings in PMv, SMG, and S1, respectively. All sorting was done prior to analysis and blind to channel or unit responses found during the task. Further, spike sorting methods can be found in Zhang et al., 2017.

#### 4.2.5 Eye Tracking

Each subject's eye position was monitored using a 120 Hz binocular eye tracking system (Pupil Labs, Berlin, Germany). If the subjects gaze shifted off the cued eye position the task was terminated and ran again ensuring that gaze position remained fixed to the cued eye position. Eye positions were synced to the task and allowed online determination of eye position. Processing of raw XY coordinates was done using Matlab 2019a (Mathworks). Coordinates were then filtered using a disk filter via the `fspecial` function. The filter was had a radius of 2, and this was done to ensure we did not exceed our sampling resolution.

#### 4.2.6 Linear Analysis for Tuning

We defined a unit as selectively tuned if the unit displayed a significant tuning based on a linear regression analysis. We created a matrix that consisted of indicator variables for each unique condition separated by either a single behavioral variable or pair, similar to (Zhang et al., 2017). For example, there were 64 unique conditions (4 eye, hand, and target positions) indicator variables were for each unique eye, hand, target, eye-hand, eye-target, and hand-target. Firing rate was estimated as a linear combination of these

indicator variables:  $FR$  is firing rate,  $X_c$  is the vector indicator variable for condition  $c$ ,  $\beta_c$  is the estimated scalar weighting coefficient for condition  $c$ , and  $\beta_0$  is the intercept.

$$FR = \sum_c \beta_c X_c + \beta_0$$

Windows were 750 ms in duration and window start times were stepped every 500 ms.

This was done for all units in each sliding window. Significance of each fit was determined using the p-value of the F-test of overall significance for the linear analysis ( $p < 0.05$ , FDR-corrected). Units that were found to be significant in this analysis were then determined to be tuned and further analyzed in the reference frame analysis.

#### 4.2.7 Reference Frame Analysis: Gradient Analysis

For every individual unit three trials per condition were analyzed. Trials were subsequently aligned to the cue execution epoch (0 s). The delay epoch is defined as -1 s to -0.25 s. Gradient analysis was used to determine the degree of modulation each behavioral variable had on the firing rate of unit when comparing across each unique combination of variable pairs (Hand-Gaze (HG), Target-Gaze (TG), and Target-Hand (TH)) (Bremner and Andersen, 2012; Buneo et al., 2002; Peña and Konishi, 2001; Pesaran et al., 2006). For each tuned unit we created a four by four matrix (response matrix) representing each unique behavioral variable position and its associated mean firing rate. We averaged across trials and the third variable. Gradients were determined using the gradient function in Matlab 2019a (Mathworks). For each gradient a resultant

angle and length are generated indicating the modulation by each variable and its strength (Fig. 4.3). However, as we can see in Fig 4.3 oftentimes the gradients show a symmetrical pattern that would result in cancellation of symmetrical angles. To avoid this, we double each angle in the matrix and represent each angle from  $0^\circ$  to  $\pm 180^\circ$ . Therefore, the summed resultant angle is represented by  $0^\circ$  for left-right patterns of gradients,  $\pm 180^\circ$  for up-down patterns of gradients, and  $-90^\circ$  for gradients pointed at the diagonal as seen in Fig 4.3A. The summed resultant angle and length however cannot be mapped directly onto the response matrix, thus we have notated the appropriate variable and combinations of variables to help with interpretation. For example, in figure 4.3A hand only (H) modulation would be found at  $\pm 180^\circ$ , gaze only (G) modulation is seen at  $0^\circ$ , H+G at  $90^\circ$ , and H-G at  $-90^\circ$ . Therefore, we can use the angle of the resultant angle as a proxy for overall orientation bias for a variable pair.

Category	HG Response Filed Orientation (degrees)	TG Response Field Orientation (degrees)	TH Response Field Orientation (degrees)
HG	-90	$\pm 180$	$\pm 180$
TG	$\pm 180$	-90	0
TH	0	0	-90
HG-TH	-90	$\neq -90$	-90
TG-TH	$\neq -90$	-90	-90
HG-TG	-90	-90	$\neq -90$
HG-TG-TH	-90	-90	-90

**Table 4.1** Criteria for Categorizing Individual Units

In each epoch gradient analyses of all tuned units were used to determine the reference frame representations. Rayleigh's test was used to assess the uniformity of circular

histograms for tuned resultant angles. Circular means were determined by weighting the contribution of each resultant angle by the resultant length. To test whether individual units coded exclusively for the target relative to the hand we categorized each unit based on the three variable-pair resultant angles. Our criteria were the following: 1) is the unit found to show significant tuning in the linear analysis; and 2) classify units based on the appropriate response field orientation for each category (tolerance  $\pm 45^\circ$  Table 4.1). This categorization scheme is similar to the one used by Bremner and Andersen, 2012.

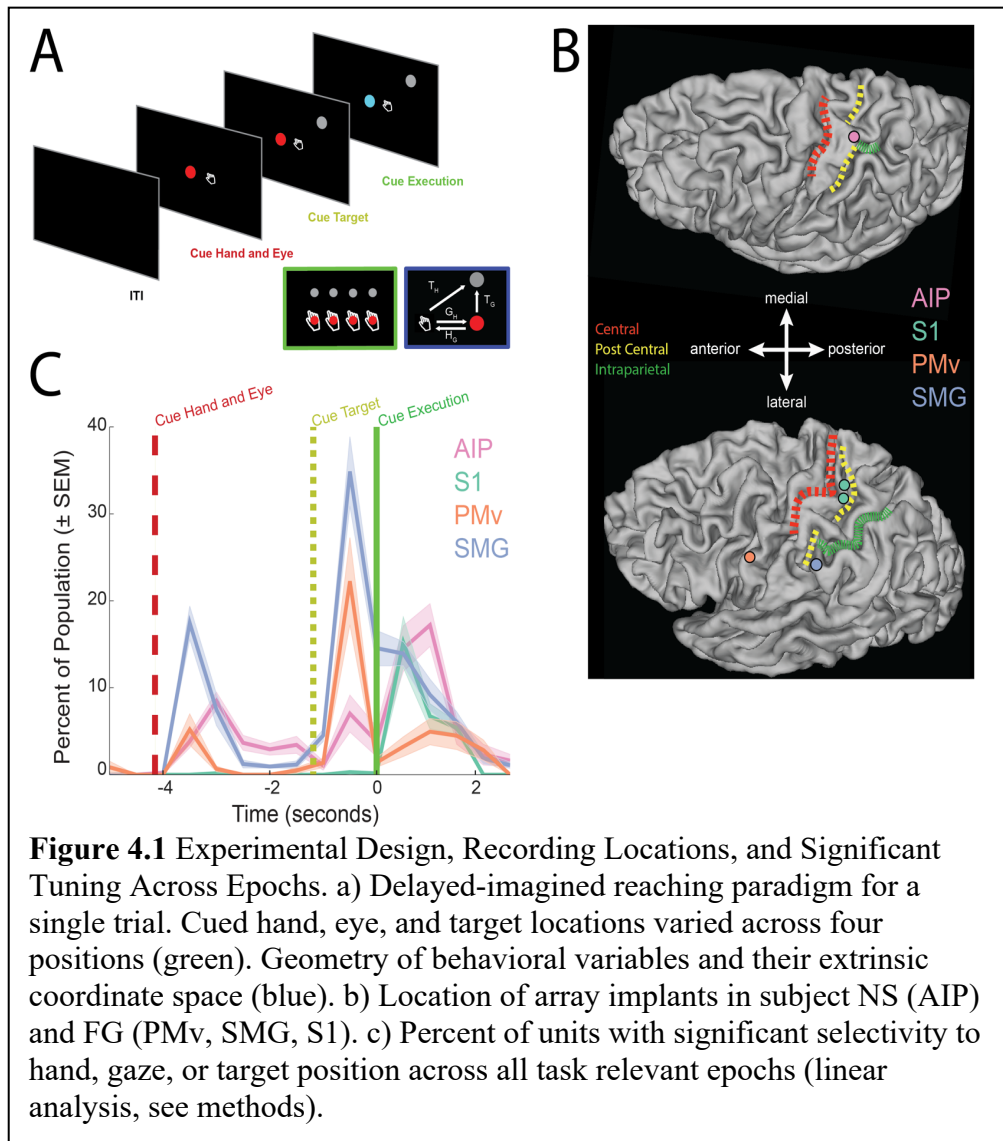
#### 4.2.8 Dimensionality Reduction

We used population level dimensionality reduction analyses to determine the most common modes of reference frame encoding over time in a brain area. The firing rates for all units, trial averages, and time points were arranged in a matrix (unique trials by unit) and reduced down using principal component analysis (Fig. 4.8). For the first 20 components we then ran a gradient analysis for each time window. Time windows were 100 ms in duration and response field angles and lengths were acquired from the start of the cue hand eye epoch to the end of the cue execution epoch. Analyses done with larger steps showed similar results. Next, we converted all resultant angles and lengths into complex numbers to account for both variables and utilized complex principal component analysis to identify the most common mode of tuning found. Previous work on geophysical data sets have successfully used similar methods for identifying dynamics (Horel, 1984). A matrix of each complex value for each time point and each component was then created and reduced to find the components that explained the greatest variance.

Furthermore, we used parallel analysis to determine which components from this dimensionality reduction were significant (Franklin et al., 1995).

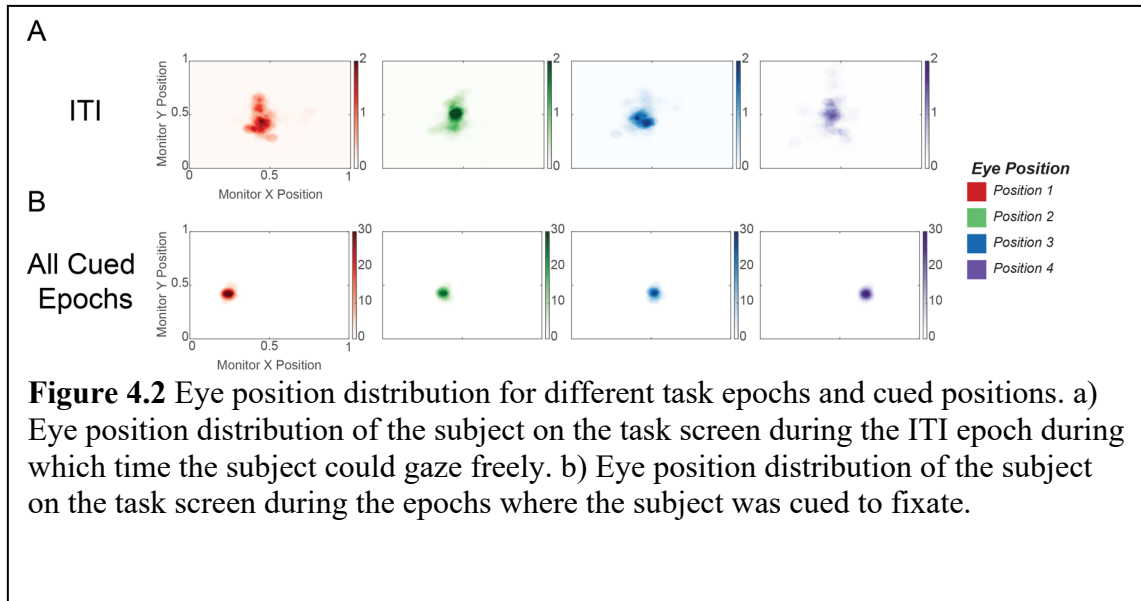
### 4.3 Results

What coordinate frame or frames do we use to encode imagined movement intentions? To answer this, we recorded neural activity in ventral premotor cortex (PMv), supramarginal gyrus (SMG), and primary somatosensory cortex (S1) in participant FG and anterior intraparietal cortex (AIP) in participant NS (Fig. 4.1B). These participants completed a delayed-reach task in which we systematically varied hand, eye, and target position in order to determine the reference frame encoding of reach intentions during planning and execution epochs (see Methods). This design allowed for us to characterize whether cell firing rates (FRs) encoded the target position relative to gaze direction (T-G), target relative to hand (T-H), hand position relative to gaze direction (H-G), or a combination of these vectors. The combination of these three vectors allows us to identify if a unit is encoding the target relative to the direction of gaze (eye-centered), the position of the hand (hand-centered), relative to the position of eye, hand, and target specifying the differences in locations (relative), or body/world centered.



The task was composed of four different phases (Fig 4.1A): 1) we cued both gaze position and hand position at one of four locations where the subject would fixate and imagine their hand (Cue Hand and Eye (CHE), 3.25 seconds), 2) while maintaining gaze fixation and imagined hand position from the previous epoch a target was presented above and in line at one of four locations, (Cue Target (CT), 1.25 second, possible locations greens) 3) a cue was given to begin the imagined reach to the target while maintaining eye fixation (Cue Execution (CE), 2 seconds), 4) an inter-trial interval with

no stimuli presented on the screen. The subject's gaze position was monitored using an eye tracker (Pupil Labs, Berlin, Germany) in order to ensure that data was not analyzed if the participant broke gaze fixation after a gaze position was cued (Fig 4.2). If the participant broke gaze fixation, we restarted the task.



#### 4.3.1 Imagined Reaching Related Activity in Human Cortex

Firing rates were analyzed using a sliding window of 750 ms throughout the entirety of the task. Using the neural (e.g. FR) and behavioral states (e.g. gaze position), we employed a linear analysis to determine significant relations between single unit activity and associated behavioral states (see methods). We found significant proportions of the population that were tuned during the CHE, CT, and CE epochs of the task. We recorded from 537 (PMv), 1066 (SMG), 651 (S1), and 421 (AIP) units across 4-6 sessions. The maximal percentage of tuned units per epoch was: 4.66%, 17.82%, 0.15%, and 8.31%



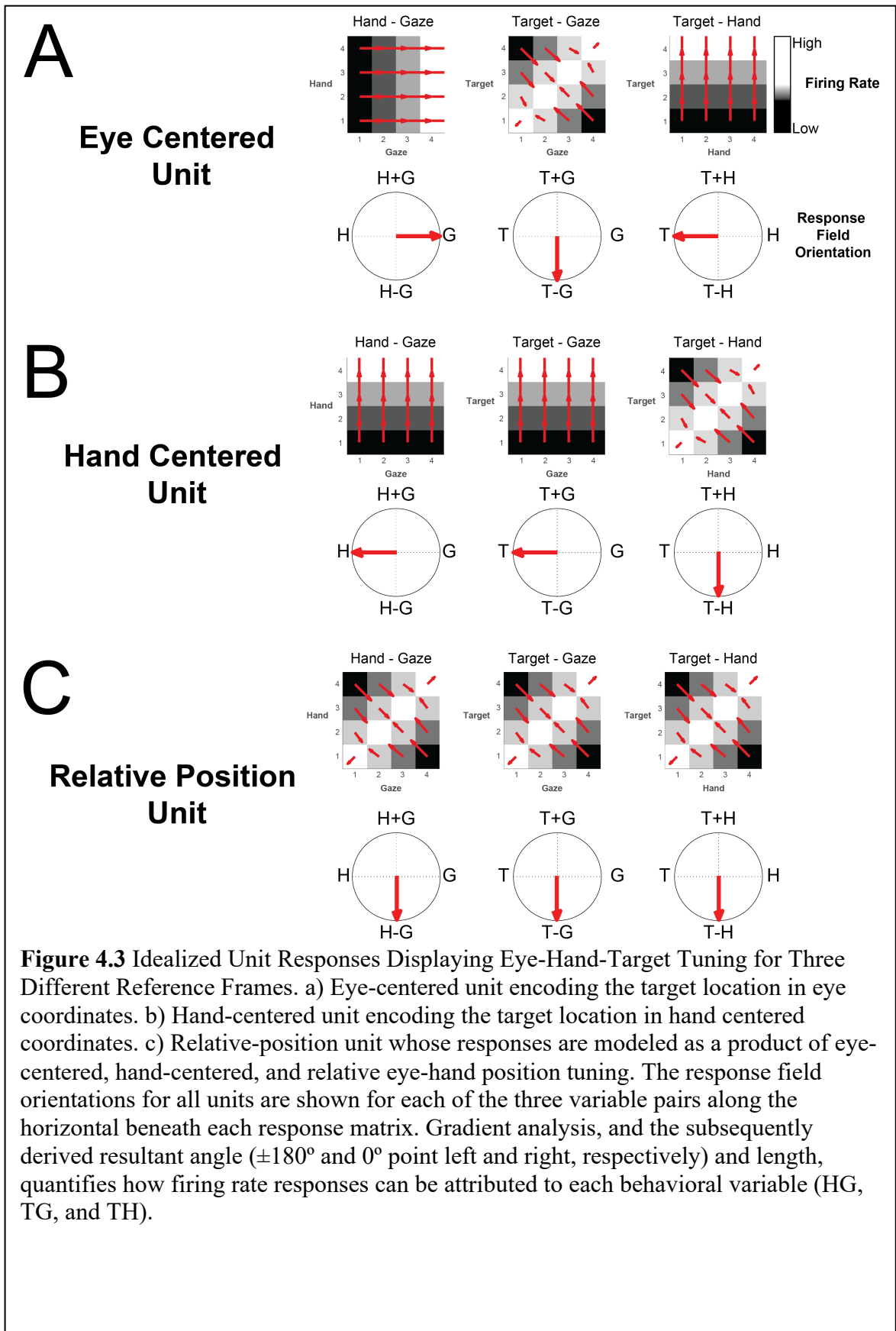
during the CE epoch ( $p < 0.0001$ ; ANOVA), 21.60%, 34.99%, 0.31%, and 6.89% of units tuned during the delay ( $p < 0.0001$ ; ANOVA) and 5.03%, 14.07%, 15.05%, 16.86% ( $p = 0.0015$ ; ANOVA) during the go epoch for PMv, SMG, S1, and AIP ( $p < 0.05$ , FDR corrected), respectively (Fig 4.1C). We find that tuning varies across all phases of the task and that tuning differs between brain regions. S1 has little to no tuning throughout the task until the cue execution epoch. In contrast, SMG shows robust tuning throughout all 3 epochs (CHE, CT, and CE).

### 4.3.2 Reference Frames

In order to determine and understand the coordinate frames in which behavioral variables are encoded, it is important we provide a brief explanation here of how we used gradient analyses to define the coordinate frame of a unit (further explained in methods and Pesaran et al., 2006). Put simply, movements in the brain can be represented in two ways: 1) an extrinsic space defined by endpoint directional movements (Fig 4.1A blue panel), and 2) an intrinsic space defined by the angles and forces required of individual muscles to make the desired movement. This distinction can be represented by the following example: saccades and reaches in the same direction can both be thought of sharing the same extrinsic space. However, because the muscle and joint movements are unique to the effector (i.e., muscle), they do not share an intrinsic space representation. One aim of this work is to transform the intrinsic commands for saccades to the reference frame of target position relative to initial gaze position (T-G). Similarly, we aim to transform intrinsic reach commands to target position relative to initial hand position (T-H). Finally, another vector can be defined by the relative position of the initial hand

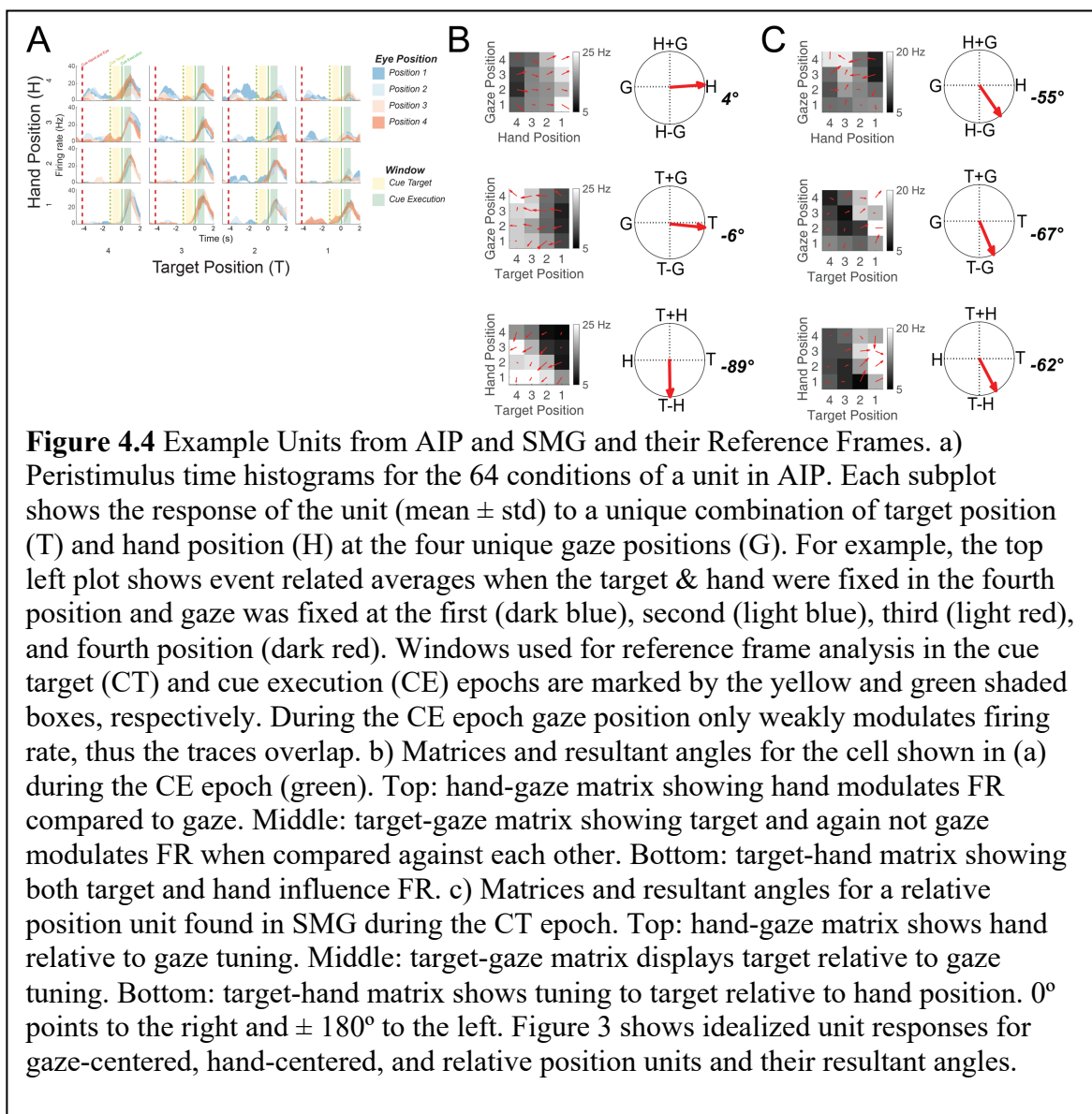
position and eye position (H-G) (Buneo and Andersen, 2006). H-G can be either gaze position in hand coordinates or hand position in eye coordinates. See Buneo and Andersen, 2005 for further discussion. For the rest of this section, we will refer to and describe H-G as hand position in eye coordinates.

The utility of a gradient analysis used here is the ability to determine how much a unit's firing rate is modulated based on either hand, eye, target position, or a combination of these. The relative relationship between hand and target in a hand centered unit is best explained by the hand and target having the same spatial positioning in order to maintain the same firing response. For example, if a hand centered cell fires maximally when the target is placed above the hand position. Assuming we shift the target over to the right by a position in order for the unit to fire at a comparable rate we must also shift the hand position. This shows that for the following example of a hand-centered unit the influence



moves upwards. In Figure 4.3 we illustrate how a matrix and gradients would appear for idealized eye-centered, hand-centered, and relative position units.

Building upon the previous efforts from Pesaran et al., 2006 in NHPs we used a similar reference frame dissociation task to independently control and minimize the possible vector representations of T-G, H-T, and H-G that might be represented by a single unit during free behavior. This task allowed us to systematically control hand, eye, and target

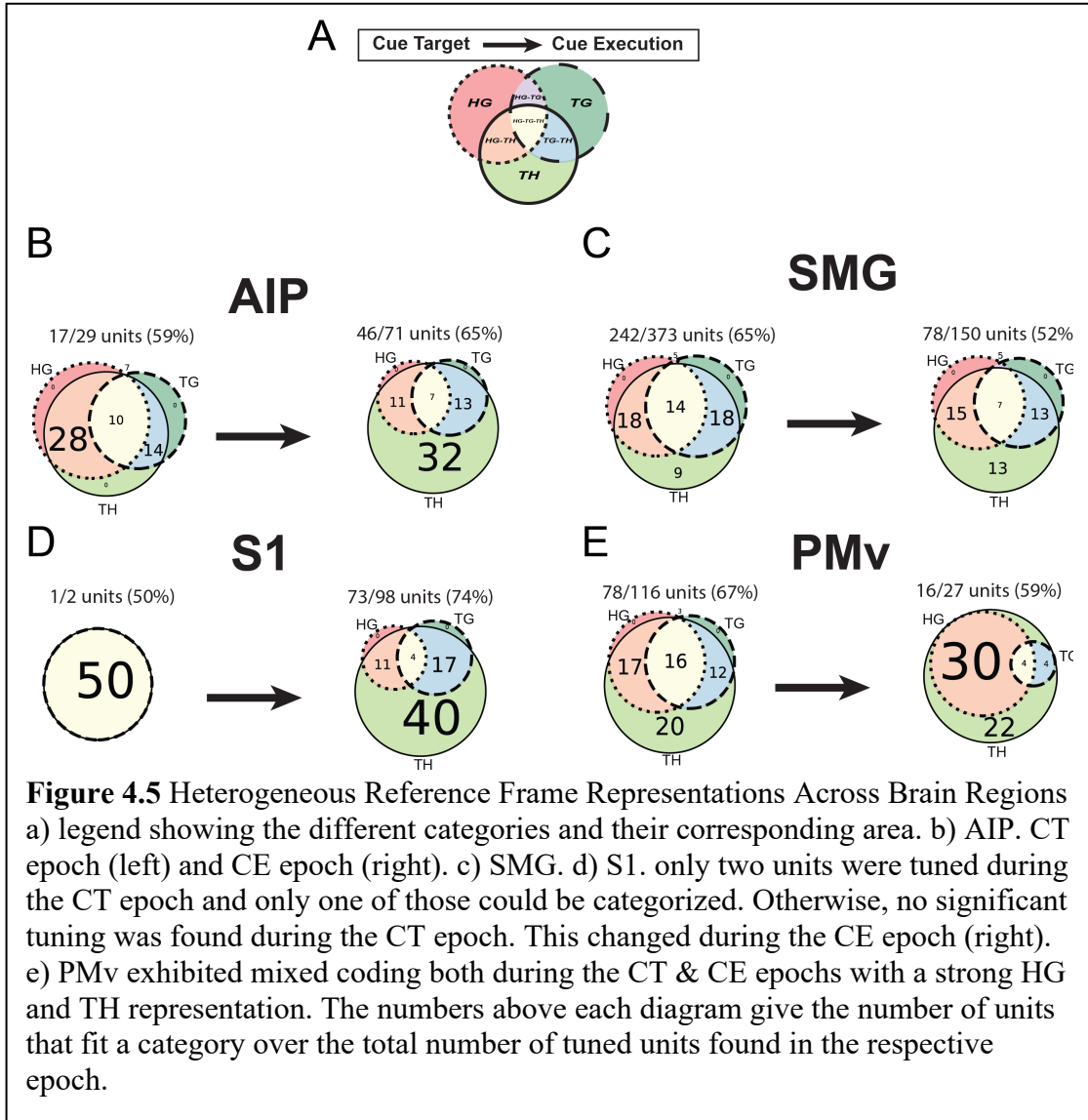


positions while using a gradient analysis to determine the coordinate frames in which these variables were represented on a single unit basis. Figure 4.4 shows an example of a cell found in AIP that codes target location in hand-centered coordinates. The peristimulus time histogram (PSTH) in Figure 4.4A is typical of a neuron found to encode the target location in hand centered coordinates. This unit showed significant activity during the CHE and CE epochs. In Figure 4.4b, we illustrate the reference frame analysis derived from the CE window of the PSTH. Furthermore, in Figure 4c, we show a sample matrix for a relative position unit. Units were sampled from AIP and SMG, respectively. The gradients for the hand centered unit show that with respect to H-G ( $4^\circ$ ) and T-G ( $-6^\circ$ ), hand and target position respectively are exerting the greatest influence on the firing rate of this unit. Thus, when we examine T-H we find that the response field for reach targets shifts with each initial hand position ( $-89^\circ$ ). In Figure 4.4c we see a different relation amongst the three vectors. In this sample cell during the CT epoch we find that H-G, T-G, and T-H all have diagonal gradient orientations, indicating that there is a relative response to each variable pair to the other ( $-55^\circ$  HG,  $-67^\circ$  TG, and  $-62^\circ$  TH).

### 4.3.3 Heterogeneous Representations of Coordinate Frames

We examined the proportion of tuned units from the linear analysis that encoded the different vectors during planning and execution epochs of the delayed imagined reaching task. We found that during the planning epoch there was a greater tendency across all brain areas to encode more than one vector. However, this overall tendency changed during the execution epoch where all areas collapsed to a largely hand centered dominant encoding of the target (Figure 4.5). Overall, of the units that were significantly tuned

during each epoch we found 20% (PMv), 9% (SMG), 0% (S1), and 0% (AIP) of the total amount of tuned units to be hand centered, and 16% (PMv), 13% (SMG), 14% (S1), and 10% (AIP) to be coding the relative position of the three behavioral variables during the planning epoch. This changed during the execution epoch with 22% (PMv), 13% (SMG), 40% (S1), and 32% (AIP) to show hand-centered tuning and 4% (PMv), 7% (SMG), 4% (S1), and 7% (AIP) encoding relative position of eye, hand, and goal (target) during the execution epoch. This uses a 45° freedom explain in methodology like those used by Bremner and Andersen, 2012 (Table 4.1).



In PMv, 78/116 (67%) units were found to encode one or multiple vectors based on the definitions for each category. Of these, 23/116 units (20%) encoded only the TH vector and 0 units for the single vector of TG or HG. The next largest proportions were found to encode multiple vectors concurrently with the TH vector. HG and TH vectors were concurrently encoded by 20/116 units (17%), while TG and TH were encoded by 14/116 units (12%). All three vectors were encoded by 18/116 units (16%). This changes during

the execution phase where 16/27 units fit our criteria. Of these, TH and HG vectors were concurrently encoded in 8/27 units (30%) or only the TH vector in 6/27 units (22%).

In SMG, 242/373 (65%) tuned units were able to be categorized based off our criteria. Of these we find a larger proportion of units to concurrently encode multiple vectors along with the TH vector. Interestingly, TG-TH and HG-TH are encoded by 69/373 (18%) and 68/373 (18%), respectively. Furthermore, we find that there is a large proportion of units that are relative position units (HG-TG-TH) 52/373 (14%), and smaller proportion of units only encoding the TH vector (34/373, 9%). Unlike PMv, we do not see as large of shifts in the proportion of units encoding each respective category. During the CE epoch we find that a greater proportion of units as compared to the CT epoch encode the TH vector only (20/150 units, 13%). Interestingly, units showing relative position coding during this epoch decreases to 10/150 (7%), while encoding of both the HG-TH and TG-TH vectors decreases minimally to 22/150 (15%) and 19/150 (13%), respectively.

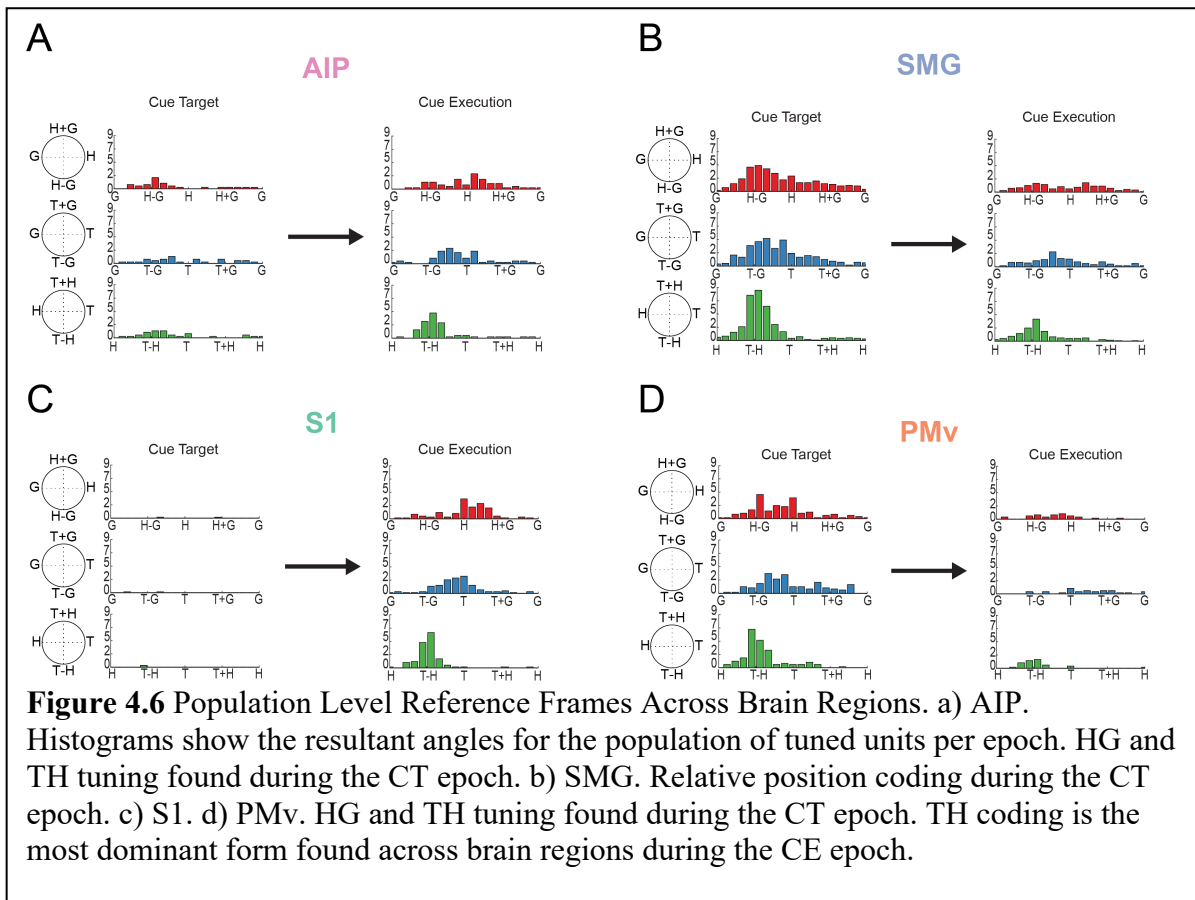
In contrast to the other brain regions, in S1 we find little to no tuning during the CT epoch. Surprisingly, during the subsequent epoch (CE) we find a majority of tuned units to be hand centered. The greatest proportion of units in S1 are found to encode TH vector only (39/98, 40%). Interestingly, of the remaining tuned units TG-TH and HG-TH are encoded by 17% (17/98) and 11% (11/98). Lastly, only a small proportion of units fall within the relative position category with 4/98 (4%) units. Overall, S1 seems to encode the behavioral variables only during the CE epoch in mostly hand centered coordinates.



In contrast to SMG we find that AIP, an area in the SPL of PPC, encoding of the HG, TG, and TH vectors differs especially during the planning epoch. We find that during planning AIP does not show large proportions of the population to be tuned to the TH vector during the CT epoch. The largest proportion of tuned units during this epoch encode two or more vectors: TH-HG 8/29 units (28%), TH and TG 4/29 (14%), all three vectors (TH, TG, HG) 3/29 units (10%). This changes during the execution epoch to resemble S1, but with a relatively smaller percentage of units encoding the TH vector only 23/71 units (32%). Also, TH-HG were concurrently encoded by 8/71 units (11%), TH-TG by 9/71 units (13%), and all three vectors by 5/71 units (7%).

#### 4.3.4 Population Level Encoding of Reference Frames

While single unit analysis displayed a common theme of heterogeneity of units, especially during the planning epoch, when looking at population level encoding more distinct reference frames emerged as a whole. This difference can be due to the categorization criteria used. Anywhere from 32-41% of the tuned population was excluded in the single unit analyses categorization analysis. Population level analyses of all tuned units included these cells and yields a clearer perspective on the overall differences and reference frame encoding used in each region.



#### 4.3.4.1 *PMv*

Population level analyses determined the reference frames of units that were found to be significantly tuned from the regression analysis. When looking at population level reference frame encoding of gaze, hand, and target we find a predominantly hand-centered encoding during the planning epoch with a distinct peak of a subset of the population encoding HG. The population of resultant angles for the HG vector was found to be unimodally distributed ( $p < 0.0001$ ; Rayleigh test) and nonuniform ( $p < 0.01$ ; Watson test) with a weighted mean direction of  $-48^\circ$  and average length of the resultant vector from the gradient analysis was 5.9. The TG vector was found to be unimodally

distributed ( $p < 0.0001$ ; Rayleigh test) and nonuniform ( $p < 0.01$ ; Watson test) with a weighted average of  $-13^\circ$  and average vector length of 3.8. The TH population vector was found to be unimodally distributed as well ( $p < 0.0001$ ; Rayleigh test) and nonuniform ( $p < 0.01$ ; Watson test) with a weighted average of  $-85^\circ$  and average resultant vector length of 11.7. However, while the mean angles of HG and TG are trending towards a difference ( $p = 0.08$ , Watson's nonparametric test) the resultant lengths of these same angles are found to be significantly different ( $p < 0.03$ ; Wilcoxon signed-rank test, Fig 4.7D). Taken together this shows that during the CT epoch both TH and HG are the most strongly represented vectors (Figure 4.6D).

In contrast, during the execution epoch we find that of the significantly smaller number of tuned units during the execution epoch the HG, TG, and TH vectors were all found to be unimodally distributed ( $p < 0.0001$ ,  $p < 0.01$ ,  $p < 0.0001$ , respectively; Rayleigh test) and nonuniform ( $p < 0.01$ ; Watson test) with weighted mean directions of  $-36^\circ$ ,  $42^\circ$ , and  $-92^\circ$ , respectively. Weighted resultant vector lengths were found to be 8.1, 4.8, and 20 for HG, TG, and TH vectors, respectively. Furthermore, when comparing population level differences across the epochs we found from planning to execution the HG vector population distributions did not significantly differ ( $p = 0.34$ ; Mardia-Watson-Wheeler test) nor did the mean resultant angles ( $p = 0.97$ ; Watson's nonparametric test).

Strikingly, the encoding of the hand relative to gaze position was maintained from planning to execution, with similar modulation ( $p = 0.46$ ; rank-sum test). TG was found to have a significantly different distribution from planning to execution ( $p = 0.005$  Mardia-Watson-Wheeler test) as well as a significant difference in the mean direction of

resultant angles ( $p = 0.003$ ; Watson's nonparametric test). Lastly, TH vector encoding remains consistent with no significant differences in the distribution or in the mean resultant angles ( $p = 0.87$  and  $p = 0.75$ ; Mardia-Watson-Wheeler test and Watson nonparametric test, respectively). Interestingly, we do however find that the resultant lengths of the TH vector are different across the epochs with greater modulation seen during the CE epoch ( $p = 0.01$ ; Wilcoxon rank-sum test). This shows that while more units are tuned during the CT epoch, and the response to changes in T and H position is the same in PMv, the magnitude of modulation for TH units is greatest during the CE epoch.

#### 4.3.4.2 SMG

The population level reference frames found in SMG were analyzed from 1066 units across 6 sessions in subject FG. Population analyses of reference frames were done on 231 and 149 units found to be significantly tuned during the planning and execution epochs, respectively. Interestingly, during the planning epoch we find that HG, TG, and TH are all unimodally distributed ( $p < 0.0001$ ; Rayleigh test) and nonuniform ( $p < 0.01$ ; Watson test) with weighted mean resultant angles at  $-63^\circ$ ,  $-44^\circ$  and  $-80^\circ$  with average resultant vector lengths of 5.8, 8.3, and 15.9, respectively. Furthermore, the tuning strength of TH is significantly greater than both TG and HG ( $p < 0.0001$ ; Wilcoxon-signed-rank test, Fig 4.7B) with TG greater than HG ( $p = 0.002$ ; Wilcoxon-signed-rank test, Fig 4.7B). While there is no significant difference in the mean ( $p = 0.31$ ; Watson's non-parametric mean) of HG compared to TG we do find that the distributions are significantly different ( $p = 0.02$ ; Mardia-Watson-Wheeler test). There is a very

concentrated amount of resultant angles encoding the target position relative to the hand (TH at  $-90^\circ$ ), which is found to have significantly different mean and distributions when compared to TG and HG ( $p < 0.0001$  Watson nonparametric test,  $p < 0.0001$ ; Mardia-Watson-Wheeler test, HG or TG vs TH). Strikingly, this lends to show that while the TH vector is mostly encoded during the planning phase there is still a moderate amount of gaze influence on unit encoding of target position (TG) and hand position (HG) (Figure 4.6B).

During execution we see an overall shift in the tuning of HG and TG response field angles from encoding a relative position encoding to a stronger representation of TH with subsequent shifts in HG and TG vectors to hand and target. The HG, TG, and TH populations were unimodally distributed ( $p < 0.0001$ ; Rayleigh test) and nonuniform ( $p < 0.01$ ; Watson test). The weighted resultant mean angles for HG, TG, and TH were found to be  $-16^\circ$ ,  $-33^\circ$ , and  $-80^\circ$  with average resultant vector lengths of 3.7, 7.9, and 13.6, respectively. The HG and TG population distributions are significantly different ( $p = 0.002$ ; Mardia-Watson-Wheeler test), but don't have significantly different means ( $p = 0.25$ ; Watson nonparametric test,  $p = 0.07$ ), and are trending towards having differences in the strength of tuning ( $p = 0.07$ ; Wilcoxon-signed-rank test, Fig 4.7B). Furthermore, the TH populations mean and distribution is significantly different from both the TG and HG populations ( $p < 0.0001$  Watson nonparametric test,  $p < 0.0001$ ; Mardia-Watson-Wheeler test, HG or TG vs TH).

Lastly, we find significant shifts in the populations from the CT to CE epochs. This is represented with significant changes in the mean and distribution of overall population responses of HG from planning to execution ( $p = 0.002$ ; Watson nonparametric test,  $p = 0.01$ ; Mardia-Watson-Wheeler test). Interestingly, we do not find a significant difference in TG or TH population mean or distribution across epochs ( $p = 0.1$  (TG) and  $p = 0.75$  (TH); Watson nonparametric test,  $p = 0.09$  (TG) and  $p = 0.48$  (TH); Mardia-Watson-Wheeler test). Interestingly, SMG displays a relative encoding of the three behavioral variables hand, gaze, and target during planning which then changes to a much more hand centric representation (TH) when the imagined reach is being made with moderate TG encoding.

#### 4.3.4.3 *S1*

Population level reference frame encoding in S1 are only analyzed during the CE epoch as this was the only phase that showed significant proportion of the population to be tuned (Figure 4.6C). During the CE epoch we interestingly find that much like the results from the individual unit analysis the population shows a very strong peak at TH.

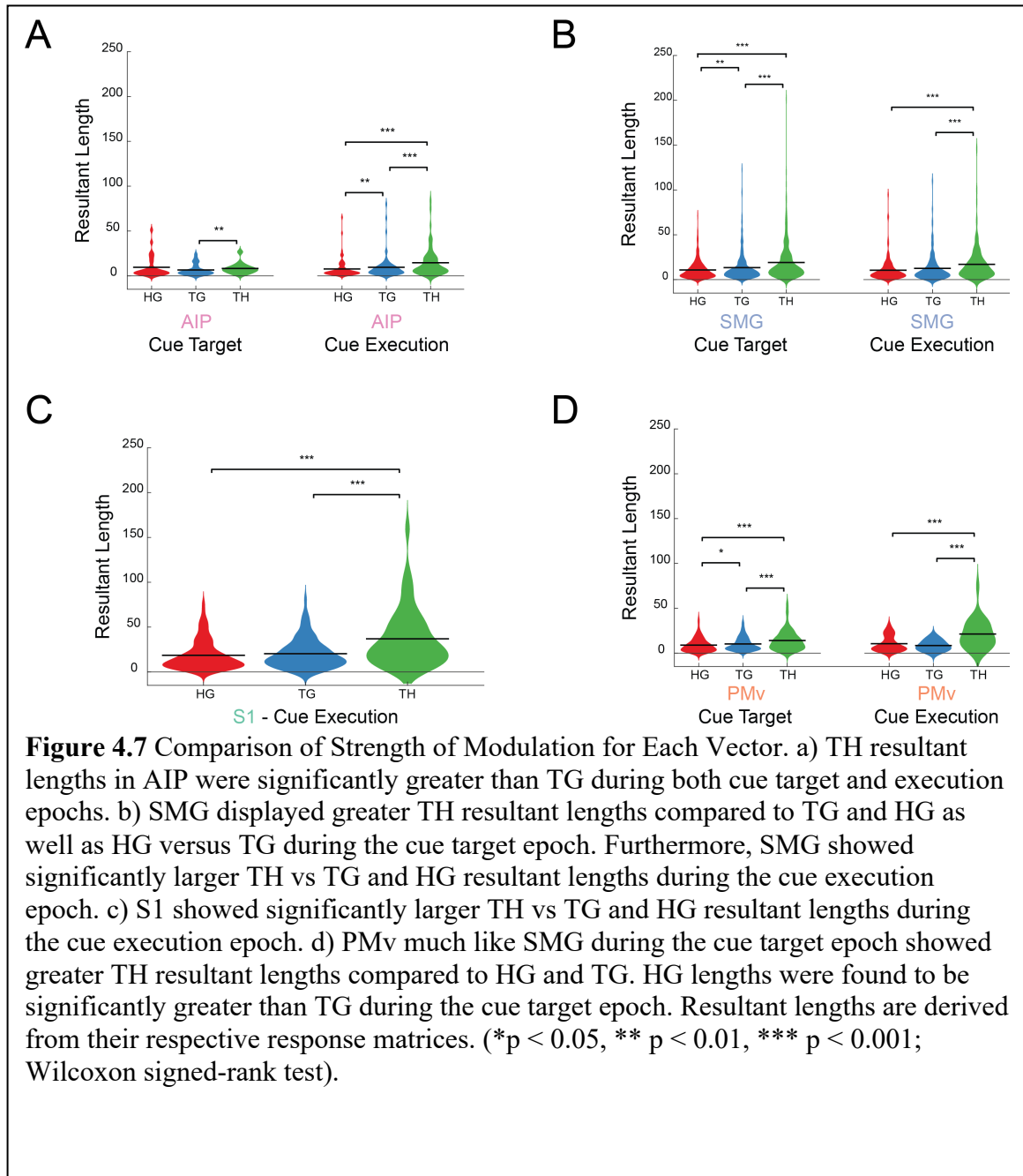
Weighted mean directions of the three vectors HG, TG, and TH were found to be  $-10^\circ$ ,  $-19^\circ$ , and  $-91^\circ$  with resultant lengths of 13, 15, and 34.8, respectively. All three vectors were also found to be unimodally distributed ( $p < 0.0001$  HG, TG, TH; Rayleigh test) and nonuniform ( $p < 0.01$ ; Watson test). Interestingly, based off these findings S1 seems to have the most homogenous representation of reference frames, with a strong encoding of the target relative to the hand during the CE epoch.

#### 4.3.4.4 AIP

A more comprehensive look at the population level tuning found in AIP interestingly shows a strong preference for the HG vector (Fig 4.6A). We find that population level resultant angles for only HG and TH are unimodal (HG:  $p < 0.0001$ , TG:  $p = 0.24$ , TH:  $p < 0.0001$ ; Rayleigh test) and nonuniform (HG:  $p < 0.01$ , TG:  $p > 0.15$ , TH:  $p < 0.01$ ; Watson test). Weighted mean resultant angles during the planning epoch in AIP for HG, TG, and TH were found to be  $-82^\circ$ ,  $-88^\circ$ ,  $-99^\circ$  with average resultant vector lengths of 7.7, 1.5, and 4.8, respectively. This tuning is suggestive of tuning of the position of the hand relative to gaze position (HG) and target location relative to hand position (TH).

In contrast, during the execution epoch we find that all vectors (HG, TG, TH) are unimodally distributed ( $p < 0.0001$ ; Rayleigh test) and nonuniform ( $p < 0.01$ ; Watson test). We find a significant concentration of the reference frame population resultant angles centered around TH with a weighted mean angle and resultant vector length of  $-84^\circ$  and 13.2, respectively. The mean weighted resultant angles and vector lengths for HG and TG were found to be  $4^\circ$ , 4.8 and  $-11^\circ$ , 7, respectively. Shockingly, here we see that during the planning epoch the HG and TH reference frame representations are present however during execution we see a shift in the HG response indicating a more defined hand centered coding of the target ( $p < 0.001$ ; Mardia-Watson-Wheeler test). We also find significant changes in the mean resultant angle of HG but not in TG or TH ( $p < 0.0001$ ,  $p = 0.3$ ,  $p = 0.96$ ; Watson's nonparametric test). Furthermore, of note is that during the planning epoch TG was not found to be unimodal or nonuniform; however this shifted during the CE epoch towards target centric tuning of the TG vector. These results

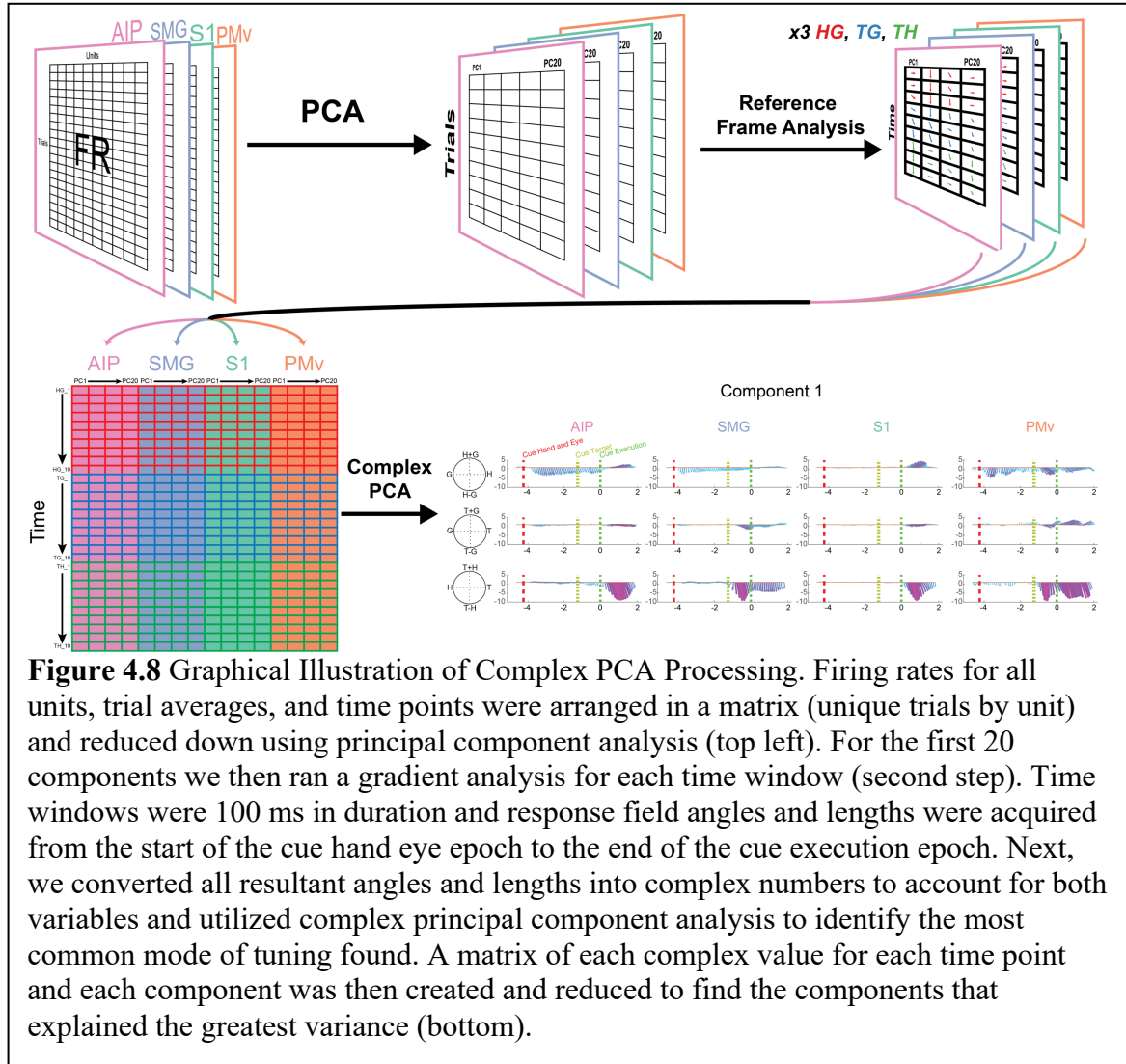
further indicate that AIP possibly encodes the relative position of the hand to gaze (HG) and target to hand (TH) during the delay epoch (CT) and the population of tuned units shifts to a more hand centric encoding of the target (TH) during the execution of the imagined reach (CE).





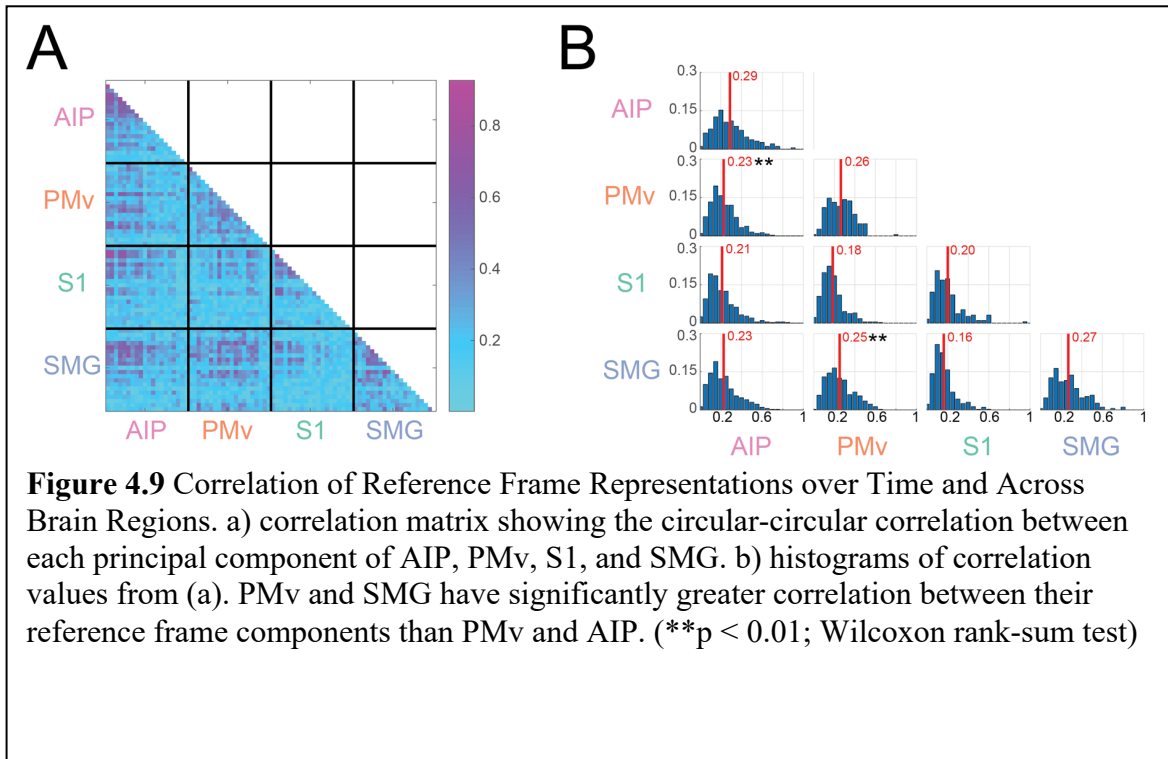
### 4.3.5 Temporal Evolution of Reference Frames

From the above single unit analyses we find that population level reference frames shift and dimensionality collapses from the CT to CE epochs. The degree to which this occurs and how reference frames evolve temporally exactly is something that potentially depends upon the cortical region. The nature of these temporal dynamics and how exactly they differ between brain areas is not clear from the single unit analyses above as they only provide a brief picture of the reference frame encoding and provide no information about how the HG, TG, and TH vectors are concurrently evolving. Furthermore, utilizing static time windows to determine reference frame representations of dynamic imagined movements fail to encompass tuning through time. To resolve this issue, we employ a population level dimensionality reduction analyses to allow us to compare brain areas at the level of the full temporally evolving dynamics across all tuned units. This allows us to determine how strongly different reference frame dynamics express across different brain areas throughout the entirety of a delayed imagined reaching task.



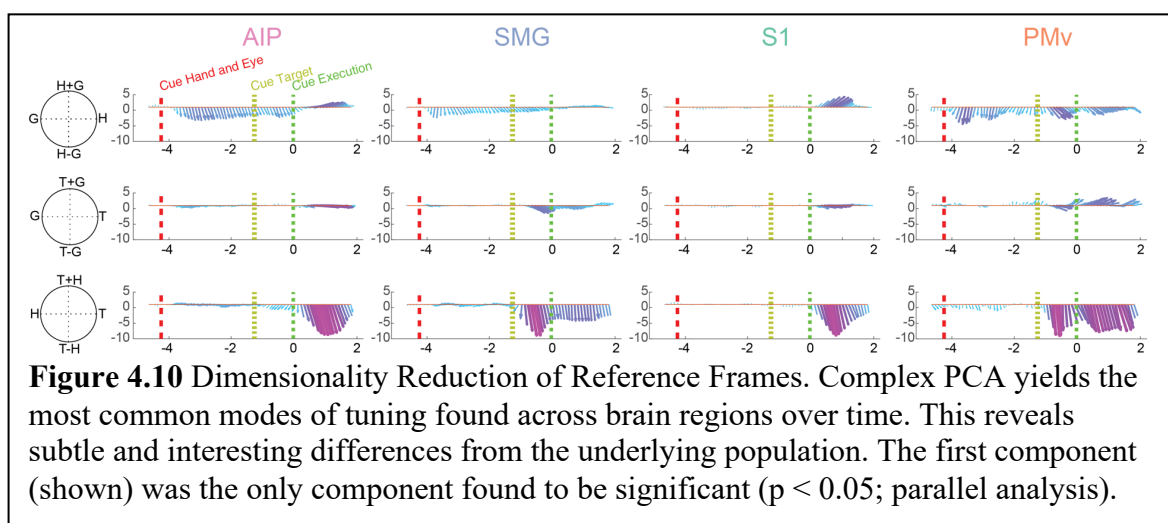
Through the steps of our dimensionality reduction we generate a correlation matrix across the first 20 principal components (Figure 4.8) of each brain region and compare the correlation of each components temporally evolving reference frame across all brain regions and their respective components (Figure 4.9A,  $\text{corr}(\text{brain region } X_i, \text{brain region } Y_j)$  where  $X$  and  $Y$  are the different brain regions and  $i$  is components 1-20). PMv and SMG have significantly greater correlation between their reference frame components than PMv and AIP. (\*\* $p < 0.01$ ; Wilcoxon rank-sum test, Figure 4.9B). This result agrees

with the NHP literature where anatomical connections between these two areas have been identified (Rozzi et al., 2008).



Using the correlation matrix, we perform a second dimensionality reduction of the HG, TG, and TH vectors and subsequently identify the components that meet a threshold determined from a parallel analysis to be significant principal components (Franklin et al., 1995). Parallel analysis reveals that one component met our stopping criteria (i.e. significance level) of 0.05 (95<sup>th</sup> percentile). In the first principal component we see the temporal evolution of reference frames across all brain areas during the imagined reaching task.

In AIP, the first principal component (38% of variance explained across all brain areas) showed strong tuning of the HG vector during the cueing of the effectors and maintenance of this tuning even after presentation of the target (Figure 4.10). We do also see small resultant vector lengths of TH during the planning. These smaller resultant lengths are suggestive of little to no tuning to TG or TH during the CT epoch. We see that this reference frame tuning changes during the execution epoch wherein we find resultant vectors evolve for all three vectors. During execution of the imagined reach the TH vector resultant length grew and encoded the relation of the target and hand position more uniformly. The HG vector progressively evolved to encode hand position and the TG vector encoded target position most likely per consequence of the strong encoding of TH during the execution epoch. This shows that in AIP the position of the hand is encoded relative to gaze position (HG) during the planning epoch with relatively subtle tuning of the target position relative to the hand; this then evolved to a more pronounced and stronger encoding of the TH vector during the CE epoch.



In PMv we found different patterns of tuning compared to AIP. During the fixation and maintenance of hand position (cueing of the effectors) there was a phasic representation of the HG vector that dissipates unlike the tonic HG representation seen in AIP and SMG. However, we found that during the planning epoch unlike the AIP area, there was strong TH representation during the planning epoch. This encoding during the planning epoch stayed consistent throughout the planning epoch and was maintained throughout the execution epoch.

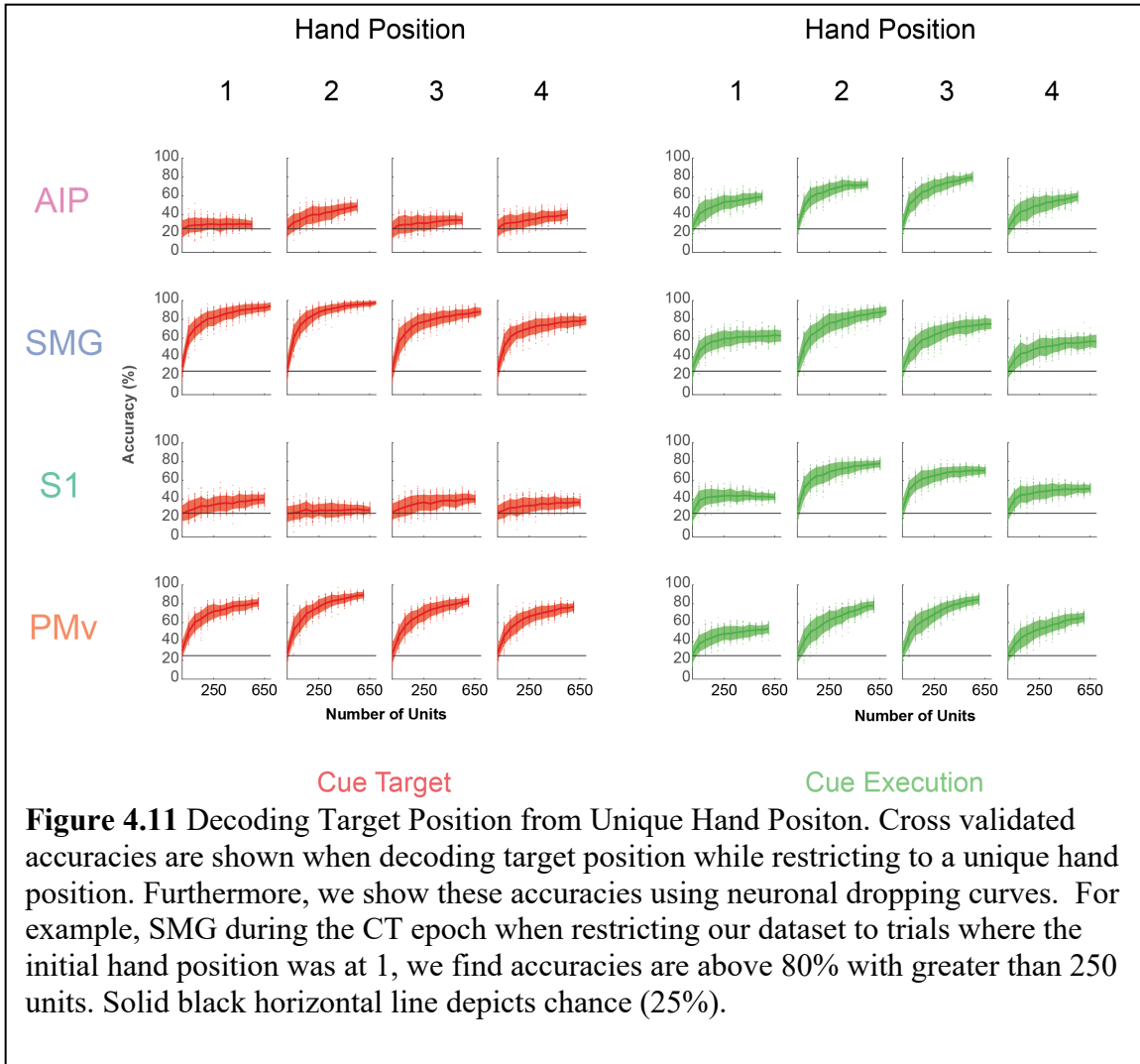
From previous work in the same patient, we elicited naturalistic responses in the arm via intracortical microstimulation of S1 (Salas et al., 2018). Utilizing the same array during our imagined reaching task we found little to no encoding of any of the vectors. This was expected, as we find no tuning above chance in S1 during the cueing of the effectors and target epochs of the delayed-imagined reaching task. Interestingly, we found strong hand centered encoding of the target (TH) during the cue execution epoch peaking around 1 second after the CE epoch is cued to begin.

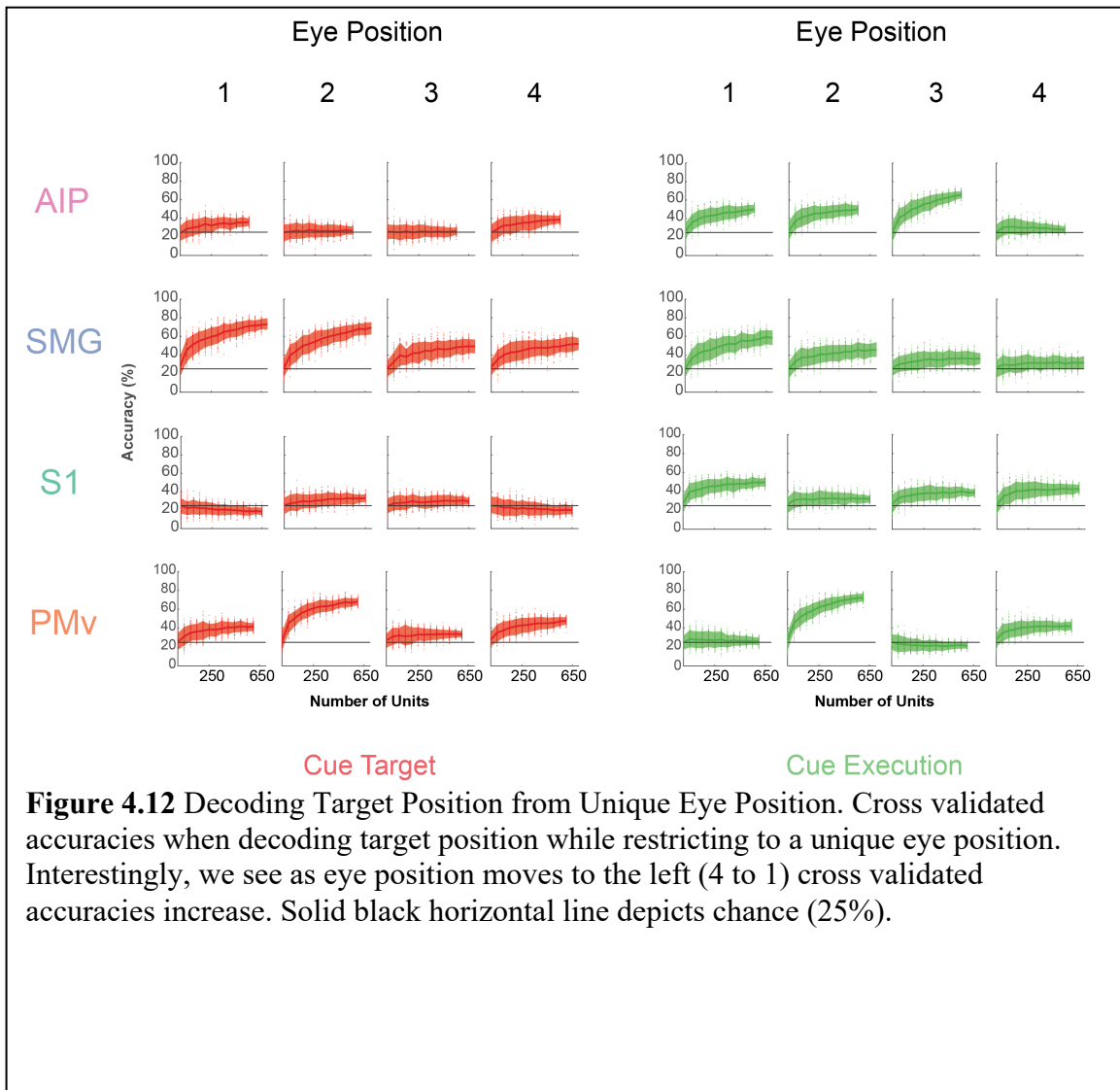
In SMG we found temporal evolution of reference frames to be similar to AIP with some subtle differences. Much like AIP during the cueing of the effectors, we found that HG tuning was prominent with TG and TH vectors pointing in the direction of G and H, respectively. During the planning epoch we found that HG tuning was maintained while TG and TH tuning evolved to encode the target relative to gaze position (TG) and target relative to the hand position (TH), respectively. Further analyses on decode performance are suggestive of an eye position effect (see below). The HG vector shifts to H while the

TH vector remains the same as it did during the delay, but with a decrease in the magnitude of the resultant vector length, indicating lower tuning strength. Interestingly, the TG vector remains oriented in the same direction as it did during the CT epoch. Thus, in SMG we find a relative position code (HG, TG, TH) during the CT epoch that shifts to TH and weak TG vector encoding during the CE epoch.

#### 4.3.6 Decoding Accuracy

Based on the findings above and noting that TH is largely encoded across most brain areas it follows that if the true encoding mechanism in that brain area is mainly hand centric then we can increase our decoding accuracy by separating out trials based upon hand position. Our reasoning is as follows, if the reference frame for example in S1 during the CE epoch is found to be TH then based off the temporal reference frame analysis target position should be encoded with respect to hand position. Thus, as we vary hand position we would expect coding for target positions to change as it is hand centered. Within a decoder framework we tested this assumption by training a linear classifier to decode target position given data from each independent hand (Figure 4.11) position and utilize dropping curves to compare decode accuracies across brain regions.





As expected based on our temporal reference frame analysis in brain regions SMG and PMV where TH vectors had large resultant vectors we find greater than 80% cross validated accuracy during the CT epoch. Interestingly, in SMG where we find strong encoding of the TG vector (Figure 4.10) we also find ascending cross validated accuracies when eye positions move from the right to left most eye positions (Figure 4.12). This is suggestive of eye position dependent modulation during this epoch with the left most eye positions having the greatest effect during the CT epoch. This trend can also be seen during the cue execution epoch, but to a lesser degree, which also corresponds to



the smaller resultant lengths (Figure 4.10 and 4.12). Conversely, in areas AIP and S1 where we found the smallest resultant vectors for TH we find cross validated accuracies to be at chance or slightly better during the same epoch. During the cue execution epoch we find cross validated accuracies to significantly be greater than chance across all brain regions. Due to the limited number of hand and target positions in our task the most lateral hand positions have the least diversity in reach directions, therefore biasing cross validated accuracies to be greatest at the centermost starting hand positions. For example, reaches are only up and away from the left and right most starting hand positions as opposed to hand positions two and three where there is greater diversity in the reach directions.

## 4.4 Discussion

Here we studied how sensorimotor reference frames are encoded and develop in four brain regions of human cortex across two patients during an imagined-delayed reaching task. The task design included a large array of combinations for the three behavioral variables that allowed us to examine this question. The percent of the population found to be tuned to any combination of the effectors varies across epochs and brain areas (Bremner and Andersen, 2012; Buneo et al., 2002; Chang and Snyder, 2010; McGuire and Sabes, 2011; Pesaran et al., 2006). The tuned units in areas near PMv, SMG, S1, and AIP showed mixed encoding of the eye, hand, and target variables more so during the planning than the execution epoch. However, the size of this effect varied based on the area being recorded from. Furthermore, utilizing dimensionality reduction techniques revealed that the evolution of reference frame encoding varies across brain areas and

epochs. The predominantly hand-centered coding found in these brain regions during the execution epoch is distinct from many of the previously reported eye-centered and heterogeneous reference frames seen in SPL areas of NHPs (McGuire and Sabes, 2011). Reference frame encoding during the planning epoch seems to be more mixed, however this seems to vary based on the area that is being recorded from. Lastly, while we find hand-centered tuning in our task paradigm we are limited by the high degree of correlation between the hand and muscle kinematics. Thus, at a first approximation, we are unable to discern between coding with respect to the hand versus coding of muscle kinematics.

There has long been a lasting debate with regards to the heterogeneity of reference frames across brain regions (Avillac et al., 2005; Batista et al., 2007; Bremner and Andersen, 2012; Chang and Snyder, 2010; McGuire and Sabes, 2011; Pesaran et al., 2010). It can be difficult to draw a single conclusion based on these reports due to behavioral and analytical differences between them. Here we aimed to resolve this by using the same behavioral and analytical techniques across brain regions. To the best of our ability, we objectively quantified common modes of tuning using gradient analyses and dimensionality reduction on the entire population of tuned neurons across brain regions. In doing so, we came to the most likely conclusion that the result of reported discrepancies is most likely due to the variable encoding of behavioral variables across brain regions. For example, we find more homogenous representations in areas like S1 compared to intermediate representations in areas SMG and PMv. This analysis differs

from previous work in that it does not require fitting responses to a model to determine reference frame representations (Batista et al., 2007; McGuire and Sabes, 2011).

Previous findings that established anatomical connections between PMv and SMG in NHPs (Clower et al., 2001; Rozzi et al., 2006, 2008) and the results here, e.g. these areas' reference frame representations had greater correlations compared to other regions, add to the growing body of work suggestive of these two areas' role in visuo- and somatomotor transformation of arm movements. We also do find that heterogeneity of brain regions is also variable in parietal cortex especially when we compare SMG and AIP. While both areas are in different subdivisions of the parietal cortex and do both encode reaches in hand centered coordinates during the cue execution epoch they encode slightly different variables during the delay. With SMG encoding TH, TG, and HG and AIP encoding the HG vector. However, we must note these conclusions are limited by the number of behavioral variables used in paradigm.

During movements we must be able to rapidly adjust and control our limbs in order to smoothly interact with our environment. Sensory delays in visual and proprioceptive feedback during these movements are delayed enough that errors cannot be appropriately integrated. Thus, previous work has hypothesized that the brain generates an internal estimate of our limbs (Miall and Wolpert, 1996). PPC, an association area at the functional interface between sensory and motor representations, is a strong candidate as an anatomical structure that might represent the internal estimate. However, it is difficult to collect direct neural evidence of this phenomenon due to the high correlation between

sensory and motor efference signals. The parietal lobe was also proposed as a candidate for encoding these state estimates with recent evidence suggesting that neurons encode internal forward models that are not available from passive sensory feedback or correlated with outgoing motor commands (Mulliken et al., 2008). In our behavioral setup we have the unique opportunity to measure the internal estimate of the limb disassociated from the motor and sensory variables during the cueing of the effectors epoch. The ability to measure these changes in the absence of sensory feedback could be highly suggestive of encoding of this estimate. In areas AIP, SMG, and PMv we found that hand position is encoded relative to gaze position during the cueing of the effectors, but not in S1 (Fig 4.10). In NHPs, PPC (AIP and SMG) has been shown to be an area that maintains an internal state estimate, and we found similar activity in an area near PMv (Mulliken et al., 2008; Stavisky et al., 2017). Although these findings contribute to the evidence that an internal state estimate is maintained in PMv, further investigation is required (see internal state estimate section).

Some studies quantify reference frames by fitting cell firing rates to models of predicted encoding schemes. This approach can be advantageous when neural signals are good fits for the proposed model, however it can fall apart when the parameters being fit cannot explain a large proportion of the variability. This can prove to be problematic when looking at a population of units that seem to be heterogeneous. Fortunately, the approach that we take allows us to determine the subtle impact that different variables have on a unit's firing rate. We take this a step further by utilizing dimensionality reduction techniques that take into consideration both the magnitude and push-pull nature that pairs

of behavioral variables have on the entire population of tuned units. Furthermore, this also yields insight into the temporal evolution and significant modulatory influences behavior variables have not just on a single unit, but across the overall population all whilst not enforcing a rigid framework to be fit.

Our results in PMv are, to the best of our knowledge, the first single unit recordings in humans showing significant tuning to an imagined reach and that these neural data can be used to decode target location. Previous work in NHPs by Kakei et al. (2001) showed that PMv neurons were directionally tuned and displayed an extrinsic like tuning. This study also went on to show that tuning to reaches was found during planning, execution, and both. Our results here suggest that direction tuning is modulated by hand position in humans. Furthermore, Kakei and colleagues did not vary the location of hand position, thus this is something that would most likely be overlooked in their task paradigm.

However, the greatest proportion of tuning we found was primarily during the planning epoch. These differences between directional and epoch relevant tuning compared to the findings of Kakei and colleagues is possibly due to the relative depth of recording. Kakei recorded at an average depth of  $2.9 \pm 0.89$  mm whereas our recordings were at  $\sim 1.5$  mm. Lastly, our findings in PMv display encoding of the hand relative to gaze position (HG) during planning and execution. More recent work from PMv has shown that hand configuration can be decoded from neural data acquired from PMv (Schaffelhofer et al., 2015). Combining these previous findings with those of Kakei suggests that PMv plays a role in encoding reaches and hand configuration (Kakei et al., 2001). Our findings in PMv during an imagined reach show HG and TH encoding during planning and

execution of the imagined movement. Further investigation is needed to determine the role of concurrent HG and TH tuning.

Previous findings in NHPs have found that the IPL, a larger area encompassing SMG, is a rich region that is responsive to different sensory stimuli and has many connections to frontal, parietal, and temporal areas such as the ventral premotor cortex (PMv), superior parietal lobule (SPL) and area MSTd, respectively (Matelli et al., 1986; Nelissen et al., 2011; Petrides and Pandya, 1984a; Rizzolatti et al., 1998; Rozzi et al., 2006, 2008).

Furthermore, functional connectivity analyses in humans have gone on to show that IPL is potentially part of a multimodal integration network that acts as a strong network interface between unimodal-related systems and cortical hubs (Sepulcre et al., 2012). In relation to these findings we find that SMG indeed displays a relative position code (concurrent HG, TG, and TH tuning) during the CT (planning) epoch which then evolves to encoding the target relative to both the hand and, to a lesser degree, gaze position (TH and TG). Interestingly, these findings compliment functional and anatomical studies that find IPL to be connected with visual areas, such as area MSTd in NHPs (Caspers et al., 2006, 2011; Nelissen et al., 2011). Further work on disassociating how reaching movements compared to eye movements could yield further insight into the potential contribution of SMG in the distributed cortical network that controls coordinated eye and arm movements, such as those proposed to be in PMd (Pesaran et al., 2010).

The results in S1 in contrast to the other areas are interesting, as we find no tuning to HG during the cueing of the effectors and little to no tuning throughout the task until the

subject imagines making a reach during the cue execution epoch. During this phase we find a strong largely homogenous hand centered representation. As mentioned in chapter 2, to the best of our knowledge these are the first human single unit findings to show S1: 1) encodes imagined reaches, 2) represents these in hand centric coordinates, and 3) has little no encoding of any behavioral variables until the imagined execution (no internal state estimate present).

In AIP, an area in PPC, we find strong HG tuning during the cueing of the effectors and delay with an even more robust encoding of the target relative to the hand. Throughout the task AIP seems to display a unitary reference frame that dominates each distinct epoch: cueing of effectors – HG, planning – HG, execution – TH. Interestingly, we find that AIP like SMG and less so PMv encodes an internal state estimate during the cueing of the effectors (Chapter 3).

Here we show that reference frames can shed light on what information is encoded in a brain region during a specific task. Using a delayed-imagined reaching task we show that imagined reaches are encoded in different reference frames among the brain areas we recorded from. However, additional work is needed to determine how different brain areas encode imagined reaches, and additionally how they encode saccades. Does spatial information about the target link the control of eye and arm movements? Or does SMG play a more direct role similar to FEF and SEF? Lastly, studying how these areas concurrently encode this information would be of value but would require simultaneous recordings to shed further light on the temporal dynamics of reference frame encoding.

## 5. Conclusion

In Chapter 2, we studied the role of primary somatosensory cortex (S1) in a cognitive motor imagery task. To the best of our knowledge, we have shown the first single unit evidence that cognitive imagery of movements is represented in the primary somatosensory area of human cortex (Chapter 2). Demonstrating S1 neurons track motor intentions in the complete absence of sensation. These findings possibly lend credence to previous findings showing S1 has direct projections to the spinal cord, and stimulation of S1 produces overt motor movements (Matyas et al., 2010; Penfield and Boldrey, 1937; Rathelot and Strick, 2006). Further investigation teasing apart whether these signals originate from S1 or copies from areas, such as M1, are still needed. Interestingly, we find that this activity is restricted to the time of imagined execution with negligible activity while the subject must actively maintain the position of the limb in memory, maintain fixation at distinct spatial locations, and maintain movement plans. These results suggest that the role of S1 in motor production is restricted to the time of movement execution. This parallels much of the NHP literature showing activity to be restricted to epochs involving active movements. However, of note is that active movements in S1 of NHPs has been shown to exhibit pre-movement activity (Fetz and Baker, 1973; London and Miller, 2013). Due to the constraints of our paradigm we are unable to test this as we have no way of determining when the subject began his imagined reach. Future studies aimed at recording S1 activity during attempted movements, at or one level above the SCI, in tetraplegic subjects would be interesting as this could elicit pre-movement activity with an associated EMG signal marking the beginning of the movement. Lastly, we show S1 activity codes the reach vector, coding motor intention



relative to the imagined position of the hand. These results implicate a role of primary somatosensory cortex in cognitive imagery, implicate a role of S1 in motor production in the absence of sensation, and suggest that S1 may provide a source of control signals for future implementations of neural prosthetic systems.

In Chapter 3, we studied if internal state estimates are stored in human posterior parietal cortex. Previous clinical reports found that subjects with parietal lesions while capable of performing activities of daily living, had unique deficits such as the inability to sense their arm if it was out of view and stationary (Wolpert et al., 1998). Here we show strong evidence for internal state estimates of the hand being encoded and stored in posterior parietal cortex (PPC). Furthermore, we find that the internal state estimate of the hand is encoded relative to the position of the eye. This holds implications for future implementations of neural prosthetics aimed at decoding hand position. While the findings shown in this dissertation provide evidence for the internal state estimate being stored in PPC, future aims towards understanding if this estimate is updated in this brain region during dynamic behaviors is required. Finally, in Chapter 4 we show that areas AIP, PMv, and SMG all exhibit HG tuning during the CHE epoch, suggesting that hand position is encoded relative to gaze position, but not in S1. Further studies, aimed at comparing how these representations differ or are similar across brain regions will aid in understanding if these are true internal state estimates in PMv and SMG. If so, is the internal state estimate stored similarly to AIP? And is it updated?

In Chapter 4, we investigated the reference frames encoded in an area near PMv, SMG, S1, and AIP. We show that reference frame representation heterogeneity is dependent upon the brain region. Further work in understanding if this heterogeneity is a by-product of sensory inputs to each brain region is needed. Interestingly, we find the most heterogeneity during the planning epoch. This evolves into a much clearer and unified hand centered reference frame across all brain regions suggesting that during a selected action the reference frame switches to the most relevant behavioral variable encoded. Further work, similar to those done by Pesaran and colleagues (2010), is needed and could be enhanced if the subjects made randomly interleaved saccades to the cued target as opposed to imagined reaches. Interestingly, we find that SMG and PMv, previously reported areas found to be reciprocally connected, share similar reference frame representations throughout our delayed-imageind-reaching task (Matelli et al., 1986; Petrides and Pandya, 1984b; Rizzolatti et al., 1998; Rozzi et al., 2006, 2008). Lastly, we show that complex PCA can be utilized to objectively reduce the dimensionality of heterogeneous reference frame representations to the most common modes found across brain regions. Future work, aimed at discerning local and long range spike field coherence will be beneficial, in so far as possibly providing mechanisms by which neurons across different brain regions coordinate their activity for reaches.

Understanding how the brain encodes behavioral variables is highly relevant to future successful implementations of brain machine interfaces (BMIs). Furthermore, how the

interplay across brain regions, can aid in finding new potential targets for BMI applications. While M1 and PPC to date have been the primary examples of successful BMI implementation we show here that areas like primary somatosensory cortex (S1) is also a region that should be used especially for closed-loop BMI applications.

Taken together the work presented here has broad applications for the successful implementation of future brain machine interfaces, decoding algorithms, neuroprosthetics, and our general understanding of how our brain helps us navigate an ever-changing world.

## 6. References

- Adrian, E.D., and Zotterman, Y. (1926). The impulses produced by sensory nerve endings. *J. Physiol.* *61*, 465–483.
- Aflalo, T., Kellis, S., Klaes, C., Lee, B., Shi, Y., Pejisa, K., Shanfield, K., Hayes-Jackson, S., Aisen, M., Heck, C., et al. (2015). Decoding motor imagery from the posterior parietal cortex of a tetraplegic human. *Science* *348*, 906–910.
- Ajiboye, A.B., Willett, F.R., Young, D.R., Memberg, W.D., Murphy, B.A., Miller, J.P., Walter, B.L., Sweet, J.A., Hoyen, H.A., Keith, M.W., et al. (2017). Restoration of reaching and grasping movements through brain-controlled muscle stimulation in a person with tetraplegia: a proof-of-concept demonstration. *The Lancet* *389*, 1821–1830.
- Andersen, R.A., and Buneo, C.A. (2002). Intentional Maps in Posterior Parietal Cortex. *Annu. Rev. Neurosci.* *25*, 189–220.
- Andersen, R.A., and Cui, H. (2009). Intention, Action Planning, and Decision Making in Parietal-Frontal Circuits. *Neuron* *63*, 568–583.
- Andersen, R.A., Essick, G.K., and Siegel, R.M. (1985). Encoding of spatial location by posterior parietal neurons. *Science* *230*, 456–458.
- Andersen, R.A., Snyder, L.H., Bradley, D.C., and Xing, J. (1997). Multimodal Representation of Space in the Posterior Parietal Cortex and Its Use in Planning Movements. *Annu. Rev. Neurosci.* *20*, 303–330.
- Andersen, R.A., Hwang, E.J., and Mulliken, G.H. (2010). Cognitive Neural Prosthetics. *Annu. Rev. Psychol.* *61*, 169–C3.
- Avillac, M., Denève, S., Olivier, E., Pouget, A., and Duhamel, J.-R. (2005). Reference frames for representing visual and tactile locations in parietal cortex. *Nat. Neurosci.* *8*, 941–949.
- Baldauf, D., Cui, H., and Andersen, R.A. (2008). The posterior parietal cortex encodes in parallel both goals for double-reach sequences. *J. Neurosci. Off. J. Soc. Neurosci.* *28*, 10081–10089.
- Batista, A.P., Santhanam, G., Yu, B.M., Ryu, S.I., Afshar, A., and Shenoy, K.V. (2007). Reference Frames for Reach Planning in Macaque Dorsal Premotor Cortex. *J. Neurophysiol.* *98*, 966–983.
- Baumann, S., Griffiths, T.D., Rees, A., Hunter, D., Sun, L., and Thiele, A. (2010). Characterisation of the BOLD response time course at different levels of the auditory pathway in non-human primates. *Neuroimage* *50*, 1099–1108.
- Bremner, L.R., and Andersen, R.A. (2012). Coding of the Reach Vector in Parietal Area 5d. *Neuron* *75*, 342–351.

- Bremner, L.R., and Andersen, R.A. (2014). Temporal Analysis of Reference Frames in Parietal Cortex Area 5d during Reach Planning. *J. Neurosci.* *34*, 5273–5284.
- Buneo, C.A., and Andersen, R.A. (2006). The posterior parietal cortex: Sensorimotor interface for the planning and online control of visually guided movements. *Neuropsychologia* *44*, 2594–2606.
- Buneo, C.A., Jarvis, M.R., Batista, A.P., and Andersen, R.A. (2002). Direct visuomotor transformations for reaching. *Nature* *416*, 632.
- Butts, D.A., Weng, C., Jin, J., Yeh, C.-I., Lesica, N.A., Alonso, J.-M., and Stanley, G.B. (2007). Temporal precision in the neural code and the timescales of natural vision. *Nature* *449*, 92–95.
- Buzsáki, G., Anastassiou, C.A., and Koch, C. (2012). The origin of extracellular fields and currents — EEG, ECoG, LFP and spikes. *Nat. Rev. Neurosci.* *13*, 407–420.
- Caspers, S., Geyer, S., Schleicher, A., Mohlberg, H., Amunts, K., and Zilles, K. (2006). The human inferior parietal cortex: Cytoarchitectonic parcellation and interindividual variability. *NeuroImage* *33*, 430–448.
- Caspers, S., Eickhoff, S.B., Rick, T., von Kapri, A., Kuhlen, T., Huang, R., Shah, N.J., and Zilles, K. (2011). Probabilistic fibre tract analysis of cytoarchitectonically defined human inferior parietal lobule areas reveals similarities to macaques. *NeuroImage* *58*, 362–380.
- Chang, S.W.C., and Snyder, L.H. (2010). Idiosyncratic and systematic aspects of spatial representations in the macaque parietal cortex. *Proc. Natl. Acad. Sci.* *107*, 7951–7956.
- Chang, S.W.C., Papadimitriou, C., and Snyder, L.H. (2009). Using a compound gain field to compute a reach plan. *Neuron* *64*, 744–755.
- Chartier, J., Anumanchipalli, G.K., Johnson, K., and Chang, E.F. (2018). Encoding of Articulatory Kinematic Trajectories in Human Speech Sensorimotor Cortex. *Neuron* *98*, 1042-1054.e4.
- Chaudhary, U., Birbaumer, N., and Curado, M.R. (2015). Brain-Machine Interface (BMI) in paralysis. *Ann. Phys. Rehabil. Med.* *58*, 9–13.
- Chivukula, S., Jafari, M., Aflalo, T., Yong, N.A., and Pouratian, N. (2019). Cognition in Sensorimotor Control: Interfacing With the Posterior Parietal Cortex. *Front. Neurosci.* *13*.
- Clower, D.M., West, R.A., Lynch, J.C., and Strick, P.L. (2001). The Inferior Parietal Lobule Is the Target of Output from the Superior Colliculus, Hippocampus, and Cerebellum. *J. Neurosci.* *21*, 6283–6291.
- Colby, C.L. (1998). Action-Oriented Spatial Reference Frames in Cortex. *Neuron* *20*, 15–24.

- Colby, C.L., and Duhamel, J.-R. (1996). Spatial representations for action in parietal cortex. *Cogn. Brain Res.* 5, 105–115.
- Collinger, J.L., Wodlinger, B., Downey, J.E., Wang, W., Tyler-Kabara, E.C., Weber, D.J., McMorland, A.J., Velliste, M., Boninger, M.L., and Schwartz, A.B. (2013). High-performance neuroprosthetic control by an individual with tetraplegia. *The Lancet* 381, 557–564.
- Davidson, T.J., Kloosterman, F., and Wilson, M.A. (2009). Hippocampal replay of extended experience. *Neuron* 63, 497–507.
- Desmurget, M., and Grafton, S. (2000a). Feedback Control for Fast Reaching Movements. *Trends Cogn. Sci.* 4, 9.
- Desmurget, M., and Grafton, S. (2000b). feedback control for fast reaching movements. *Trends Cogn. Sci.* 4, 9.
- Desmurget, M., Epstein, C.M., Turner, R.S., Prablanc, C., Alexander, G.E., and Grafton, S.T. (1999). Role of the posterior parietal cortex in updating reaching movements to a visual target. *Nat. Neurosci.* 2, 563–567.
- Duhamel, Colby, C.L., and Goldberg, M.E. (1992). The updating of the representation of visual space in parietal cortex by intended eye movements. *Science* 255, 90–92.
- Duhamel, J.-R., Bremmer, F., BenHamed, S., and Graf, W. (1997). Spatial invariance of visual receptive fields in parietal cortex neurons. 389, 4.
- Ethier, C., Oby, E.R., Bauman, M.J., and Miller, L.E. (2012). Restoration of grasp following paralysis through brain-controlled stimulation of muscles. *Nature* 485, 368–371.
- Fetz, E.E. (2007). Volitional control of neural activity: implications for brain-computer interfaces: Volitional control of neural activity. *J. Physiol.* 579, 571–579.
- Fetz, E.E., and Baker, M.A. (1973). Operantly conditioned patterns on precentral unit activity and correlated responses in adjacent cells and contralateral muscles. *J. Neurophysiol.* 36, 179–204.
- Fetz, E., King, J.E., and Mam, M. (1969). Operant Conditioning of Cortical Unit Activity. 5.
- Fletcher, S.N., Collinger, J.L., Foldes, S.T., Weiss, J.M., Downey, J.E., Tyler-Kabara, E.C., Bensmaia, S.J., Schwartz, A.B., Boninger, M.L., and Gaunt, R.A. (2016). Intracortical microstimulation of human somatosensory cortex. *Sci. Transl. Med.* aaf8083.

- Franklin, S.B., Gibson, D.J., Robertson, P.A., Pohlmann, J.T., and Fralish, J.S. (1995). Parallel Analysis: a method for determining significant principal components. *J. Veg. Sci.* *6*, 99–106.
- Fujiwara, Y., Lee, J., Ishikawa, T., Kakei, S., and Izawa, J. (2017). Diverse coordinate frames on sensorimotor areas in visuomotor transformation. *Sci. Rep.* *7*.
- Fusi, S., Miller, E.K., and Rigotti, M. (2016). Why neurons mix: high dimensionality for higher cognition. *Curr. Opin. Neurobiol.* *37*, 66–74.
- Georgopoulos, A.P., Kalaska, J.F., Caminiti, R., and Massey, J.T. (1982). On the relations between the direction of two-dimensional arm movements and cell discharge in primate motor cortex. *J. Neurosci. Off. J. Soc. Neurosci.* *2*, 1527–1537.
- Glaser, J.I., Chowdhury, R.H., Perich, M.G., and Miller, L.E. Machine learning for neural decoding. *24*.
- Gomi, H., and Kawato, null (1996). Equilibrium-point control hypothesis examined by measured arm stiffness during multijoint movement. *Science* *272*, 117–120.
- Goodale, M.A. (1998). Vision for perception and vision for action in the primate brain. *Novartis Found. Symp.* *218*, 21–34; discussion 34–39.
- Gréa, H., Pisella, L., Rossetti, Y., Desmurget, M., Tilikete, C., Grafton, S., Prablanc, C., and Vighetto, A. (2002). A lesion of the posterior parietal cortex disrupts on-line adjustments during aiming movements. *Neuropsychologia* *40*, 2471–2480.
- Harris, K.D., Quiroga, R.Q., Freeman, J., and Smith, S.L. (2016). Improving data quality in neuronal population recordings. *Nat. Neurosci.* *19*, 1165–1174.
- He, S.Q., Dum, R.P., and Strick, P.L. (1993). Topographic organization of corticospinal projections from the frontal lobe: motor areas on the lateral surface of the hemisphere. *J. Neurosci. Off. J. Soc. Neurosci.* *13*, 952–980.
- Hernández, A., Nácher, V., Luna, R., Zainos, A., Lemus, L., Alvarez, M., Vázquez, Y., Camarillo, L., and Romo, R. (2010). Decoding a Perceptual Decision Process across Cortex. *Neuron* *66*, 300–314.
- Hochberg, L.R., Serruya, M.D., Friehs, G.M., Mukand, J.A., Saleh, M., Caplan, A.H., Branner, A., Chen, D., Penn, R.D., and Donoghue, J.P. (2006). Neuronal ensemble control of prosthetic devices by a human with tetraplegia. *Nature* *442*, 164–171.
- Holdefer, R.N., and Miller, L.E. (2002). Primary motor cortical neurons encode functional muscle synergies. *Exp. Brain Res.* *146*, 233–243.
- Horel, J.D. (1984). Complex Principal Component Analysis: Theory and Examples. *J. Clim. Appl. Meteorol.* *23*, 1660–1673.

- House, W.F. (1976). Cochlear implants. *Ann. Otol. Rhinol. Laryngol.* *85 suppl 27*, 1–93.
- Inoue, K., Kawashima, R., Satoh, K., Kinomura, S., Goto, R., Koyama, M., Sugiura, M., Ito, M., and Fukuda, H. (1998). PET Study of Pointing With Visual Feedback of Moving Hands. *J. Neurophysiol.* *79*, 117–125.
- Jordan, M.I., and Rumelhart, D.E. (1992). Forward models: Supervised learning with a distal teacher. *Cogn. Sci.* *16*, 307–354.
- Takei, S., Hoffman, D.S., and Strick, P.L. (2001). Direction of action is represented in the ventral premotor cortex. *Nat. Neurosci.* *4*, 1020–1025.
- Kao, J.C., Nuyujukian, P., Ryu, S.I., Churchland, M.M., Cunningham, J.P., and Shenoy, K.V. (2015). Single-trial dynamics of motor cortex and their applications to brain-machine interfaces. *Nat. Commun.* *6*, 7759.
- Katayama, M., and Kawato, M. (1993). Virtual trajectory and stiffness ellipse during multijoint arm movement predicted by neural inverse models. *Biol. Cybern.* *69*, 353–362.
- Kim, S.-P., Simeral, J.D., Hochberg, L.R., Donoghue, J.P., and Black, M.J. (2008). Neural control of computer cursor velocity by decoding motor cortical spiking activity in humans with tetraplegia. *J. Neural Eng.* *5*, 455–476.
- London, B.M., and Miller, L.E. (2013). Responses of somatosensory area 2 neurons to actively and passively generated limb movements. *J. Neurophysiol.* *109*, 1505–1513.
- Makin, T.R., and Bensmaia, S.J. (2017). Stability of Sensory Topographies in Adult Cortex. *Trends Cogn. Sci.* *21*, 195–204.
- Matelli, M., Camarda, R., Glickstein, M., and Rizzolatti, G. (1986). Afferent and efferent projections of the inferior area 6 in the macaque monkey. *J. Comp. Neurol.* *251*, 281–298.
- Matyas, F., Sreenivasan, V., Marbach, F., Wacongne, C., Barsy, B., Mateo, C., Aronoff, R., and Petersen, C.C. (2010). Motor control by sensory cortex. *Science* *330*, 1240–1243.
- McGuire, L.M.M., and Sabes, P.N. (2009). Sensory transformations and the use of multiple reference frames for reach planning. *Nat. Neurosci.* *12*, 1056–1061.
- McGuire, L.M.M., and Sabes, P.N. (2011). Heterogeneous Representations in the Superior Parietal Lobule Are Common across Reaches to Visual and Proprioceptive Targets. *J. Neurosci.* *31*, 6661–6673.
- van der Meer, M.A.A., Johnson, A., Schmitzer-Torbert, N.C., and Redish, A.D. (2010). Triple dissociation of information processing in dorsal striatum, ventral striatum, and hippocampus on a learned spatial decision task. *Neuron* *67*, 25–32.



- Miall, R.C., and Wolpert, D.M. (1996). Forward Models for Physiological Motor Control. *Neural Netw.* *9*, 1265–1279.
- Morrow, M.M., and Miller, L.E. (2003). Prediction of Muscle Activity by Populations of Sequentially Recorded Primary Motor Cortex Neurons. *J. Neurophysiol.* *89*, 2279–2288.
- Mulliken, G.H., Musallam, S., and Andersen, R.A. (2008). Forward estimation of movement state in posterior parietal cortex. *Proc. Natl. Acad. Sci.* *105*, 8170–8177.
- Musallam, S., Corneil, B.D., Greger, B., Scherberger, H., and Andersen, R.A. (2004). Cognitive Control Signals for Neural Prosthetics. *Science* *305*, 258–262.
- Nelissen, K., Borra, E., Gerbella, M., Rozzi, S., Luppino, G., Vanduffel, W., Rizzolatti, G., and Orban, G.A. (2011). Action observation circuits in the macaque monkey cortex. *J. Neurosci. Off. J. Soc. Neurosci.* *31*, 3743–3756.
- Nelson, R.J. (1987). Activity of monkey primary somatosensory cortical neurons changes prior to active movement. *Brain Res.* *406*, 402–407.
- Norman, S.L., McFarland, D.J., Miner, A., Cramer, S.C., Wolbrecht, E.T., Wolpaw, J.R., and Reinkensmeyer, D.J. (2018). Controlling pre-movement sensorimotor rhythm can improve finger extension after stroke. *J. Neural Eng.* *15*, 056026.
- Nuyujukian, P., Sanabria, J.A., Saab, J., Pandarinath, C., Jarosiewicz, B., Blabe, C.H., Franco, B., Mernoff, S.T., Eskandar, E.N., Simeral, J.D., et al. (2018). Cortical control of a tablet computer by people with paralysis. *PLOS ONE* *13*, e0204566.
- Pandarinath, C., O’Shea, D.J., Collins, J., Jozefowicz, R., Stavisky, S.D., Kao, J.C., Trautmann, E.M., Kaufman, M.T., Ryu, S.I., Hochberg, L.R., et al. (2018). Inferring single-trial neural population dynamics using sequential auto-encoders. *Nat. Methods* *15*, 805–815.
- Peña, J.L., and Konishi, M. (2001). Auditory spatial receptive fields created by multiplication. *Science* *292*, 249–252.
- Penfield, W., and Boldrey, E. (1937). Somatic motor and sensory representation in the cerebral cortex of man as studied by electrical stimulation. *Brain* *60*, 389–443.
- Pesaran, B., Nelson, M.J., and Andersen, R.A. (2006). Dorsal Premotor Neurons Encode the Relative Position of the Hand, Eye, and Goal during Reach Planning. *Neuron* *51*, 125–134.
- Pesaran, B., Nelson, M.J., and Andersen, R.A. (2010). A Relative Position Code for Saccades in Dorsal Premotor Cortex. *J. Neurosci.* *30*, 6527–6537.
- Petrides, M., and Pandya, D.N. (1984a). Projections to the frontal cortex from the posterior parietal region in the rhesus monkey. *J. Comp. Neurol.* *228*, 105–116.

- Petrides, M., and Pandya, D.N. (1984b). Projections to the frontal cortex from the posterior parietal region in the rhesus monkey. *J. Comp. Neurol.* *228*, 105–116.
- Pouget, A., and Snyder, L.H. (2000). Computational approaches to sensorimotor transformations. *3*, 7.
- Pouget, A., Deneve, S., and Duhamel, J.-R. (2002). A computational perspective on the neural basis of multisensory spatial representations. *Nat. Rev. Neurosci.* *3*, 741–747.
- Quiroga, R.Q., Snyder, L.H., Batista, A.P., Cui, H., and Andersen, R.A. (2006). Movement Intention Is Better Predicted than Attention in the Posterior Parietal Cortex. *J. Neurosci.* *26*, 3615–3620.
- Rathelot, J.-A., and Strick, P.L. (2006). Muscle representation in the macaque motor cortex: an anatomical perspective. *Proc. Natl. Acad. Sci.* *103*, 8257–8262.
- Rathelot, J.-A., Dum, R.P., and Strick, P.L. (2017). Posterior parietal cortex contains a command apparatus for hand movements. *Proc. Natl. Acad. Sci.* *114*, 4255–4260.
- Revechakis, B., Aflalo, T.N., Kellis, S., Pouratian, N., and Andersen, R.A. (2014). Parietal neural prosthetic control of a computer cursor in a graphical-user-interface task. *J. Neural Eng.* *11*, 066014.
- Rigotti, M., Barak, O., Warden, M.R., Wang, X.-J., Daw, N.D., Miller, E.K., and Fusi, S. (2013). The importance of mixed selectivity in complex cognitive tasks. *Nature* *497*, 585–590.
- Rizzolatti, G., Luppino, G., and Matelli, M. (1998). The organization of the cortical motor system: new concepts. *Electroencephalogr. Clin. Neurophysiol.* *106*, 283–296.
- Rozzi, S., Calzavara, R., Belmalih, A., Borra, E., Gregoriou, G.G., Matelli, M., and Luppino, G. (2006). Cortical Connections of the Inferior Parietal Cortical Convexity of the Macaque Monkey. *Cereb. Cortex* *16*, 1389–1417.
- Rozzi, S., Ferrari, P.F., Bonini, L., Rizzolatti, G., and Fogassi, L. (2008). Functional organization of inferior parietal lobule convexity in the macaque monkey: electrophysiological characterization of motor, sensory and mirror responses and their correlation with cytoarchitectonic areas. *Eur. J. Neurosci.* *28*, 1569–1588.
- Rushworth, M.F.S., Nixon, P.D., and Passingham, R.E. (1997). Parietal cortex and movement I. Movement selection and reaching. *Exp. Brain Res.* *117*, 292–310.
- Russo, A.A., Bittner, S.R., Perkins, S.M., Seely, J.S., London, B.M., Lara, A.H., Miri, A., Marshall, N.J., Kohn, A., Jessell, T.M., et al. (2018). Motor Cortex Embeds Muscle-like Commands in an Untangled Population Response. *Neuron* *97*, 953-966.e8.

- Salas, M.A., Bashford, L., Kellis, S., Jafari, M., Jo, H., Kramer, D., Shanfield, K., Pejsa, K., Lee, B., Liu, C.Y., et al. (2018). Proprioceptive and cutaneous sensations in humans elicited by intracortical microstimulation. *ELife* 7, e32904.
- Serruya, M.D., Hatsopoulos, N.G., Paninski, L., Fellows, M.R., and Donoghue, J.P. (2002). Instant neural control of a movement signal. *Nature* 416, 141–142.
- Shadmehr, R., and Krakauer, J.W. (2008). A computational neuroanatomy for motor control. *Exp. Brain Res.* 185, 359–381.
- Singh, C., and Levy, W.B. (2017). A consensus layer V pyramidal neuron can sustain interspike-interval coding. *PLOS ONE* 12, e0180839.
- Sirigu, A., Duhamel, J.-R., Cohen, L., Pillon, B., Dubois, B., and Agid, Y. (1996). The Mental Representation of Hand Movements After Parietal Cortex Damage. *Science* 273, 1564–1568.
- Spence, C., and Driver, J. (2004). Multimodal spatial representations in the primate parietal lobe." *Crossmodal Space and Crossmodal Attention*. J. Driver and C. Spence (Eds.) pp. 99-122, Oxford University Press (OUP Oxford).
- Stavisky, S.D., Kao, J.C., Ryu, S.I., and Shenoy, K.V. (2017). Trial-by-Trial Motor Cortical Correlates of a Rapidly Adapting Visuomotor Internal Model. *J. Neurosci.* 37, 1721–1732.
- Stein, R.B., Gossen, E.R., and Jones, K.E. (2005). Neuronal variability: noise or part of the signal? *Nat. Rev. Neurosci.* 6, 389–397.
- Sugata, H., Hirata, M., Yanagisawa, T., Matsushita, K., Yorifuji, S., and Yoshimine, T. (2016). Common neural correlates of real and imagined movements contributing to the performance of brain–machine interfaces. *Sci. Rep.* 6.
- Tibshirani, R., Walther, G., and Hastie, T. (2001). Estimating the number of clusters in a data set via the gap statistic. *J. R. Stat. Soc. Ser. B Stat. Methodol.* 63, 411–423.
- Trotter, Y., and Celebrini, S. (1999). Gaze direction controls response gain in primary visual-cortex neurons. *Nature* 398, 239–242.
- VanRullen, R., Guyonneau, R., and Thorpe, S.J. (2005). Spike times make sense. *Trends Neurosci.* 28, 1–4.
- Velliste, M., Perel, S., Spalding, M.C., Whitford, A.S., and Schwartz, A.B. (2008). Cortical control of a prosthetic arm for self-feeding. *Nature* 453, 1098–1101.
- Vidal, J.J. (1973). Toward Direct Brain-Computer Communication. *Annu. Rev. Biophys. Bioeng.* 2, 157–180.

Wander, J.D., Sarma, D., Johnson, L.A., Fetz, E.E., Rao, R.P.N., Ojemann, J.G., and Darvas, F. (2016). Cortico-Cortical Interactions during Acquisition and Use of a Neuroprosthetic Skill. *PLoS Comput. Biol.* *12*.

Welker, W.I., Benjamin, R.M., Miles, R.C., and Woolsey, C.N. (1957). Motor effects of stimulation of cerebral cortex of squirrel monkey (*Saimiri sciureus*). *J. Neurophysiol.* *20*, 347–364.

Wolpaw, J., and Wolpaw, E.W. (2012). *Brain-Computer Interfaces: Principles and Practice* (Oxford University Press, USA).

Wolpert, D.M., and Ghahramani, Z. (2000). Computational principles of movement neuroscience. *3*, 6.

Wolpert, D., Ghahramani, Z., and Jordan, M. (1995a). An internal model for sensorimotor integration. *Science* *269*, 1880–1882.

Wolpert, D.M., Ghahramani, Z., and Jordan, M.I. (1995b). An internal model for sensorimotor integration. *Science* *269*, 1880–1882.

Wolpert, D.M., Goodbody, S.J., and Husain, M. (1998). Maintaining internal representations: the role of the human superior parietal lobe. *Nat. Neurosci.* *1*, 529–533.

Zhang, C.Y., Aflalo, T., Revechkis, B., Rosario, E.R., Ouellette, D., Pouratian, N., and Andersen, R.A. (2017). Partially Mixed Selectivity in Human Posterior Parietal Association Cortex. *Neuron* *95*, 697-708.e4.

Zhang, K., Ginzburg, I., McNaughton, B.L., and Sejnowski, T.J. (1998). Interpreting neuronal population activity by reconstruction: unified framework with application to hippocampal place cells. *J. Neurophysiol.* *79*, 1017–1044.

Zipser, D., and Andersen, R.A. (1988). A back-propagation programmed network that simulates response properties of a subset of posterior parietal neurons. *Nature* *331*, 679–684.

(2015). National Spinal Cord Injury Statistical Center, Facts and Figures at a Glance.